LA-UR-03-4819

Approved for public release;
distribution is unlimited.

Title: VADOSE-ZONE FLUID AND SOLUTE FLUX: ADVECTION AND DIFFUSION AT THE AREA 5 RADIOACTIVE WASTE MANAGEMENT SITE

Author(s): Andrew Wolfsberg and Philip Stauffer

Submitted to: U.S. Department of Energy
National Nuclear Security Administration
Nevada Site Office

Form 836 (8/00)

This work was supported by the U.S. Department of Energy,
National Nuclear Security Administration, Nevada Site Office.

Los Alamos National Laboratory, an affirmative action/
equal opportunity employer, is operated by the University
of California for the United States Department of Energy
under contract W-7405-ENG-36.

LA-UR-03-4819

VADOSE-ZONE FLUID AND SOLUTE FLUX: ADVECTION AND DIFFUSION AT THE AREA 5 RADIOACTIVE WASTE MANAGEMENT SITE

Andrew Wolfsberg and Philip Stauffer

Earth and Environmental Sciences Division

Los Alamos National Laboratory

Submitted to

U.S. Department of Energy

National Nuclear Security Administration

Nevada Site Office

July 2003

This Page Intentionally Left Blank

Revision History

Revision 1	Draft report submitted May 2003
Revision 2	Revised report submitted July 2003
Revision 3	Final report, revised per OPAI review and submitted July 2003

Acknowledgements

Michelle Walvoord provided invaluable input to this effort. Her contribution in implementing the DASH model with FEHM prior to this project, her collaboration in the analyses presented here, and her discussion of ongoing research at other relevant field sites are greatly appreciated. Mike Young, Clay Cooper, and David Shafer at DRI provided significant insight into the properties and results reported in their 2002 manuscript and they provided valuable comments on the draft report. We also thank Bruce Crowe, Vefa Yucel, Mike Sully, John Tauxe, Katie Catlett, Tom Stockton, and Paul Black for the discussions they generated, the information they provided regarding the performance assessment use of this type of process model, and their detailed reviews of this work. James Craig provided exceptional programmatic support and budget tracking, for which we are grateful. Finally, we thank the U.S. Department of Energy (DOE) and the DOE Waste Management project manager, Jhon Carilli, for providing funding to accomplish this work, which was performed under contract number W-7405-ENG-36.

Acronyms and Abbreviations

a	volumetric air content
α	Equilibrium Fractionation Factor
atm	Atmosphere
Cl	Chlorine
cm	centimeter
CW	Conca-Wright
D	Deuterium
δ	delta notation
DASH	Deep Arid Systems Hydrodynamics Model
D_{eff}	Effective Diffusion Coefficient
D_o	Free Diffusion Coefficient
DRI	Desert Research Institute
ϕ	porosity
FEHM	Finite Element Heat and Mass Transport Code
g	gram
H	Hydrogen
k	Permeability
K	Hydraulic Conductivity
ka	Thousand Years Before Present
kg	kilogram
K^H	Henrys Law Constant
K^H_{ND}	Nondimensional Henrys Law Constant
ky	Thousand Years
L	Liquid
LANL	Los Alamos National Laboratory
m	Meter
mg	Milligram
mm	Millimeter
mMQ	Modified Millington-Quirk
MPa	Mega-Pascal
MQ	Millington-Quirk
M_w	Molecular Weight
NTS	Nevada Test Site
O	Oxygen
P	Pressure
p	Partial Pressure
PA	Performance Assessment
q	Flux
θ	volumetric water content
R	Relative Permeability
R	Universal Gas Constant
REECo	Reynolds Electrical and Engineering Company, Inc.
RMS	Root Mean Square
RWMS	Radioactive Waste Management Site
s	second
SMOW	Standard Mean Ocean Water
T	Temperature
V	Vapor
yr	Year

Executive Summary

Performance assessment (PA) for the Area 5 Radioactive Waste Management Site (RWMS) on the Nevada Test Site considers, among other processes, both liquid- and vapor-phase solute transport via advection and diffusion to the accessible environment. In support of the PA, this study develops estimates of present-day liquid and vapor fluxes at three well locations near the Area 5 RWMS. It also evaluates liquid- and vapor-phase solute diffusion models. Predictions of fluxes and evaluations of diffusion model formulations are based upon matching field data for chloride, stable isotopes of oxygen and hydrogen, and water potentials measured in the three wells.

Present-day liquid and vapor flux estimates are sensitive to several uncertain parameters, the most important being the timing of the shift from a cool, mesic climate to a warm, arid climate between 26 thousand years (ky) ago and 13 ky ago. As the climate changed to drier conditions, vegetation changes caused a major shift in the vadose-zone liquid and vapor flow patterns as observed in the matric potentials and chloride accumulation profiles in the shallow vadose zone. The system continues to dry, so the duration of the post climate-change period affects estimates of present-day fluxes. Other factors affecting estimates of liquid and vapor fluxes are, in order of importance determined in this study, a) material properties and their vertical distribution, b) root-zone capillary pressure, and c) infiltration rates during the pluvial period prior to the climate change.

The estimated liquid and vapor flux profiles vary with depth, material properties, and time since the most recent major climate change. In all cases, upward liquid fluxes vary between 0.0 and 0.02 mm/yr, with the transition between upward and downward flux occurring at depths between 20 and 70 m. The maximum upward liquid flux tends to occur between depths of 5 and 20 m, depending upon the simulation conditions. Vapor fluxes are always upward, with marked increases to as high as 0.03 mm/yr occurring above depths of 10 to 30 m, depending on simulation conditions. Below those depths, upward vapor fluxes are on the order of 0.0025 mm/yr.

Due to the low estimated liquid and vapor fluxes, diffusion may be a more important process for contaminant migration at the Area 5 RWMS. Diffusion model formulations for chloride, a liquid-phase solute, and heavy oxygen and hydrogen isotopes in water molecules, which migrate in both the liquid and vapor phases, are evaluated by comparison of predicted solute profiles with measured field data. As with the flux estimates, multiple parameter uncertainties must be considered, leading to a range of predicted solute concentration profiles. The results are split with more diffusive model combinations leading to better matches to data at some wells and less diffusive model combinations matching the data at other wells. In general, the stable isotope simulations support a shorter warm, dry period. Thus, if climate warming occurred concurrently with end of the pluvial period, the stable isotope simulation results support a shorter vadose-zone drying period and the lower present-day upward fluxes associated with such timing.

The simulations in this study seek to match data resulting from complex subsurface process occurring over the tens of thousands of years. Multiple uncertainties in those processes affect the simulations. Further, the nature of predictive modeling is to abstract and simplify complex processes into a manageable framework. Overall, the models yield good, but imperfect matches to the field data. No single model matches all data sets better than another. Thus, because the predicted fluxes are very low for all situations considered and because the diffusion models capture the observed trends and often the match the data well, this study supports the following recommendations:

a) Consider equally all fluxes estimated with post-pluvial periods of 13 ky and 26 ky.

b) Consider both the more diffusive and the less diffusive model formulations presented in this study in the PA and investigate whether the model formulation differences lead to significant differences in contaminant flux estimates at the ground surface.

This Page Intentionally Left Blank

TABLE OF CONTENTS

1. Introduction

Performance assessment (PA) for the Area 5 Radioactive Waste Management Site (RWMS) on the Nevada Test Site considers, among other processes, both liquid- and vapor-phase solute transport to the accessible environment. Due to the relatively shallow depths of disposal in a system with hundreds of meters of unsaturated media above the water table, upward migration of contaminants to the ground surface has become a greater concern than downward migration to the aquifer. This concern is compounded by recent studies indicating the existence of driving forces that yield upward liquid and vapor fluxes in a system previously thought to have either small or zero downward fluxes. However, direct measurement of liquid or vapor fluxes in arid vadose zones is virtually impossible. Thus, the fluxes must be estimated using simulation techniques integrated with field and laboratory measurements of material properties and environmental tracers.

1.1 Objectives

The objective of the present study is to develop a process model for simulating gas and liquid-phase flow and solute transport in the unsaturated zone of the Area 5 RWMS that is consistent with measured and observed data. The results of simulations with the model will be used to provide estimates of liquid and vapor fluxes and an evaluation of gas-phase and liquid-phase diffusion model components in the PA for the RWMS. The development of this model is based on the following approaches:

1. Use results and concepts from several previous studies to develop a comprehensive vadose-zone flow and transport model for this system.
2. Use existing data sets to constrain and confirm model parameters, boundary conditions, and initial conditions.
3. Provide multiple results to indicate ranges in model flux predictions based upon multiple boreholes and their associated material properties, chloride concentrations, and stable isotope ratios.
4. Provide results that either validate or increase confidence in individual components of the overall system model used for performance assessment.

1.2 Nomenclature:

Predictions of present day liquid and gas fluxes depend on hydrologic processes that occurred over many tens of thousands of years. In the present study, there are multiple references to the timing and duration of a pluvial period during the Pleistocene, when percolation exceeded evaporation and transpiration, resulting in net downward flow. Prior to that pluvial period, dry conditions are assumed to have been prevalent for tens of thousands of years, resulting in massive accumulation of chloride in the shallow vadose zone. To describe the evolution of the hydrologic system in this study, the following nomenclature for time is adopted:

- ka = thousand years before present
- ky = thousand years

The system considered involves multiphase movement of water. The terms liquid and vapor are used, respectively, to describe the two phases of water, whereas fluid refers to either the liquid or vapor phases, depending on the context. The term “water” is used exclusively to refer to the liquid phase, to maintain consistency with such terms as “water content”, and air refers to the gas phase in the porous media of which a fraction is water vapor.

Matric potential, water potential, capillary pressure, and suction are terms found in the literature to describe the energy state in partially saturated porous media. In this document and the associated model, we rely on the following relation for capillary pressure (P_{cap}), vapor pressure (P_{vapor}), and water pressure (P_{water}),

$$P_{cap} = P_{vapor} - P_{water}$$

where P_{vapor} is atmospheric pressure (with a correction for vapor pressure lowering discussed in Section 1.5.3) and P_{water} is used to solve the liquid volume flux (**q**) equation as:

$$\mathbf{q} = -(kR/\mu)\ \mathrm{grad}(P_{water} - \rho\mathbf{g})$$

where k is the permeability, R is the relative permeability, μ is viscosity, ρ is liquid density, and **g** represents the acceleration due to gravity. The data cited later are given in terms of water potential or matric potential, which corresponds to the P_{water} term. The magnitude of atmospheric pressure is quite low (0.1 MPa) compared to the measured water pressures (less than –1.0 MPa) and modeled root-zone capillary pressures (4.0-8.0 MPa), so that the capillary pressures discussed are approximately equal to the negative of the reported water pressures.

1.3 Background

Several previous studies have produced data, conceptual models, and flux interpretations for the system under investigation. REECo (1994) describes the development and data collection in three deep pilot wells surrounding the Area 5 RWMS. These wells, UE5-PW-1, UE5-PW-2, and UE5-PW-3, are referred to in other reports and from here on as PW-1, PW-2, and PW-3 (Figure 1). REECo (1994) provides parameter estimates of soil-water retention and unsaturated hydraulic conductivity relationships for multiple samples at varying depths in each well. The relationships are based upon the van Genuchten- Mualem formulations for these properties in unsaturated porous media (Mualem, 1976, van Genuchten, 1980). They also provide tables of chloride mass measured in core and cuttings, $^{36}Cl/^{35}Cl$ measurements, oxygen and hydrogen stable isotope ratio measurements, water potential measurements, porosity, and bulk density with depth in the wells. Young et al. (2002) report on a new set of material property data from the upper 32 m of Area 5, measured directly on samples from PW-1 and the Science Trench (ST) boreholes ST-1 and ST-2 (Figure 1). Whereas previous methods involved estimating unsaturated hydraulic conductivities from soil water retention relationships (Mualem, 1976; van Genuchten, 1980), this data set was developed by measuring the unsaturated hydraulic conductivities directly using an Unsaturated Flow Apparatus (UFA). The material property fits have quite different van Genuchten (1980) empirical fitting parameters than those estimated by REECo (1994) (see Table 1 through Table 4). However, the new parameters lead to very similar characteristic curves within the water content ranges of interest for this study and help support the conclusions of the modeling. The REECo (1994) and the Young et al. (2002) data sets are used to parameterize the model in the present study and are discussed later in this report.

Tyler et al. (1996) discuss the role of paleoclimate in recharge and describes the use of chloride, chlorine-36, and stable isotopes in assessment of historic vadose-zone flow, using data from PW-1, PW-2, and PW-3. Key conclusions Tyler et al. (1996) make that form the basis for future conceptual models of Area 5 vadose-zone flow (e.g. Shott et al. 1998, Young et al. 2002, and the present study) are that:

- Deep vadose-zone data can be used to interpret paleohydrologic behavior
- Infiltration at PW-1, PW-2, and PW-3 likely occurred during past pluvial climates and is not occurring under present conditions. Pluvial climates most likely developed prior to full glacial maximum conditions approximately 20 and 120 ka.
- The most recent pluvial period (20 ka) may not have been sufficient to induce deep infiltration everywhere and recharge to the water table is not widespread.
- Surface geomorphology influences areas of infiltration during pluvial climates.

Tyler et al. (1996) discuss distinct double bulges in chloride data in PW-1 and PW-3 and apply a simple analytical model to estimate infiltration rates during the most recent pluvial period. They do not seek to explain the processes controlling the shape of the first chloride bulge in all three wells. Also, their discussion of soil-water age based on chloride accumulation in the three wells provides valuable insight for the predictive modeling discussed later in this report.

Tyler et al. (1999) apply the stable-isotope decay-length method of Barnes and Allison (1983) to estimate upward fluxes at all of the wells shown in Figure 1. Scanlon (2000) used the same method for study sites in the Chihuahuan Desert of Texas. In both cases, the estimated upward fluxes are high. An upper bound as high as 0.2 mm/yr was estimated by Tyler et al. (1999). However, there are some assumptions associated with that method that should be examined. First, the method assumes equilibrium between downward diffusion of isotopically enriched water with upward advection of isotopically depleted water. As discussed later in this report, it is unlikely the system is in such equilibrium. Downward diffusion of dissolved chloride and isotopically enriched water appears to be in a transient state. Second, the method was originally developed for very shallow soils. The applications cited here extend the method to systems below xeric root zones. However, the analytical solution does not seek to account for that added complexity. Detailed evaluation of the decay-length method for estimating upward advection is beyond the scope of the present study. Here we note that process model estimates of upward fluxes (Shott et al., 1998; Young et al., 2002; Walvoord et al., 2002a,b; and the present study), incorporating more detailed material properties as well as plant/soil interactions are well below the analytically derived upper bound of 0.2 mm/yr.

Shott et al. (1998) develop a conceptual model delineating the movement of moisture in the vadose zone beneath the Area 5 RWMS into four regions. The upper region, zone I is characterized by upward liquid flow toward the large capillary pressure created by transpiring plants. Zone II is described by Shott et al. (1998) as being static and of variable thickness. They estimate a static zone at PW-1 between 40 and 90 meters deep. Zone III is described as existing under quasi-steady state conditions, being dominated by gravity drainage or vertical downward flow, conditions reached a considerable time after the end of a much wetter past climatic period. Finally, Zone IV is characterized as the lowest portion of the vadose-zone, where the hydraulic potential is near zero. Shott et al. (1998) consider both liquid and vapor flow. However, they disregard vapor flow, suggesting the thermal-driven vapor flow would only be significant in the top meter and that pressure gradients are insufficient for isothermal vapor flow. Contrary to the estimates by Tyler et al. (1999), Shott et al. (1998) argue that upward fluxes are very small and can be ignored in PA calculations. Shott et al. (1998) also conducted transient liquid-phase flow simulations to assess the potential for episodic rainfall to infiltrate below the root zone. A key conclusion of that study is that the maximum depth of infiltration during a 14-year simulation was less than 0.5 m. An additional conclusion addressed in greater detail here is that the potential for diffusion of solutes in the upper zone is eliminated due to the dry conditions.

Young et al. (2002) extend upon the conceptual model of Shott et al. (1998), seeking to better constrain upward liquid flux at the Area 5 site (specifically near PW-1). The report contains information on climate reconstruction and a new set of material property data from the upper

32 m of the Area 5 site, measured directly on samples from PW-1, ST-1, and ST-2 (Figure 1). The climate reconstruction provides temperature and precipitation variations for 8 intervals with period lengths ranging from 500 to 5000 years extending back 24 ky. Their numerical model, similar to that of Walvoord et al. (2000a) described below, prescribes a boundary condition in the root zone that effectively sets a very large capillary pressure and removes water flowing to that node in the model. Thus, no infiltration penetrates below the root-zone node during the entire 24 ky sequence and the large capillary pressure provides an upward pressure gradient. Although multiple sensitivity runs were conducted accounting for uncertainty in the climate variations over the past 24 ky, the simulated water velocities, capillary pressures, and water saturations are virtually identical in all runs, due to the control exerted by the root-zone boundary condition node. Upward liquid velocities estimated by Young et al. (2002) for the PW-1/ST-1 vicinity range from 0.0 to 0.05 mm/yr, with the largest flux occurring about 4 m below ground surface.

Walvoord et al. (2002a,b) develop the deep arid system hydrodynamics (DASH) conceptual model and generate fully coupled numerical simulations of time-dependent chloride transport in the PW wells. The conceptual model of Walvoord et al. (2002a,b) provides the basis for most of the simulations presented herein, and is described in more detail in Section 1.4. Walvoord et al. (2002b) modeled chloride transport at PW-1, PW-2, and PW-3 with a multiphase flow and transport model in the presence of a geothermal gradient and a high root-zone capillary pressure. A key result of the paper with respect to the chloride data is that the variation in measured core chloride between the three wells is fit reasonably well by varying the magnitude and timing of the pluvial flux. The flow and transport model of Walvoord et al. (2002a,b) assumed homogeneous properties, based upon arithmetic averages for material properties for the three PW wells and utilized high thermal gradient estimates. Although not vital to the conclusions of their paper, estimates of liquid and vapor fluxes in the current analysis are improved using more detailed material property analyses, more reasonable thermal gradients, and incorporating uncertainty in root-zone capillary pressure and extent and date of the recent pluvial period. Thus in this work, we revisit the chloride modeling of Walvoord et al. (2002b), building on their conceptual model to better define flux in the subsurface at the Area 5 RWMS.

1.4 Conceptual Model

The deep arid system hydrodynamics model (DASH) is based upon the conceptual model and its implementation as a numerical model described by Walvoord et al. (2002a,b). The model links vegetation changes that occurred during the last climate change to the driving function for current liquid and vapor fluxes in the system. Also part of the model, although less important to net liquid and vapor flux, are the nonisothermal conditions that exist between ground surface and the water table. A key component of this conceptual model is that the transition to a warmer and drier climate and replacement of mesic vegetation with xeric (desert) vegetation induced the development and maintenance of very large capillary pressures in the root zone. The root-zone capillary pressure during this dry period is large enough that episodic infiltration events are damped in the shallow subsurface and do not penetrate to the deeper vadose-zone flow regime. Andraski (1997) supports this conceptual model, showing constant damping of water content, temperature, and capillary pressure fluctuations with depth to the base of the roots in the shallow vadose zone over a 5-year period that included a fairly wet El Niño climate.

Figure 2 provides a schematic of the conceptual model, showing the flow direction reversal that occurred due to the vegetation shift associated with climate change after the last pluvial period. Figure 3 shows the transport processes under present day climatic conditions. One of the key uncertainties affecting predictions of liquid and vapor fluxes is when the last pluvial period occurred. Data sets for vadose-zone chloride, water pressure, and stable isotopes from the Area 5 site are used here to build the conceptual model and later to serve as simulation targets for the process model.

1.4.1 Chloride Profiles

The chloride profiles from PW-1, PW-2, and PW-3 (Figure 4) and the chloride accumulation profiles (Figure 5) are described in detail by Tyler et al. (1996). The depths to the water table are approximately 235 m, 256 m and 270 m for the three wells, respectively. PW-1 and PW-3 are predominantly sandy from the ground surface to the water table, whereas PW-2 has relatively clay rich and gravel rich intervals at depth. For each of the three wells, high chloride concentration near the base of the root-zone indicates that downward percolation of water is not occurring under present conditions. Rather, chloride deposited at ground surface as dry or wet fallout is carried into the root zone with precipitation and deposited there as the water is then transpired to the atmosphere. Walvoord et al. (2002a) suggest that plants exclude salts from entering the roots. However, a prevalent plant in Frenchman Flat, Atriplex (saltbush), sequesters chloride in leaf-bladder cells and then releases it back to the environment when those cells rupture. The net effect, however, is that chloride is concentrated in the root-zone, just as with plants that exclude the salt.

The presence of secondary chloride bulges in PW-1 and PW-3, but not in PW-2 provide insight regarding the climate prior to the last pluvial period and the spatial variability of factors affecting infiltration. The absence of a deep secondary chloride bulge at PW-2 suggests that the last pluvial period fully flushed the vadose zone at that location. Tyler et al. (1996) note that PW-2 is located along an intersection of two alluvial fans, which may have focused overland flow and enhanced percolation rates below the root zone during the last pluvial period. Discussion of alluvial fan mechanics with John Whitney (USGS Denver, personal communication) highlight that the complex nature of drainage on these systems could easily allow sites within a few kilometers to experience quite different magnitudes of infiltration during the proposed pluvial period. Thus, PW-2 shows only elevated chloride concentrations since the last pluvial period, whereas, assuming 105 mg/m^2-yr constant deposition (Tyler et al., 1996), approximately 100 ky of chloride accumulation is present in PW-1 and PW-3 , indicating incomplete flushing during the past pluvial period. The location and shape of the secondary bulge is directly related to chloride accumulation prior to the last pluvial, strength of the last pluvial, and to a lesser degree, timing of the last pluvial. Matching the shape and location of the secondary bulge provides a simulation target in the present study.

Uncertainty regarding the timing of the most recent pluvial is addressed in several studies (c.f. Tyler et al., 1996; Walvoord et al., 2002a,b; and Walvoord et al., 2003). Tyler et al. (1996) compare multiple different records used for estimating when the last pluvial period ended, showing a range from about 10 ka to 50 ka. The more recent values are based upon glacial stage analyses and the older values are derived from analyses of the chloride accumulation (Figure 5). Whereas the PW-2 record indicates flushing about 25 ka, infiltration may not have penetrated below the root zone in PW-1 and PW-3 more recently than 50 ka. In specifying the recent pluvial period at about 13 ka, Walvoord et al. (2002b) invoke arguments and citations to local lake level increases from 14.5 to 13 ka and vegetation changes from woodland to desert scrub between 15 ka and 12 ka. Their modeling using that date results in reasonable matches to the chloride data for cores; they did not use the cuttings chloride data. Walvoord et al. (2003) describe uncertainty in estimating the timing of the last pluvial period, depending upon which method is used in the estimate. They note that locally, stable isotope analyses predict a range between 16 ka and 8 ka; capillary pressure analyses predict 32 ka (and longer); chloride deposition estimates predict between 16 ka and 32 ka. They also note that within these broad ranges, there is no transition time that wholly satisfies all lines of data.

The climate reconstruction of Young et al. (2002) is consistent with the chloride analysis in the present report, where the maximum time since the last period of flushing is about 25 ky, depending on local factors. Uncertainty in estimates of the time of hydraulic transition from a

pluvial period to a dry period is treated in the present study by considering both 13 ka and 26 ka for the time of its occurrence.

1.4.2 Chlorine-36 Data

In predictive simulations, the time since the last pluvial period affects estimates of present day fluxes. As discussed above, the exact timing of the last pluvial period is uncertain. Chlorine-36 data collected by REECo (1994) provide an independent indicator of the duration of recent dry climatic conditions in which percolation below the root zone has not occurred.

^{36}Cl (half-life 301,000 years) is produced via neutron activation of ^{35}Cl and spallation of K and Ca in the atmosphere and carried underground with percolating soil water. High concentrations of ^{36}Cl were added to meteoric water during a period of global fallout from atmospheric testing of nuclear devices in the 1950s and 1960s. Prior to 1950, ^{36}Cl/Cl ratios ranged between 450 and 550 x10^{-15} for approximately the past 10,000 years. However, prior to about 11 ka, ^{36}Cl/Cl ratios were higher than they are now due to geomagnetic field fluctuations (Plummer et al., 1997, Wolfsberg et al. 2000). REECo (1994, Appendix E.2) reports ^{36}Cl/Cl ratios measured in samples from PW-1, PW-2, and PW-3. Although the data are sparse, plotted in Figure 6, they show a consistent trend decreasing initially with depth in each of the three wells, and stabilizing below 30 m in PW-3 and below 40 m in PW-1 (no data are available for PW-2 below 20 m).

Two different conceptual models are considered to explain the high signals decreasing with depth in the three wells. The first involves mixing of recent bomb-pulse with pre-bomb modern water. For this conceptual model, liquid-phase water percolating below the root zone in the last 40 years would have penetrated to depths greater than 30 m, bringing some component of bomb-pulse fallout to such depths. Because the bomb-pulse fallout occurred less than 40 years prior to these measurements, diffusion is not a reasonable explanation for the downward migration. However, if advective flux carried the bomb-pulse chlorine-36 to such depths, it also would have flushed the chloride bulge observed in the upper 10 meters, putting this first conceptual model in conflict with other lines of evidence discussed in this report. Tyler et al. (1999) note that sampling in the region indicates that bomb-pulse chlorine-36 has not penetrated below about 2 m in the alluvial material.

The second conceptual model (REECo, 1994; Tyler et al., 1999) suggests that the elevated signals represent the ^{36}Cl/Cl ratios in fallout during the last period of geomagnetic fluctuations that occurred prior to 11 ka. Consistent with other measurements at the NTS, the bomb-pulse signal would be only in the upper few meters (e.g. Fabryka-Martin et al., 1998; Tyler et al., 1999), and thus was not found by REECo (1994) at the depths sampled. We extend upon this interpretation and consider why the signals stabilize below 40 and 30 m, respectively, in PW-1 and PW-3. With a half-life of 301,000 years, radioactive decay alone cannot explain the decrease from 800 to 500x 10^{-15} in the ^{36}Cl/Cl ratios in PW-1. However geomagnetic fluctuations resulting in decreases in the fallout signal and mixing with much older (dead or decayed with respect to chlorine-36) porewater during the last pluvial period are possible explanations. Fabryka-Martin et al. (1997, Figure 3-2) show the reconstructed atmospheric ^{36}Cl/Cl ratio may have varied between 2 and 1.5 times the present (pre-bomb) ratios, with the minimum occurring about 25 ka. Tyler et al. (1999) show a similar plot with the ^{36}Cl/Cl ratio in atmospheric fallout 25 ka only slightly greater than the modern signal, whereas it was nearly two times as great as 15 ka. Thus, if the last pluvial flushing the system was about 25 ka (discussed in Section 1.4.1), then the ratios measured at depth in PW-1 and PW-2 may represent the fallout during that time period. A single sample ratio of 184 x 10^{-15} in PW-1 is explained by Tyler et al. (1999) as likely due to measurement error. It could also be that the sample represents a small isolated zone that never experienced downward flow in the last several hundred thousand years. With this conceptual model, the highest values in the shallow vadose zone reflect the peak fallout ratio of about

1000×10^{-15} 15-24 ka. In conjunction with the other lines of evidence indicating no recent downward flow below the root zone, bomb-pulse chlorine-36 in only the upper two meters of alluvium, and up to 30 ky of chloride accumulation in the upper 20 m, this second conceptual model provides a compelling independent complement.

1.4.3 Capillary Pressure

Capillary pressures measured by REECo (1994) are shown in Figure 7 for boreholes PW-1, PW-2, and PW-3. The two methods used by REECo (1994) for measuring capillary pressure, FP (a filter paper technique) and CX-2 (a water activity meter), are valid at high and low capillary pressure, respectively. Thus, the data are used qualitatively in the present study. These profiles have been considered by Shott et al. (1998), Walvoord et al. (2002b), and Young et al. (2002) in development of the large capillary-pressure root-zone conceptual model. The curves exhibit the exponential character representative of transient response to a step change in capillary pressure in the root zone at the end of the last pluvial period due to vegetation shifts (Walvoord et al. 2002b).

1.4.4 Stable Isotopes

Because they are a component of the water molecule itself, the stable isotopes of hydrogen (D and H) and oxygen (^{16}O and ^{18}O) are good tracers of water movement (REECo, 1994; Tyler et al., 1996, 1999). Unlike chloride, which serves as a tracer for liquid-phase water only, these stable isotopes trace water movement in both the liquid and vapor phases. Further, due to the mass differences between $H_2{}^{16}O$, $HD^{16}O$, and $H_2{}^{18}O$ water molecules, measurements of these stable isotopes provide insight into evaporation and condensation processes in this nonisothermal multiphase system. Stable isotope data are reported as ratios in delta notation as

$$\delta^{18}O = 1000 \times \frac{\left[\left(\frac{^{18}O}{^{16}O}(\text{sample}) - \frac{^{18}O}{^{16}O}(\text{standard}) \right] \right.}{\frac{^{18}O}{^{16}O}(\text{standard})}$$

$$\delta D = 1000 \times \frac{\left[\left(\frac{D}{H}(\text{sample}) - \frac{D}{H}(\text{standard}) \right] \right.}{\frac{D}{H}(\text{standard})}$$

where the standard ratio is the standard mean ocean water (SMOW) ratio. Tyler et al. (1996, 1999) report the stable isotope measurements in the three PW wells and several other boreholes in the vicinity of the Area 5 RWMS. These data, plotted in Figure 8 and Figure 9, show the enrichment of both oxygen and hydrogen isotopes near the surface and the depletion with depth. The shallow enriched values indicate substantial evaporation whereas the deeper, depleted values indicate a past cooler climate where liquid percolated to depth before substantial evaporation could occur. The shape of these curves indicates downward diffusive mass transport of the enriched signal. Assuming liquid and vapor fluxes are upward just below the root zone, the net diffusive mass transport downward must therefore be stronger than the advective mass transport upward. Whereas these data describe a system with a downward concentration gradient because the soil water is most enriched in stable isotopes near the surface, upward concentration gradients would exist for contaminants emplaced at depth.

These data, described in greater detail by Tyler et al. (1996), are used in this study to evaluate the DASH model formulation for vapor diffusion and fractionation between liquid and vapor species.

There are several features in the stable isotope profiles that warrant consideration with regard to this project. These are discussed in greater detail by Tyler et al. (1996) and are summarized here.

- PW-2 shows significant variations in δD and $\delta^{18}O$ at about 50 m, 150 m, and 225 m. With a chloride age date in the entire profile of less than 35 ky, variations in the input signal would not be entirely damped out due to diffusion. Thus variations in the stable isotope signal penetrating below the root zone prior to and during the last major pluvial period are preserved somewhat in the depth profile.
- PW-1 and PW-3 show only modest variations in δD and $\delta^{18}O$ below 100 m depth. The chloride age dates for these deep liquids approaches 100 ky. Small time-scale variations would not be preserved over this time frame due to diffusion. The variations at about 250 m in both wells, however, implies a fairly long-time variation that occurred under higher recharge rates long before the PW-2 profile flushed completely.

For the purposes of this project, we do not seek to reconstruct the stable isotope input function to the deep vadose zone for the past 100 ky or more. Such an effort would be valuable, but would require more detailed climate reconstruction than has been done in past studies and linkage of the climate reconstruction to precipitation and vegetation. Because we are most interested in vapor phase diffusion, liquid-vapor partitioning, and fractionation as it might be relevant to performance assessment modeling of present-day conditions, we focus primarily on the upper, shallow portions of these profiles. The process for assigning boundary conditions is discussed in Section 3.2.3 and the model results are discussed in Section 4.3.

1.5 Modeling Approach

1.5.1 Story Board

The remainder of this report describes the modeling approach, data sets, model parameters, boundary conditions, uncertainties, and predictive results. In this section, the overall process is described. A catalog of the resultant simulations is discussed in Section 4 after the above-mentioned items have been introduced. A simple flow chart for the flow model process is shown in Figure 10 and summaries of the simulations are presented in Table 6 and Table 7. Discussion regarding material properties, variable parameters, and model assumptions are provided in the remaining sections of this report.

1.5.2 Approach

Using material property parameters compiled in other studies, one-dimensional column models are constructed to estimate vertical vadose-zone fluxes and transport processes at wells PW-1, PW-2, and PW-3. Present day fluxes are sensitive to the timing of the last pluvial period when infiltration persisted below the root zone. The chloride profiles measured in the three wells provide evidence for when the last pluvial period occurred. Therefore, coupled transient flow and transport models are advanced from approximately 100 ka, seeking to match field observations of chloride while considering uncertainty in the timing of the last pluvial period. Liquid and vapor-phase stable isotope transport is simulated with these models from the end of the last pluvial period to the present, with the goal of representing the upper portion of those profiles for which boundary conditions and initial conditions are more certain. The chloride transport models are used to estimate deep percolation rates during the last pluvial period, the timing of which is treated as an uncertain parameter in these simulations. Whereas the chloride transport simulations are used to constrain assumptions and parameters of the model that affect present day liquid and vapor fluxes, the stable isotope simulations are used to confirm the duration, or at least the range of values considered, of the present dry climate and to evaluate the diffusion model.

The material property parameters used to populate the models are obtained from previous studies in which they were either estimated or measured directly. For each well, homogeneous and heterogeneous property distributions are used in the models. For the homogeneous parameter models (also referred to as uniform property models), average values for each parameter are applied over the entire model domain. For the heterogeneous models, zones associated with specific samples are populated with the parameters measured on those samples. Table 1 through Table 4 list the properties specified for each of the different models considered in this study.

Boundary and initial conditions are required for the flow and transport components of the model. Perhaps the most important boundary condition is the fixed root-zone capillary pressure. This boundary condition is varied to examine its sensitivity on model results. Other boundary and initial conditions include the percolation rate and time of occurrence and duration of the last pluvial period, the chloride deposition rate, and the stable isotope concentrations in the shallow vadose zone.

1.5.3 FEHM Flow and Transport Code

As described in Walvoord et al. (2002a), the finite element heat and mass transfer (FEHM) computer code [Zyvoloski et al., 1997] is used for simulating unsaturated flow and transport in accordance with the DASH conceptual model. FEHM is maintained in software configuration management in accordance with the Yucca Mountain Software Quality Assurance Program. Version 2.21 was used in this study. FEHM simulates nonisothermal, multiphase, multicomponent flow in porous media. For vapor transport, FEHM incorporates 1) pressure driven vapor flux following Darcy's law and 2) diffusive vapor flux driven by vapor pressure gradients. Vapor pressure gradients can be caused by thermal variations and vapor pressure lowering at large capillary pressures. The latter has a much larger impact on vapor flux in the present system and is discussed in greater detail in Section 3.3.

The van Genuchten relative permeability function [van Genuchten, 1980] describes the relationships between permeability and saturation and between pressure and saturation. Assumptions inherent in FEHM include: (1) Darcy's Law appropriately describes the movement of liquid and vapor, (2) local thermal equilibrium between the fluid and the rock is maintained, and (3) solute transport does not affect the transfer of fluid or heat. Additional assumptions imposed in this study, but not inherent to FEHM, include (1) 1-D vertical flow adequately represents the hydrodynamics, (2) air flow is negligible, (3) chloride behaves conservatively (nonsorbing and nonreactive) and is nonvolatile, and (4) fractures, macropores, or other preferential flow paths do not affect the system. Chloride is assumed not to exit the soil through plant liquid uptake. Although saltbush does, in fact, sequester chloride in leaf bladder cells, the chloride is released when the cells rupture, thus allowing it to mix back in with the shallow surface soils, consistent with the approximation specified in the model.

The models and solution algorithms for FEHM are described in detail by Tseng and Zyvoloski [2000] and Zyvoloski et al. [1997]. In this study, one-dimensional columns are simulated with finite-element grids of variable vertical spacing. Each system considered (PW-1, PW-2, PW-3) is modeled with a 225-node, one-dimensional finite-element grid. Increased resolution (0.1 m) is applied near boundaries and coarser resolution (1.0 m) is used elsewhere. The pressures on bottom boundary nodes are fixed at atmospheric pressure to represent water table conditions.

Fixed temperatures are specified at the top and bottom boundaries establishing a heat flux through the vertical column that is fairly uniform and quite low. The air column remains static (the air pressure gradient is zero), volume changes and vapor-phase displacements induce a minor component of advective vapor flux (recall vapor refers to water vapor). Most movement of vapor is via diffusion from a vapor pressure gradient.

The boundary conditions at the top of the model are specified differently depending upon whether the time period of consideration is associated with a dry climate and xeric vegetation or with a pluvial climate and mesic vegetation. The timing of these events, discussed in Section 1.4, is summarized here. Dry climates are considered for the time period from approximately 100 ka to the most recent pluvial period, and since the end of the most recent pluvial period until the present (discussed in Section 1.4).

During the two dry periods, a constant, large capillary pressure boundary condition is specified at approximately the base of the root zone, 3 m below ground surface. Due to the large capillary pressure specified at this location in the model, water-pressure gradients cause flow toward this specific node. Water is drawn to this node from above and below and it is removed as it arrives, approximating the process of transpiration. In addition to Walvoord et al. (2002a,b), Young et al. (2002) and Scanlon et al. (2003) implement a similar root-zone boundary condition. During the two dry periods, water is applied at the top of the model at a concentration and rate appropriate to provide a chloride deposition rate of 105 mg/m^2-yr (Tyler et al., 1996). All of the water applied at the surface is subsequently removed by the large capillary pressure boundary node at 3 m depth, leaving the chloride behind at this depth. Hence, the chloride bulges develop in the root zones at all three wells.

During the pluvial period, the root-zone boundary condition is turned off, making the infiltration rate at the top node an important model parameter. During this period, the infiltration rate represents the deep infiltration that penetrates below the root zones of mesic vegetation. It is a model parameter determined to yield results that best match the secondary chloride bulges in PW-1 and PW-3, and the apparent complete flushing of any previously accumulated chloride in PW-2.

The equations governing the conservation of liquid mass, energy, and noncondensible gas mass equations are solved in a quasi-coupled formulation with the solute mass-transport equations. The transport equations use the flow rates and temperatures obtained in the heat- and mass-transfer solution at each time step. Therefore, fully coupled flow and transport (without feedback from the transport solution) is approximated by using small time steps in the simulations. Some of the unique modeling components implemented in this study include vapor pressure lowering (important in the root zone increased capillary pressures lead to reduced vapor), and moisture-dependent solute diffusion in both the vapor and liquid phases. Vapor moves predominantly via diffusion from the vapor pressure gradient. Vapor displacements induce a minor component of advective flux vapor flux. In the solute transport equations, FEHM uses a standard mathematical formulation for the solute dispersion coefficient. Moisture-dependent diffusion coefficients for liquid and vapor phase solutes, based on the Millington Quirk formulation (Jury et al., 1991) and the modified Millington Quirk formulation (Jin and Jury, 1996), are employed. Liquid-diffusion based on the Conca and Wright (1992) model are also employed.

All simulations conducted in this study use FEHM's standard pure implicit formulation for discretization of the time derivatives. Upstream weighting is used in the spatial discretization using FEHM's finite-volume formulation.

2. Data Sources

Multiple data sets are used to parameterize the model and to check its reliability. In addition to porosity, the primary material property parameters describe the constitutive relationship between hydraulic conductivity and capillary pressure. Chloride measurements provide targets with which to constrain the coupled flow and transport model. Stable isotope data are used as confirmation targets and to evaluate the vapor and liquid diffusion component of the transport model. The chloride data, capillary pressure data, and stable isotope data were presented in Section 1.4. Here the material properties used to populate the models are reviewed.

2.1 Constitutive Relationships

Relative conductivity and capillary pressure are modeled as functions of water content following the relationships developed by van Genuchten (1980). These relationships are based on measurements of moisture content at several capillary pressures and measurements or estimates of both saturated hydraulic conductivity (Ksat) and residual moisture content. Whereas REECo (1994) estimated the hydraulic conductivity-water content relationships, Young et al. (2002) measured them directly. With these measurements, the data were fit to van Genuchten's equations resulting in two fitting parameters (alpha and n) for each soil sample. Figure 11 to Figure 14 show the van Genuchten curves for hydraulic conductivity as a function of water content for measured data from REECo (1994) for boreholes PW-1, PW-2, and PW-3 as well as the new data from Young et al. (2002) for PW-1. The parameters are listed in Table 1 through Table 4. Throughout this report, the Young et al. (2002) data are often referred to as DRI and the REECo (1994) data are referred to as REECo. These figures also include an average curve for each borehole dataset that was generated by using the geometric means of Ksat and alpha, and the arithmetic means of porosity, residual water content, and n. The average curves are used in calculations of transport that assume a homogeneous soil profile. Justification for using the geometric mean for alpha and Ksat can be found in Zhang (2002). Finally, in the PW-1 and PW-3 REECo (1994) dataset, several measurements were removed from the calculation of the average curve because they have very high alpha values that are outside of accepted values from the literature (Carsel and Parrish, 1988). One explanation for the high reported alpha values is that the analysis, as performed in 1993, required subjective visual curve fitting. It is possible that the high values represent local minima in the solution space that should have been rejected. They are rejected here because the fit parameters are not physically viable.

2.2 Measured Material Properties

In addition to the van Genuchten properties derived from core samples, measurements of capillary pressure, porosity, bulk density, and in-situ moisture content are available for various samples. The parameter discussion sections below address measurement issues and utility of the data sets in the current modeling effort.

2.2.1 Porosity

Porosity ties hydraulic conductivity to a specific moisture content in the numerical model. Further, FEHM implements molecular diffusion in both the liquid and vapor phase as a function of both porosity and moisture content (see Section 3.3.1)

REECo (1994) calculated core porosities from measured dry bulk densities assuming a grain density of 2.65 g/cm^3. They also measured water-saturated porosities on samples used to estimate hydraulic conductivities. Errors due to water loss during measurement render the measured porosities unreliable (REECo, 1994). Therefore, only calculated porosities are used in this report.

In most cases, several porosity values are calculated within 1 m of each of the samples REECo (1994) used to compute hydraulic conductivity. These values are arithmetically averaged to generate a singe porosity associated with each retention curve used to compute van Genuchten fitting parameters. Then, homogeneous and heterogeneous porosity distributions are used to populate the numerical models, just as was done with the retention curve parameters (Table 1 through Table 4). The average porosities for PW-1, PW-2, and PW-3 are 40%, 37%, and 35% respectively.

2.2.2 Bulk Density

Bulk density was measured by REECo (1994) on the samples used to calculate porosity. It is also used in this study to calculate chloride mass as a function of depth.

2.2.3 Water Content

Volumetric water content measured on core samples tends to be quite low throughout the unsaturated zone with the mean volumetric water contents ranging from 7.9% in PW-3 to 10.9% in PW-2 and 12% in PW-1 (REECo, 1994). In-situ moisture content is perturbed by the air drilling process and is used in this modeling study in a qualitative manner only.

3. Predictive Model Design

3.1 Overview

Starting with constitutive relationships for material properties, boundary and initial conditions are assigned and simulations are conducted to match observations of solute concentration and, qualitatively, capillary pressure. These simulations lead to predictions of liquid and vapor fluxes. A formal calibration procedure was not implemented due to scope constraints on this project and boundary condition uncertainty for the flow and transport models. Thus an intuitive approach was taken to refine the model to provide reasonable matches with observations while generating ranges in the fluid fluxes representing system uncertainty.

The conceptual model upon which the simulations are based suggests that the system has been in a transient, drying state since the end of the last pluvial. The duration of this drying period impacts predictions of vadose-zone liquid and vapor fluxes. The root-zone capillary pressure exerted by xeric vegetation drives the upward fluid movement under current conditions. Thus, predicted fluxes should be sensitive to the specified root-zone capillary pressure. Additionally, fluxes should be somewhat sensitive material to properties in the vadose zone. Therefore, various property sets are considered in simulations at three-different locations near the Area 5 RWMS. For each property set modeled, the timing of the last pluvial period and the present day capillary pressure are varied to examine predicted flux sensitivities to those parameters. These two parameters exert the greatest influence on flux predictions. Several other parameters associated with the chloride and stable isotope simulations are held constant. These include the chloride deposition rate and the duration of the last pluvial period. For either of these, variation in advance parameter estimation studies along with the other parameters could lead to optimization in the matches between simulations and observations. The fixed and variable parameters are discussed in more detail later in this section.

3.1.1 Multiple Wells and Property Sets

Material property data from the three PW wells are used to create a variety of simulations that represent a range of possible subsurface conditions. For the purposes of generating a range of possible flux behavior in the face of uncertainty in material properties, we present simulations that incorporate both the heterogeneous properties measured for each borehole, as well as homogeneous property simulations that use the average curves shown in Figure 11 to Figure 14. For PW-1, we present simulations using both the REECo (1994) and Young et al. (2002) data sets for van Genuchten properties. Thus, we have 8 distinct material distributions based on 4 homogeneous and 4 heterogeneous material property sets. In the heterogeneous property sets, intervals are defined by the midpoint between measurement locations. This method leads to zoned heterogeneity with sharp property changes that do not capture the true spatial variability of

material properties on the meter to sub-meter scale. Nevertheless, the heterogeneous simulations demonstrate how material variability affects chloride distribution and flux in a gross manner.

3.2 Boundary and Initial Conditions

Flow and transport model boundary conditions are based either on present day measurements or on estimates from previous studies. The key boundary and initial conditions for the model are described in the next several subsections. At each of the locations representative of PW-1, PW-2, and PW-3, one-dimensional finite-element grids are constructed. The grids are of variable resolution, with higher resolution near the surface. The bottom boundary is specified with water table conditions. The upper boundary and root-zone nodes are specified according to the climate state. For the dry climates prior to and since the most recent pluvial period, high capillary pressures are specified in the root zones and water is applied at the surface, primarily as a mechanism to introduce chloride to the system. During the pluvial period, the root-zone boundary is turned off and the rate of infiltration at the top of the model is specified (determined subjectively) to best simulate the transport of pre-pluvial chloride at each well (see Section 1.5.3).

3.2.1 Root-Zone Capillary Pressure

Fluxes in the DASH model are controlled by the root-zone capillary pressure. Whereas low capillary pressure must have prevailed in past wet climates, high capillary pressure is required to prevent downward percolation as implied by the chloride data. Measurements of sap potential in creosote bush suggest that root-zone capillary pressure as high as 8 MPa could be maintained at the site (Odening et al., 1974) and we use this value as a maximum. Simulations using 4 MPa are also presented to show predictive sensitivity to this boundary condition. The double-bulge chloride data at PW-1 and PW-3 suggest that very little downward flow below the root zone occurred for a long period of time prior to the last pluvial. Furthermore, data from all three PW wells support more than 10 ky of chloride accumulation in the shallow vadose zone since the most recent pluvial flushing (Tyler et al., 1996). Thus, the simulations of all PW wells are designed to provide three periods including a dry period with high root-zone capillary pressure, then a wet pluvial period with low root-zone capillary pressures and significant downward percolation, and finally another dry, high root-zone capillary pressure period leading up to the present. The magnitude of the root-zone potential and the timing of the pluvial flushing are treated as uncertain parameters. For the purposes of this study, the duration of the pluvial is treated as a fixed value of 1 ky. Other paleoclimate studies have indicated that the most recent pluvial period was of short duration (c.f. Walvoord et al., 2002b). To a first order, the model is sensitive to the total volume of infiltration, the product of infiltration rate and pluvial duration. Our scoping studies show that halving the duration of the pluvial and doubling the infiltration rate or doubling the pluvial period and halving the infiltration rate lead to nearly identical predictions of chloride profiles and present day fluxes (in each case, the duration of the pluvial period is less than 15% of the present dry period duration). Thus, for the purposes of this study, the pluvial period duration is held fixed and the infiltration rate is varied to subjectively match the secondary bulge shape and location in the three wells.

3.2.2 Chloride Deposition Rate

Chloride loading as a function of time through the last 120 ky at Area 5 has been considered in several previous studies (e.g. Tyler et al., 1996, 1999). Our analysis uses a constant chloride deposition rate of 105 (mg/m^2-yr) as proposed by Tyler (1996). Scanlon (2000) calculates a value of 87 mg/m^2-yr for chloride deposition in the Chihuahuan desert of Texas while Phillips (1994) measured values between 75-125 mg/m^2-yr in New Mexico. Two studies, soon to be published, have begun to investigate predictive uncertainty to the chloride deposition rate since the end of

the last pluvial period (Scanlon et al., 2003 and Walvoord et al., 2003), the latter at the Amargosa Desert Research Site, near Death Valley National Monument. Refinement to the model presented herein might benefit from similar consideration in future iterations. The sensitivity of chloride accumulation in transport simulations to chloride deposition rate is linear in time. If the simulated rate is decreased by 20%, the simulated time to develop the post pluvial chloride mass must increase by 20%. As expected, Walvoord et al. (2003) show that a greater period of time is required to form a chloride bulge for low deposition rates. Within the range of uncertainty in chloride deposition rates, Walvoord et al. (2003) achieved reasonable matches to the data for post-pluvial periods of chloride accumulation between 16 and 32 ky. In the present study, although we only consider a single chloride deposition rate, we consider post-pluvial periods (the parameter affecting flux predictions) of 13 ky and 26 ky, consistent with Walvoord et al. (2003).

3.2.3 Stable Isotope Ratios

Stable isotopes of hydrogen and oxygen offer a unique tracer of water in both the liquid and vapor phase. The enriched ratios of the stable isotopes in the shallow vadose-zone result from the present dry climate and the depleted ratios at depth are indicative of cooler wetter past climates (Figure 8 and Figure 9). The extension of enriched ratios below the root zone indicates that the enriched source diffuses downward, counter to the upward liquid and vapor flow identified with the chloride transport modeling. To a first approximation, one can assume that the enriched ratios represent the warm dry climate since the end of the last pluvial and the depleted ratios are due to cooler and wetter conditions during and possibly before the past pluvial. Making that assumption, Walvoord et al. (2001, 2003) simulate present-day stable isotope profiles with the following steps:

1. Prescribe a depleted ratio throughout the entire profile as an initial condition representative of the system immediately after the most recent pluvial period during the Pleistocene. Examination of Figure 8 indicates ratios of –14 and –110 per mil for delta ^{18}O and delta D, respectively, may be reasonable.
2. Set the water table isotopic ratio boundary condition to the values chosen in step 1.
3. Set the root-zone enriched ratio boundary condition to the contemporary values measured between 2 and 3 m. Examination of Figure 9 indicates –4 and –75 per mil for delta ^{18}O and delta D, respectively, may be reasonable.
4. Simulate flow and transport with the full, non-isothermal, multiphase model to identify most reasonable duration of the recent post-pluvial warm and dry conditions.

Given the assumptions described above, this approach provides a starting point for predicting the timing of the pluvial period and evaluation of vapor diffusion models for partially saturated porous media.

Closer examination of the stable isotope profiles in Figure 8 indicates complex location-specific trends indicative of climatic and possibly hydraulic changes on time scales smaller than the single pre- and post-pluvial periods considered in the present study. Most noticeable are the “S” shaped stable isotope profiles at PW-2. At approximately 40 m below ground surface, the ratios for both stable isotopes are depleted more than 10% less than the values cited in item (1) above. At greater depths, the ratios increase substantially above the “Pleistocene” values, indicating enrichment prior to the last pluvial period. Near the water table, the ratios appear to return to those observed in other wells, indicating the influence of the current groundwater composition. The depleted ratios at 40 m are the most difficult to reconcile conceptually. They most likely indicate that the timing of infiltration that penetrated to this depth is somewhat different than at the other two wells. These ratios represent the lightest, coldest water. However, at greater depths, less depleted and even enriched ratios are observed, indicating the isotopic signal of infiltrating

water at PW-2 varied quite a bit (Recall the total chloride inventory in PW-2 indicates ages less than 35 ky). The deep enriched isotopic ratios are likely remnants of the shallow vadose-zone porewater composition just prior to the last pluvial period, not unlike the enriched signals that have developed since the last pluvial period.

The stable isotope profiles at PW-3 also deviate from the assumptions listed above. Although not as pronounced, they show an "S" shaped curve, too, with the greatest depletion at about 40 m. As with PW-2, the depleted signals likely represent variations in temperature and timing of infiltration during the last pluvial period. The depth of the isotopic ratio depletion maxima corresponds with the portion of the chloride profile associated with the last pluvial period.

PW-3 and PW-1 show minor enriched excursions at great depth. These depths are well below the secondary chloride bulges, thus indicating enrichment by some combination of surficial enrichment and/or enriched saturated-zone compositions well before the last pluvial period. Unraveling that paleoclimatic response is beyond the scope of this project and would have little impact on predictions of present day fluxes in the shallow subsurface.

In this study, we focus on the upper portions of the stable isotope profiles. The deeper portions should be examined in the context of a broader paleoclimate study. Two approaches are taken for specifying boundary and initial conditions. One approach follows steps 1 through 4 stated above, seeking a best match to all three-profiles for the same uniform initial condition and root-zone boundary conditions. The second approach considers that the amount of enrichment occurring in the shallow soils and the timing (and hence specific ratios) of Pleistocene infiltration could vary between the three locations. With this approach, the initial condition is set to match the specific well's most depleted stable isotope ratios. Thus, whereas the boundary and initial conditions for PW-1 are set as stated above, the initial condition for PW-2's stable isotopes is –16 and –128 per mil, respectively for delta ^{18}O and delta D. For PW-3, they are set at –14 and –120 per mil respectively.

3.3 Processes and Parameters

The liquid and vapor in all simulations are governed by the same basic driving forces, which include gravity-driven liquid flow, capillary pressure, and vapor pressure gradients. During the pluvial period, percolating water flows to depth under the force of gravity. During the non-pluvial periods, capillary pressure at the root zone provides a strong driving force that overcomes the force of gravity to pull liquid up from depth. Vapor pressures are lowered throughout the domain, according to the Kelvin effect, which arises from the energy balance across curved liquid surfaces causing vapor pressure to be a function of capillary pressure (Case, 1994). At a constant temperature, as capillary pressure rises, the equilibrium vapor pressure is lowered, leading to an isothermal gradient in vapor pressure that causes water vapor transport from regions of low capillary pressure toward regions of high capillary pressure (the root zone in this case). The geothermal gradient also contributes to the net water vapor pressure gradient that drives vapor toward the surface from below the root. The thermal gradient is quite small in the Area 5 wells, however, and contributes to less than 1/10 of the total calculated vapor flux.

Diffusive chemical flux in all simulations follows the formulation described in Section 3.3.1, while the advective component of liquid and vapor chemical transport is coupled to the physics of the phase flux as described above (Section 1.5.3).

3.3.1 Liquid and Vapor Diffusion Model

Liquid and vapor-phase diffusive flux of solutes is governed by concentration gradients as described by Fick's Law. In porous media, the tortuous pathways the solutes take in either of the phases effectively reduce the mass flux. Therefore, effective diffusion coefficients are needed to

reduce the mass flux by scaling the free air or free liquid diffusion coefficients for individual solutes. One model that applies for both liquid and vapor phase solutes in unsaturated is porous media is the Millington-Quirk formulation (c.f. Jury et al., 1991; page 204). This model reduces the free air diffusion coefficient as a function of volumetric air content and material porosity. Similarly, it reduces the free liquid diffusion coefficient as a function of volumetric water content and porosity. The Millington-Quirk relationships are

$$D_{effV} = a^{10/3}/\phi^2 \, D_{oV}$$

$$D_{effL} = \theta^{10/3}/\phi^2 \, D_{oL,}$$

And a modified Millington-Quirk relationship for vapor diffusion (Jin and Jury, 1996) is

$$D_{effV} = a^2/\phi^{2/3} \, D_{oV}$$

where D_{eff} is the is the effective porous media diffusion coefficient that is fit to the mass flux equation (Fick's Law) as:

$$\text{Mass flux} = -D_{eff} \, \text{grad}(C).$$

D_o is the diffusion coefficient for a species in the absence of a porous medium, (V) and (L) subscripts refer to vapor and liquid, a is the volumetric air content, θ is the volumetric water content, and ϕ is the porosity of the media. With water contents of about 10% and air contents of more than 30%, the reduction factors for liquid phase diffusion are substantially greater than for vapor diffusion. Jury et al. (1991) also show that for very dry systems such as Area 5, the Millington-Quirk model and other models converge to the same value for D_{effV}. Although most dissolved chloride transport simulations presented are computed using the Millington-Quirk formulation, we present some results using the Conca-Wright (1992) model for diffusion as a function of water content. The Conca-Wright model is a based on a large data set containing gravels, sands, and intact tuffs and was developed with measurements of electrical conductivity through solutions of NaCl and KCl. The best-fit equation to the data curve of Conca-Wright is:

$$D_{effL} = 10^{(-4.1 + 2.7*\log10(\theta) + 0.32*\log10(\theta))}$$

At low water content, the Conca-Wright model for the effective liquid diffusion coefficient can be approximately an order of magnitude higher than predicted using the Millington-Quirk model. Therefore, the Conca-Wright model is compared with the Millington-Quirk model in two dissolved chloride transport simulations discussed in Section 4.2.1.

3.3.2 Phase Partitioning and Fractionation of Stable Isotopes

To simulate D and ^{18}O transport, the isotopic water species, $H_2{}^{16}O$, $H_2{}^{18}O$ and $HD^{16}O$, are treated as separate volatile species with different mass-based diffusion coefficients and different phase partitioning according to Henry's Law. As such, both kinetic and equilibrium fractionation are enabled. $H_2{}^{18}O$ and $HD^{16}O$ constitute only trace fractions of total number of water molecules in any sample; In natural waters, the proportions of $H_2{}^{16}O$, $H_2{}^{18}O$ and $HD^{16}O$ are 1000:2:0.32 (Merlivat and Coantic, 1975) Thus, as in the reactive geochemical transport model PHREEQC (Thorstenson and Parkhurst, 2002; Parkhurst and Appelo, 1999), the equation structure in FEHM assumes the presence of only one solvent, liquid $H_2{}^{16}O$. To simulate D and ^{18}O transport, the isotopic water species, $H_2{}^{18}O$, and $HD^{16}O$, are treated as electrically neutral solutes.

The concentration of water molecules in the gas phase is approximated using Henry's law equilibrium partitioning coefficients for the dominant water molecule $H_2{}^{16}O$ (c.f. Jury et al., 1991; page 235). The molecules with the heavier trace isotopes, $H_2{}^{18}O$ and $HD^{16}O$, do not partition between the liquid and gas phases with the same equilibrium ratios as the dominant $H_2{}^{16}O$. Their concentrations in the vapor phase are estimated by converting equilibrium fractionation factors

into Henrys Law coefficients, $K^{H}_{H_2{}^{18}Og}$ and $K^{H}_{HD^{16}Og}$, similar to Thorstenson and Parkhurst (2002, Table 2.), as follows:

$$\log K^{H}_{H^{18}O_g} = \log K^{H}_{H_2{}^{16}O_g} + \log(\alpha^{^{18}O}_{H_2{}^{16}O_l - H_2{}^{16}Og})$$

$$\log K^{H}_{HDO_g} = \log K^{H}_{H_2{}^{16}O_g} + \log(\alpha^{D}_{H_2{}^{16}O_l - H_2{}^{16}Og})$$

where $K^{H}_{H_2{}^{16}Og}$ is the Henrys law constant for water and α^{i} are the equilibrium fractionation factors for ^{18}O and D. The equilibrium fractionation factors can be defined as ratios of saturation vapor pressures (Friedman & O'Neil, 1977; Merlivat and Coantic, 1975) as follows:

$$\alpha^{D}_{H_2{}^{16}O_l - H_2{}^{16}Og} = \frac{p(H_2{}^{16}O)}{p(HD^{16}O)} = 1.0850$$

$$\alpha^{^{18}O}_{H_2{}^{16}O_l - H_2{}^{16}Og} = \frac{p(H_2{}^{16}O)}{p(H_2{}^{18}O)} = 1.0098$$

Henrys law constants in FEHM are specified in units of MPa, to solve the equation

$$P_v = K^{H} X$$

where P_v is the vapor pressure of either $H_2{}^{18}O$ or $HD^{16}O$, X is their mole fraction in water, and K^{H} is the Henrys Law constant. Henrys law constants are often reported in the literature (e.g. Jury et al. 1991) in the non-dimensional form

$$K^{H}_{ND} = \frac{C_g}{C_l}$$

where C_g and C_l are gas and liquid concentrations, respectively. Converting between the two is accomplished with (Jury et al. 1991)

$$K^{H} = K^{H}_{ND}\left(\frac{RT\rho_w}{M_w}\right)F$$

Where

- R is the universal gas constant (8.206×10^{-5} atm-m^3/mol-K)
- T is degrees Kelvin (293 used here)
- ρ_w is the density of water (1×10^{6} g/m^3 used here)
- M_w is the molecular weight of water (18 g/mole)
- F converts atm to MPa (9.87 MPa/atm)

The dimensional Henrys Law constants used in this study are listed in Table 5.

Kinetic fractionation is captured in the model as a result of different vapor diffusivities for $H_2{}^{16}O$, $H_2{}^{18}O$, and $HD^{16}O$. Here, we use the measured ratios of the vapor diffusivities provided in Merlivat (1975) as listed in Table 5. Although small kinetic fractionation processes due to evaporation and diffusion in the vadose zone are captured with this model, the dominant effect associated with the stable isotope profiles is due to the enriched ratios resulting from substantial

evaporation in the shallow vadose zone. This is represented in the model through specification of root-zone stable isotope ratio boundary conditions.

4. Model Simulations

4.1 Overview

A series of simulations is conducted with the objective of matching observed chloride, capillary pressures, and stable isotope data while predicting liquid and vapor flux profiles at PW-1, PW-2, and PW-3. Table 6 provides an overview of the flow simulations used to develop the liquid and vapor flux profiles. Table 7 provides an index of the flow simulations to cross reference to the figures listed later in this report and to the companion model parameter and output tables.

4.1.1 Variable Parameters

Several model parameters are varied as part of the qualitative sensitivity analysis. For these varying parameters, their impact on liquid and vapor fluxes are examined in the results. They are listed below with a brief discussion.

- Root-zone capillary pressure: Set at 8 MPa and 4 MPa during the dry period since the last pluvial period
- Time of transition from pluvial to drying conditions: Set at 26 ka and 13 ka.
- Material properties for each borehole model: Uniform and heterogeneous material property distributions are used
- The liquid diffusion coefficient was based on either the Millington-Quirk or the Conca-Wright models for partially saturated porous media.

For the three locations there are a total of 8 different property sets. For each property set, the two different root-zone potentials and the time of the last pluvial are considered, leading to 32 liquid and vapor flux profiles for consideration. Variation in the liquid diffusion model is presented with respect to the simulated chloride profile giving 36 chloride simulation results for statistical comparison. When the liquid diffusion model is changed, the pluvial infiltration rate is changed to best match to observed chloride profiles.

4.1.2 Fixed Parameters

For all simulations, the pre-pluvial period duration is 79 ky and is a function of the assumed chloride mass loading rate (105 mg/m^2-yr). For a smaller mass-loading rate, we would require a longer pre-pluvial period to generate the mass found in the secondary chloride bulges in PW-1 and PW-3. For all simulations the pluvial period duration is 1 ky. Whereas the pluvial period duration is held constant, the infiltration rate during that period is varied to best match profiles of the secondary chloride bulges, including the absence of one in PW-2. Obviously, varying the duration of the pluvial period, as a sensitivity parameter, would impact the pluvial infiltration rate for simulations that best fit the chloride profile. However, Walvoord et al. (2002b) cite additional paleolacustrine studies supporting the assumption of a very short-duration pluvial period. During the pluvial period, large capillary pressures are not prescribed at the root-zone model node and infiltration moves downward from the surface. Post-pluvial, dry period durations of 26 ky and 13 ky are considered to reasonably sample the uncertainty in the parameters discussed previously.

Several parameters are held constant in the simulations. They are listed below with a brief discussion.

- Root-zone potential prior to the last pluvial period: This is set at 8 MPa. Variability would mostly be either damped out over time or reset during the pluvial period (at least in the upper vadose zone).
- Duration of the dry period prior to the last pluvial: This is set at 79 ky to preserve the chloride inventory in PW-1 and PW-3, using the fixed chloride deposition rate.
- Chloride deposition rate: Set at 105 mg/m^2-yr. Although uncertain, this parameter is inversely related to the amount of time required to develop the integrated post-pluvial chloride seen in the shallow subsurface of the PW wells.
- Duration of the pluvial flushing period: Although uncertain, this is set to 1000 years (after Walvoord et al., 2002b). Reduction in the duration would require increase in the pluvial flow rate, leading to the same liquid mass flow over the pluvial period and minor impacts on the predicted present-day flow rates.
- Pluvial infiltration rate: Assuming a 1000 year period, the pluvial infiltration rate is subjectively fit to match the predicted and observed location of the secondary chloride bulge. Thus, it is a unique, but fixed parameter for each simulation. It is large for PW-2 as is required to flush the entire secondary bulge from the system and smallest for PW-1, where the downward migration rate of the secondary bulge is smallest.
- Stable isotope concentrations below the root zone since the last pluvial period: Lacking a detailed process model for estimating isotopic enrichment in shallow vadose-zone material since the last pluvial, these are set to the present day measured values. Walvoord et al. (2003) note that the present isotopic composition may be more enriched than at earlier times since the last pluvial period due to warmer temperatures for the last 8 ky.
- Stable isotope concentration in the entire vadose zone immediately after the pluvial period: These too are fixed to measured values, thus missing fluctuations resulting from climate changes before and after the pluvial period.

4.2 Flow Fields Based on Chloride Simulations

The following sections present results from the numerical modeling of chloride transport. The simulations assume that chloride is a conservative tracer that moves only in the liquid phase. The three PW wells, each with distinct material properties and varied history of chloride transport allow us to create a set of simulations spanning a wide range of behavior since 106 ka. The output from these simulations provides a range of reasonable vapor and liquid fluxes that we would currently expect to find in the undisturbed subsurface near the Area 5 RWMS. The simulated results are plotted with the data in Figure 15 through Figure 22 for the different wells, property distributions, and timing of pluvial period, and boundary conditions discussed in the next section.

4.2.1 Matching Chloride Observations

Figure 5 compares cumulative chloride mass profiles in the three PW wells with simulation results assuming the pluvial period was 26 ka (referred to from here on as 26 ky after the pluvial period) and using an 8 MPa root-zone capillary pressure boundary condition. Assuming a constant chloride deposition rate of 105 mg/(m^2-yr), the length of the pre-pluvial period was adjusted to align the total mass in the PW-3 simulation with the data. PW-3 was chosen to fit the pre-pluvial period because it has the best signal throughout the borehole and also contains both the pre-pluvial and post-pluvial chloride bulges. Infiltration rates during the pluvial period

(assumed to have lasted 1 ky) were fit individually at each well to translate the pre-pluvial chloride bulge to depth. In the case of PW-2, this involved flushing it from the vadose zone. The PW-1 total chloride curve is affected by the lack of data in the shallow vadose zone (analysis of chloride measurements in ST-1 would benefit future studies). PW-2 has much less chloride in the upper 150 m, however the simulated chloride inventory with depth is similar to the data, due to the large infiltration rate prescribed during the pluvial period.

For the purpose and scope of this study, best-fit simulations for chloride in each of the three boreholes were achieved visually (and subjectively). Then common statistical methods (Boas, 1983) were used to compare visually-similar results. Future studies would benefit from quantitative parameter estimation seeking to minimize the difference between simulated and observed chloride concentrations by varying all parameters to which the results are sensitive, and minimizing the difference between observed and simulated chloride profiles.

The initial visual data matching was based on two factors. First, the location of the peak of the secondary (deep) chloride bulge was quite sensitive to the volume of liquid allowed to infiltrate during the 1 ky pluvial period (Table 8 and Table 9). Therefore, the pluvial infiltration rate was adjusted by 0.5 mm/yr increments in boreholes PW-1 and PW-3 until the best visual match was achieved. In borehole PW-2, infiltration was increased until the pre-pluvial chloride was pushed below a depth of 150 m.

The visual match of mass and depth of chloride within the post-pluvial, primary bulge was used to check the goodness of fit. Because of the chloride profile shape in the upper 30 m in PW-1, and in considering the other citations for a less recent pluvial period discussed in Section 1.4, we considered a 26 ky post-pluvial duration in addition to the 13 ky period evaluated by Walvoord et al. (2002b). Consideration of the other paleoclimate records described by Tyler et al. (1996) and Walvoord et al. (2003) supports this extension. Additionally, the shape of the upper 50 m of the PW-3 chloride profile led us to explore the Conca-Wright diffusion model as a way to simulate more chloride mass transport to depth.

Figure 15 to Figure 18 show that for PW-1, the simulated chloride profile at 26 ky post-pluvial period matches the data better than at 13 ky post-pluvial. The visual match is confirmed by the statistics shown in Table 8, where the RMS error for 26 ky is consistently lower than for 13 ky for the PW-1 simulations run with the Millington-Quirk diffusion model. In addition to a lower RMS error, the 26 ky simulations also have lower variance. Of the PW-1 simulations, the best fit is found in the homogeneous REECo simulation using the MQ diffusion model (RMS is 23 and the variance is 353.6).

For the PW-2 simulations using Millington-Quirk (Figure 19 and Figure 20), the statistics show that a 13 ky post-pluvial period has a lower RMS than a 26 ky post pluvial period. However, the mean residual (data minus model) results for PW-2 show that the best-fit post-pluvial duration is between 13 ky and 26 ky, because the mean residual is positive at 13 ky and negative for the 26 ky simulations. For example, a simulation for which the pluvial was 20 ka yields a mean residual of only 4.8 and an RMS (29.9), which is less than either the 13 ky or 26 ky simulations. Although the global minimum best fit has not been found, the model results suggest that the pluvial period was likely between 13 and 26 ka.

Simulation results for PW-3 using the Millington-Quirk diffusion model (Figure 21 and Figure 22) are less conclusive. In the homogeneous case, the lowest RMS error is found with a 26 ky post-pluvial period, while the heterogeneous simulation has a lower RMS for the 13 ky simulation. In either case, the match to the data is poor in the upper 50 m of the domain as indicated by the high variance for these simulations. One explanation is that the process model is under-predicting diffusive mass flux. Therefore, the Conca-Wright (1992) diffusion model was implemented to reevaluate the PW-3 chloride profile; results for the homogeneous case are shown in Figure 21. Because the new diffusion model affects the shape and position of the deep chloride

bulge, the pluvial infiltration rate was adjusted to from 9 to 7 mm/yr (Table 8). With the higher diffusion predicted by the Conca-Wright model, chloride transport simulations match the data much better. At 26 ky post-pluvial the RMS error is reduced from 35.1 to 21.1, and the variance drops significantly from 1231 to 447. The Conca-Wright model was also run on the PW-1 homogeneous case, with decidedly different results. The pluvial infiltration rate was adjusted to 2mm/yr to achieve a reasonable visual fit to the deep chloride bulge; the resulting chloride profile is shown in Figure 21.The higher diffusion of the Conca-Wright model leads to smearing of the deep front and a less definitive shape to the chloride bulge around 45 m. The statistics show that the 13 ky simulation has an RMS error of 23.7 compared to 29.8 for the 26 ky simulation. Furthermore, the variance of both 13 ky and 26 ky is much higher than the MQ simulation at 26 ky. Thus we are left with one set of simulations supporting the MQ diffusion model (PW-1) while the simulations for PW-3 support the Conca-Wright diffusion model. Although the chloride transport simulations are sensitive to the diffusion model, the effect on flux is minimal. For example, the simulations in PW-1 and PW-3 modified for the Conca-Wright diffusion model lead to vapor and liquid flux results that are within 1% of those achieved with the base, MQ diffusion model (Section 4.2.3).

Another possible explanation for the chloride profile at PW-3 is that substantial chloride from the shallow vadose zone was only partially transported to greater depth during the pluvial flushing period (Tyler et al., 1996). Conceptually, this type of behavior is explained with a dual-porosity model, in which solutes can diffuse into immobile porewater, or porewater can imbibe into low permeability zones. The result of such processes is the apparent retardation of solutes relative to the percolating liquid velocity. This may explain the elevated chloride values between 20 and 50 m depth in PW-3, however further investigation would be required to substantiate this hypothesis.

4.2.2 Water Pressure

Figure 23 to Figure 26 show the simulated water pressures (negative of capillary pressures) versus the data for the three PW boreholes. Two methods (FP and CX-2) were used for collection of the data (REECo, 1994), but these methods were not used consistently at each measurement point. As described previously, the filter paper method (FP) is more appropriate at lower capillary pressure while the CX-2 method is more appropriate at higher capillary pressure. The data do, however, support the use of a high capillary-pressure root-zone boundary (4-8 MPa). Also of interest is the fact that only the simulations using the Young et al. (2002) van Genuchten property set are able to maintain capillary pressure of 0.5 MPa below 50 m depth. This is of particular note because the data indicate that the capillary pressure does not drop as quickly as the simulations using the REECo (1994) data would suggest. However, as seen in the following section, the resulting fluxes of liquid and vapor are very low for all the simulations regardless of which van Genuchten data set was used.

4.2.3 Resultant Liquid and Vapor Fluxes

Figure 27 to Figure 34 show the liquid and vapor volume fluxes generated for all simulations considering pluvial periods at 13 ka and 26 ka, and with root-zone capillary pressure of 4 MPa and 8 MPa. Volume flux (volume per area time) is often called Darcy flux or Darcy velocity. Multiplying the vapor flux by the ratio of vapor phase density to liquid phase density (1.2/1000) converts vapor flux to equivalent liquid flux. Thus, in the simulations, the vapor flux is actually 833 times the reported liquid equivalent. To convert these values to the true pore velocity in the unsaturated zone, one must divide by the phase content (air content or water content). In the 30 m below the root zone, water content in the simulations is typically around 8-12%, while air content is about 28 to 32%. Thus the true velocity of the liquid phase is approximately 10× the

reported volume flux, while the true velocity of the water vapor is on the order of 2500× the reported liquid equivalent flux (833×3). Flux toward the surface is positive while flux toward the water table is negative.

In all cases, the upward volume flux of liquid toward the root zone is less than 0.025 mm/yr while the maximum upward volume flux of vapor (as liquid equivalent) is always less than 0.035 mm/yr.

The maximum liquid flux toward the surface is seen in the heterogeneous PW-3 simulation with an 8 MPa root pressure and a 13 ky post-pluvial period at depth of approximately 10 m (Figure 28). The exact depth of the maximum flux is related to the depth of the root-zone boundary condition, specified in these simulations at 3 m below these ground surface. Thus, shifting the depth of the root-zone boundary condition (by a meter or two) in the model would lead to associated shifts in resultant flux profiles. The maximum upward liquid flux generated in any simulation depends on the complex interaction between hydraulic conductivity, water content, and capillary pressure. Although a given simulation may have a high capillary gradient, if the liquid saturation is low, the resulting flux will be low if the van Genuchten relationship yields a very low hydraulic conductivity. The fact that the region below the root zone is drying in response to the capillary pressure of the root-zone is the main reason the estimated liquid fluxes at 26 ky post-pluvial are lower than at 13 ky post pluvial. The maximum upward vapor flux toward the root zone is also seen in the heterogeneous PW-3 simulation with an 8 MPa root zone at 13 ky post-pluvial in the region immediately below the root zone (Figure 32). Maximum upward vapor flux is controlled by the magnitude of the water vapor pressure gradient. In the FEHM simulations, the vapor pressure of water is mainly controlled by the vapor pressure lowering relationship, with only a minor component of the vapor pressure gradient contributed by the temperature gradient. The vapor pressure lowering relationship is based on the fact that water vapor pressure at high capillary pressure is much lower than water vapor pressure at low capillary pressure. Therefore, water vapor will diffuse from areas of low capillary pressure to areas of high capillary pressure. In these simulations, the highest capillary pressure is at the root zone, and high capillary pressure propagates below the root with the drying front in the post-pluvial period. Initially, when the drying front is located near the root zone, the water vapor gradient is high because of the short distance between the wet and dry sediments, however as time passes and the dry region below the root zone expands, the gradient is reduced and the vapor flux decreases. This behavior explains the reduction in vapor flux from 13 ky to 26 ky post-pluvial. As expected, the vapor flux for the 4 MPa root is lower (0.024 mm/yr) than the 8 MPa root (0.032 mm/yr) because the water vapor pressure in the 4 MPa root zone is higher than in the 8 MPa root zone. Vapor pressure lowering is non-linear so the flux is not reduced by a factor of two.

Figure 35 through Figure 38 show liquid and vapor flux as a function of time at the root zone and 5 m below the root zone for the 8 MPa root simulations. In all cases, the liquid and vapor fluxes appear to asymptotically approach a steady value. At 5 m below the root zone, the PW-1 simulation using data from REECo (1994) adjusts more rapidly to the post-pluvial change in root-zone capillary pressure than the simulation of PW-1 using the Young (2002) van Genuchten properties. Simulations of PW-3 show that for the heterogeneous case, changes in liquid flux at 5 m below the root zone take up to 20 ky to approach equilibrium with the root-zone capillary pressure.

4.3 Stable Isotopes

Stable isotope transport in the vadose-zone is simulated from the end of the last pluvial period to the present. In these simulations, a uniform ratio for the oxygen and hydrogen isotopes is prescribed over the entire column at the end of the last pluvial period and an enriched ratio is prescribed at the ground surface (see Section 3.2.3). Coupled liquid and vapor flow and transport

are then simulated. For each well, uniform and heterogeneous material properties were considered, including both the REECo (1994) and Young et al. (2002) property sets for PW-1.

All simulations focus primarily on the upper portion of the stable isotope profiles. As discussed previously, enrichment below the shallow depleted signals (in PW-2 and PW-3) indicates climate change variations prior to the last pluvial period, for which consistent local reconstruction has not been adequately reported in the literature. However, the upper portions of the profiles (above about 60 m deep) represent the depletion due to cool Pleistocene infiltration during the last pluvial period and then enrichment in the very shallow vadose zone associated with the recent period of warmth and drying. It is important to note, however, that the isotopic enrichment in shallow soils is due to evaporation during warm climatic conditions, the duration of which may not perfectly coincide with the duration of the post-pluvial period; cool conditions may have persisted for some time after the climate changed to dryer conditions. Thus, in simulating the propagation of enriched isotopic ratios downward, we are really considering the time since the climate warmed causing such enrichment.

Enriched stable-isotope ratios are prescribed at the base of the root zone and depleted ratios are set as the initial condition over the entire depth of the profiles. The transient flow fields described previously for dissolved chloride transport simulations are used for these stable isotope transport simulations. Simulations were conducted varying a) the duration of the present dry (warm) period since the end of the last pluvial period and b) the diffusion model. Resolving the duration of the present dry period could be used to weight the flux profiles presented previously for dry periods of 26 ky and 13 ky. Resolving the appropriate diffusion model (vapor and liquid) could be used to condition the diffusive flux component in the PA model. The results in this section show that it may be most appropriate to consider post-pluvial period durations between 13 and 26 ky. However, if the Conca-Wright liquid diffusion model and the modified Millington-Quirk vapor diffusion can be shown to be most appropriate for these material properties, then a 13 ky post-pluvial period (or at least period since warmer conditions caused substantial enrichment in shallow soils) is most likely when considering the stable isotope profiles.

These simulations do not generally seek to represent the complex profile shapes in PW-2 and PW-3 below the first stable isotope depletion minima (between 60 and 75 m deep). To do so, simulations would have to represent climatic variations prior to the last pluvial period for which more and less enrichment occurred in the shallow vadose zone and in the groundwater. Thus, the results for PW-2 and PW-3 do not match the deeper profiles well. However, one set of scoping simulations were conducted in which the initial conditions were set at the isotopic depletion minima over the entire column, but then as the root-zone isotopic ratios were enriched for post-pluvial conditions, so were the groundwater isotopic ratios. Although these simulations do not lead to excellent matches to the data, they do highlight the influence from both the surface and the groundwater on stable isotope profiles in the vadose zone.

Stable isotope transport simulations were conducted for all flow fields described in the previous sections. The only parameters that caused variations were the duration of the post-pluvial warm period and the form of the diffusion model. Results for homogeneous and heterogeneous material properties were nearly identical. Thus, only results that show predictive variations are shown in the following sections.

4.3.1 PW-1 Simulations

An initial simulation compares simulated stable oxygen isotope profiles using different diffusion model formulations and different durations of the post-pluvial warm dry period at PW-1 (Figure 39). For the same material properties (Young et al., 2002) and a fixed post-pluvial root-zone capillary pressure of 8 MPa, the results show that using the Millington-Quirk (MQ) model for both liquid and vapor leads to the least downward diffusive flux and the modified Millington-

Quirk (mMQ) vapor diffusion model coupled with the Conca-Wright (CW) liquid diffusion model leads to the greatest diffusive flux of the enriched stable isotopes. Comparing the model simulations with the data highlights a feature in the PW-1 data indicative of a boundary change more recently than the beginning of warming after the last pluvial period. It appears that the enriched ratios in the shallow vadose zone may have decreased in the last 5 to 10 ky, contrary to indications of even warmer temperatures during this most recent period (e.g. Kaufman, 2003). Such "kinks" in the data are not observed in PW-2 or PW-3 profiles where more detailed shallow vadose-zone data are also available. Thus we focus on the portion of the curve representative of changes that occurred closer to the time of major climate transition. The more diffusive combination of models (mMQ-CW) match the profiles better for a 13 ky post-pluvial warm period and the least diffusive models (MQ-MQ) match the data better for a 26 ky post-pluvial warm period.

Simulations of the PW-1 stable isotope profiles are shown in Figure 40 and Figure 41 for REECo (1994) and Young et al. (2002) properties using different vapor and liquid diffusion models. `The combinations considered are Millington-Quirk for both liquid and vapor (MQ-MQ) and Conca-Wright for liquid and modified Millington-Quirk for vapor (CW-mMQ). In each case, simulated profiles are shown for 10, 13, and 26 ky after the climate warmed and dried, creating the enriched upper boundary condition. For the least diffusive model formulation (MQ-MQ), the best fits to the upper portions of the profiles indicate that the warming began as long ago as 26 ky. However, the most diffusive model formulation (CW-mMQ) provides a better fit to the data if the shift to warmer conditions were 10 to 13 ka. Note, however, that even if the enrichment required to form the upper boundary condition ratios for these simulations occurred 13 ka, that does not directly mean that the pluvial infiltration period ended then. It only means that the climate warmed enough to cause such evaporative enrichment of the stable isotopes in the shallow vadose zone.

4.3.2 PW-2 Simulations

Starting with the same upper isotopic ratio boundary conditions used for PW-1 and the flow fields developed to best match the chloride in PW-2, Figure 42 and Figure 43 show model results for PW-2 for different vapor and liquid diffusion models combinations 10, 13, and 26 ky after the last pluvial period. The initial isotopic ratio specified at the end of the pluvial throughout the entire column and the lower isotopic ratio boundary condition were set to the most depleted ratios measured in PW-2 (between 35 and 70 m). Unlike the PW-1 results, warm, dry periods of 26 ky lead to over prediction of the enriched front's downward migration for all diffusion models considered. Also, the enrichment bulges below 50 m are clearly not captured in the simulations. Those represent climatic variation prior to the last pluvial period not captured in this model. However, to examine the effect within the vadose-zone profile of isotopic ratio changes at both the surface and the water, a scoping calculation was performed in which the initial condition following the last pluvial period was set as the most depleted isotopic ratios, but the water table boundary was then set to present day isotopic ratios measured in the groundwater. The results, shown in Figure 43 show the influence of saturated zone isotopic composition on vadose-zone profiles. Matching the enriched bulges below 50 m would require additional information climate variations prior to the last pluvial to enable more accurate specification of boundary and initial conditions. For example, it is highly unlikely that the depleted ratios observed between 35 and 75 m represent the conditions of the entire column at the end of the last pluvial period. Thus the results present here focus primarily on matching the portions of the profiles representative of the period since the last pluvial period.

4.3.3 PW-3 Simulations

As with PW-2, simulations of 26 ky post pluvial warm, dry periods over predict the downward migration of the enriched stable isotope fronts, regardless of which diffusion model combination is used at PW-3 (Figure 44). However, the CW-mMQ combination over predicts the enriched front migration for warm dry periods as short as 10 ky. Thus, at this location, if the enriched isotopic ratios have existed in the shallow vadose zone for at least 10 ky (regardless of exactly when the pluvial deep infiltration occurred), the MQ-MQ diffusion model combination would appear to provide more accurate results. It is notable that the chloride data at this location were matched much better with the CW liquid diffusion model (Figure 21). However, the gas diffusion model, not the liquid diffusion model, dominates the enriched stable isotope front migration. Thus, the indications here are that MQ may be somewhat more accurate than mMQ, or that climatic variations affecting boundary conditions are not resolved in great enough detail in this model.

Also similar to PW-2, the stable isotope profiles at PW-3 show enriched isotopic bulges at depth, peaking at about 200 m. This depth is much greater than the secondary chloride bulge at PW-3 (Figure 21), indicating a climatic temperature change well before the last pluvial period that may have affected both shallow vadose-zone and saturated-zone isotopic compositions. A simple scoping calculation was performed in which the saturated zone delta D was increased to present day conditions after the depleted initial condition was specified over the entire column at the end of the pluvial period (Figure 45). The results show that changes in the saturated zone have an impact on the vadose-zone profile, but that more detailed climate and water composition changes over up to the past 100 ky might be needed. As stated above, the primary objective here was to study the upper portion of the stable isotope profiles representative of the period since the last pluvial period.

5. Summary

Two important conclusions for performance assessment (PA) modeling can be drawn from the present study. The first is that present-day liquid and vapor fluxes in the shallow vadose-zone near the Area 5 RWMS are estimated to be upward, but of very small magnitude. The fluxes are so small that liquid-phase chloride and isotopically enriched water vapor diffuse in the opposite direction due to downward concentration gradients. The second conclusion is that the liquid and vapor diffusion models considered, which correct free-vapor and free-liquid diffusion coefficients for tortuosity in partially saturated porous media, provide reasonable bounds with the more diffusive Conca-Wright (liquid) and modified Millington Quirk (vapor) models leading to better matches to field observations in some cases whereas the less diffusive Millington Quirk (liquid and vapor) models lead to better fits in other cases. Given other uncertainties associated with chloride deposition rates, past timing of climate changes, and governing processes, this study suggests that PA models should consider both the more- and less-diffusive combinations of liquid and vapor models to bound process model uncertainty.

The process model development and implementation for this project involved constructing a multiphase, nonisothermal, vadose-zone flow and transport simulator with FEHM to implement the DASH conceptual model. Models at three different locations, PW-1, PW-2, and PW-3 were populated with material property parameters derived from previous field investigations and analyses of material from these wells. Boundary and initial conditions were determined from previous studies and from contemporary conditions derived from field observations.

The approach for each well was to simulate, for each property set, a three-period system consisting of the dry pre-pluvial period lasting 79 ky, the pluvial period of 1000-year duration and the dry post-pluvial period of 13 or 26 ky. Thus, the total simulation time is either 93 ky or

106 ky, depending upon the duration of the present, post pluvial period. The primary objective of this process was to capture the cumulative chloride distribution in the wells and to reproduce the shape of the chloride profiles, thus constraining model uncertainty. Uncertainty in pluvial infiltration rates, duration of the dry post-pluvial period, and post-pluvial root-zone capillary pressure lead to a set of 32 simulations, each yielding a unique liquid and vapor flux profile (Figure 27 to Figure 34). The liquid and vapor flux profiles vary with depth, location, material properties, time since period of pluvial infiltration, and root-zone capillary pressure. In all cases, upward liquid fluxes vary between 0.0 and 0.02 mm/yr, with the transition between upward and downward flux occurring at depths between 20 and 70 m. The maximum upward liquid flux tends to occur between depths of 5 and 20 m, depending upon the simulation conditions. The base of the root zone was specified as 3 m in all simulations. Shifting that value by a meter or two would lead to similar shifts in the simulated flux profiles. Location and property variations lead to differences of up to a factor of 4 (peak flux). Simulations for which the pluvial infiltration period was 13 ka yield present day fluxes about twice as large as those predicted if the pluvial infiltration period was 26 ka. Varying the root-zone capillary pressure between 8 MPa or 4 MPa has less impact on predicted fluxes than material property variations or time of last pluvial period. Vapor-phase fluxes are always upward, with marked increases occurring above depths of 10 to 30 m, depending on simulation conditions. Below those depths, upward vapor fluxes are on the order of 0.0025 mm/yr. Above those depths, vapor fluxes increase to as high as 0.03 mm/yr. Variations in the shapes of the vapor flux profiles depend on the same factors listed above for the liquid flux profiles. Peak upward vapor fluxes occur just below the root zone and vary, for the same boundary conditions, by about a factor two, depending upon location and material properties. Simulations for which the pluvial infiltration period was 13 ka yield present day vapor fluxes about twice as large as those predicted if the pluvial infiltration period was 26 ka. As with the liquid flux profiles, root-zone capillary pressure variations had the smallest impact on predicted flux profiles.

The simulations that yielded the best matches with the chloride data were then re-simulated with the transport of oxygen and hydrogen stable isotopes. These simulations focus on the evolution of the stable isotope profiles during the warm, dry climate since the last pluvial period. Thus, the simulations are primarily compared with the upper portions of the stable isotope profiles representing the most recent climatic changes. Variations at great depth in the stable isotope indicate complex climatic variations prior to the last pluvial period, for which reconstruction is beyond the scope of this project.

Simulated stable isotope profiles are sensitive to the duration of the post-pluvial warm, dry period and to the form of the diffusion models (primarily vapor). Reasonable matches to the data can be achieved by varying either of these components of the model within their ranges of uncertainty. For the more diffusive model configuration, the duration of the post-pluvial warm, dry period would need to be around 10 to 13 ky. For the less diffusive model configuration, the warm, dry period could have been as long as 26 ky. These results lead to the recommendation at the beginning of this section. Reduction in uncertainty regarding either the most accurate diffusion model formulation or the post-pluvial warm, dry period would lead to refinement of the recommendation.

The current performance assessment model for the Area 5 RWMS does not simulate liquid or vapor fluxes. Thus, this study provides a set of flux-with-depth profiles the performance assessment model can draw upon. The performance assessment model does simulate solute diffusion. This study suggests PA consideration of two liquid diffusion and two gas diffusion model formulations for partially saturated porous media.

6. References

Andraski, B. J., Soil-water movement under natural-site and waste-site conditions: A multiple-year field study in the Mojave Desert, Nevada, Water Resour. Res., 33, 1901– 1916, 1997.

Barnes, C. J., and G. B. Allison, The distribution of deuterium and oxygen-18 in dry soils, I, Theory, J. Hydrol., 60, 141–156, 1983.

Boas, M.L., Mathematical Methods in the Physical Sciences, second edition, Wiley and Sons, NY, 1983.

Carsel, R.F. and R.S. Parrish., Developing joint probability distributions of soil-water retention characteristics, Water Resour. Res., 24(5), 755-769, 1988.

Case, C.M., Physical Principals of Flow in Unsaturated Porous Media, Clarendon Press, Oxford, 1994.

Conca, J.L., and J. Wright, Flow and Diffusion of Unsaturated Gravel, Soils, and Whole Rock, Applied Hydrogeology, International Association of Hydrologists, Vol. 1, 5-25, 1992.

Fabryka-Martin, J.T., A.L. Flint, D.S. Sweetkind, A.V. Wolfsberg, S.S. Levy, G.J.C. Roemer, J.L. Roach, L.E. Wolfsberg, and M.C. Duff, Evaluation of flow and transport models of Yucca Mountain, based on chlorine-36 studies for FY97, Los Alamos National Laboratory, Yucca Mountain Project Milestone Report SP2224M3, 1997.

Fabryka-Martin, J.T; A.V. Wolfsberg; S.S. Levy; K. Campbell, P. Tseng, J.L. Roach, and L.E. Wolfsberg, Evaluation of flow and transport models of Yucca Mountain, based on chlorine-36 and chloride studies for FY98, Milestone Report SP33DDM4, Los Alamos National Laboratory, Los Alamos, NM, 1998.

Jin, Y. and W.A. Jury., Characterizing the Dependence of Gas Diffusion Coefficient on Soil Properties, Soil Sci. Soc. Am. J., 60: 66-71, 1996.

Jury, W.A., W.R. Gardner, and W.A. Gardner, Soil Physics, Wiley and Sons, NY, 1991.

Kaufman, D., Amino acid paleothermometry of Quaternary ostracodes from the Bonneville Basin, Utah, Quat. Sci. Rev. 22:899-914, 2003.

Merlivat, L. Molecular diffusivities of H216O, HD16O, H218O in gases, J. Chem. Phys, 69, 2864-2871, 1978.

Merlivat L., and M. Coantic, Study of mass transfer at the air-water interface by an isotopic method, J. Geophys. Res., 80, 3455-3464, 1975.

Mualem, Y., A new model for predicting the hydraulic conductivity of unsaturated porous media, Water Resour. Res. 12:513-522, 1976.

Odening, W.R., B.R. Strain, and W.C. Oechel, The effect of decreasing water potential on net CO2 exchange of intact desert shrubs, Ecology, 55, 1086-1095, 1974.

Parkhurst, D.L., and C.A.J. Appelo, User's guide to PHREEQC (version 2)--A computer program for speciation, batch-reaction, one-dimensional transport, and inverse geochemical calculations, U.S. Geological Survey Water-Resources Investigations Report 99-4259, 312 p., 1999.

Phillips, F. M., Environmental tracers for water movement in desert soils of the American southwest, Soil Sci. Soc. Am. J., 58, 15-24, 1994.

Plummer, M.A., Phillips, F.M., Fabryka-Martin, J.T., Turin, H.J., Wigand, P.E., and Sharma, P., Chlorine-36 in fossil rat urine: an archive of cosmogenic nuclide deposition during the past 40,000 years, Science, 277: 538-541, 1997.

Reynolds Electrical and Engineering Company, Inc. (REECo), Site characterization and monitoring data from area 5 pilot wells, Nevada Test Site, Nye County, Nevada, Contract. Rep. DOE/NV/11432-74, Nev. Oper. Off., U. S. Dep. of Energy, Las Vegas, 1994.

Scanlon, B.R., Uncertainties in estimating water fluxes and residence times using environmental tracers in an arid unsaturated zone, Water Resour. Res. 36:395-409, 2000.

Scanlon, B.R., K. Keese, R.C. Reedy, J. Simunek, and B.J. Andraski, Variations in flow and transport in thick desert vadose zones in response to paleoclimatic forcing (0–90 kyr): field measurements, modeling, and uncertainties, Water Resour. Res., In Press, 2003.

Shott, G.J, L.E. Barker, S.E. Rawlinson, M.J. Sully, and B.A. Moore, Performance assessment for the Area 5 Radioactive Waste Management Site at the Nevada Test Site, Nye County, Nevada, Revision 2.1. DOE/NV/11718-176. 1998.

Smiles, D.E., W.R. Gardner, and R.K. Schulz, Diffusion of tritium in arid disposal sites, Water Resour. Res. 31(6), 395-409, 1995.

Thorstenson, D.C. and D.L. Parkhurst. Calculation of individual isotope equilibrium constants from implementation in geochemical models, U.S. Geological Survey WRIR 02-4172, Denver Colorado, 2002.

Tyler, S.W., J.B. Chapman, S.H. Conrad, D.P. Hammermeister, D.O. Blout, J.J. Miller, M.J. Sully, and J.M. Ginanni, Soil-water flux in the southern Great Basin, United States: Temporal and spatial variations over the last 120,000 years, Water Resour. Res., 32, 1481-1499, 1996.

Tyler, S., J. Chapman, C. Cooper. Estimates of evaporation at the Area 5 Radioactive Waste Management Site, Nevada Test Site: Evaluation of estimates based on stable isotopes and comparisons to other methods. Desert Research Institute, Publication No. 45169. DOE/NV/11508-46, 1999.

Tseng, P.H. and G.A. Zyvoloski, A reduced degree of freedom method for simulating non-isothermal multi-phase flow in a porous medium, Adv. Water Res., 23(7), 731-745, 2000.

van Genuchten, M.Th. A closed-form equation for predicting the hydraulic conductivity of unsaturated soils, Soil Sci. Soc. Am. J. 44:892- 898, 1980.

Walvoord, M. A., F. M. Phillips, and A. V. Wolfsberg. Deuterium, Oxygen-18 and Chlorine-37 Stable Isotope Profiles as Clues Into the Recharge Histories of Desert Vadose Zones, abstract Eos Trans. AGU, 82(47), Fall Meet. Suppl., Abstract H41G-08, 2001

Walvoord, M. A., M. A. Plummer, F. M. Phillips, and A. V. Wolfsberg, Deep arid system hydrodynamics 1: Equilibrium states and response times in thick desert vadose zones, Water Resour. Res., 38, 15pp. 2002a.

Walvoord, M. A., F. M. Phillips, S. W. Tyler, P. C. Hartsough, Deep arid system hydrodynamics 2: Application to paleohydrologic reconstruction using vadose-zone profiles from the northern Mojave Desert, Water Resour. Res., 38, 12 pp., 2002b.

Walvoord, M.A., D.A. Stonestrom, B. J. Andraski, and R.G. Streigl. Constraining the paleohydrologic evolution of a deep unsaturated zone in the Amargosa Desert, submitted to Vadose Zone Journal, 2003.

Wang, J.H., Robinson, C.V., and Edelman, I.S., Self-diffusion and structure of liquid water III. Measurements of the self-diffusion of liquid water with H2, 3H3, and O18 as tracers, J. Amer. Chem. Soc, 75, 466-470, 1953.

Wolfsberg, A.V., K. Campbell, and J.T. Fabryka-Martin. Use of chlorine-36 data to evaluate fracture flow and transport models at Yucca Mountain, Nevada, Geophysical Monograph: Dynamics of Fluids in Fractured Rocks, 349-362, American Geophysical Union, Washington D.C., 2000.

Young, M., C. Cooper, S. Sharpe, J. Miller, and D. Schafer, Upward advection: Dynamic simulation of vadose zone moisture flux, unpublished draft DRI report submitted to U.S. Department of Energy, Nevada Site Office, Las Vegas, May, 2002.

Zhang, D., Stochastic Methods for Flow in Porous Media: Coping with Uncertainties, pp. 350, Academic Press, San Diego, 2002.

Zyvoloski, G. A., B. A. Robinson, Z. V. Dash, and L. L. Trease, Summary of the models and methods for the FEHM application – A finite-element heat-and mass-transfer code, Los Alamos National Laboratory Report LA-13307-MS, Los Alamos, NM, 1997.

This Page Intentionally Left Blank

7. Tables

Table 1. PW-1 Hydrogeologic Data (REECo, 1994)

Depth(m)	Ksat (cm/s)	Residual Water Content	alpha (1/cm)	n	porosity
14.6304	1.10E-03	8.6	0.0211	1.73	0.43
17.9832	6.20E-04	6.7	0.0237	1.53	0.43
23.7744	2.30E-03	8.3	0.0305	1.77	0.49
39.3192	2.20E-03	2	0.0939	1.21	0.43
48.4632	7.70E-04	6.3	0.0376	1.42	0.37
54.5592	2.90E-03	3.9	0.1038	1.28	0.34
78.9432	4.40E-03	4.8	0.0899	1.33	0.39
91.44	5.40E-04	4.7	0.0957	1.27	0.34
109.728	9.80E-05	9.1	0.0197	1.44	0.35
121.92	1.50E-03	7.8	0.0494	1.68	0.36
140.208	6.50E-04	8.8	0.0146	1.55	0.36
152.0952	3.30E-03	10.8	0.0246	1.43	0.42
164.8968	5.50E-04	9.2	0.016	1.71	0.42
177.0888	4.90E-04	6.8	0.0241	1.61	0.38
188.6712	1.00E-03	8.4	0.0295	1.63	0.38
201.168	5.80E-03	7.3	0.028	1.58	0.51
213.36	2.40E-03	6.4	0.0213	1.77	0.43
225.552	3.00E-03	6.5	0.0382	1.82	0.34
231.648	2.90E-03	7.3	0.0344	1.78	0.39
Homog	1.32E-03	7	0.0343	1.54	0.4

Table 2. PW-1 Hydrogeologic Data (Young et al., 2002)

Begin Depth (m)	End Depth (m)	Avg. Depth (m)	Ksat (cm/s)	Residual Water Content	alpha (1/cm)	n	Porosity
0	2.75	1.375	0.23	0.215	0.0764	1.22	0.43
2.75	6.5	4.625	1.2	0.798	0.3528	1.25	0.42
6.5	9.75	8.125	1	0.792	0.2744	1.23	0.44
9.75	11.5	10.625	0.2	4.84	0.147	1.28	0.44
11.5	12.5	12	0.48	1.998	0.1274	1.21	0.37
12.5	15.75	14.125	0.18	6.615	0.1372	1.26	0.35
15.75	19	17.375	0.02	6.342	0.0431	1.31	0.42
19	24.25	21.625	0.09	6.29	0.0853	1.34	0.37
24.25	29.75	27	0.01	7.622	0.0392	1.41	0.37
29.75	29.75	29.75	0.31	3.588	0.1666	1.29	0.46
Homog	NA	NA	0.175	3.91	0.116	1.28	0.407

Table 3. PW-2 Hydrogeologic Data (REECo, 1994)

Depth(m)	Ksat cm/s	Residual Water Content	alpha (1/cm)	n	porosity
0.3	5.20E-04	5.4	0.0185	1.4	0.38
0.9	3.00E-05	3.6	0.018	1.25	0.37
9.1	5.30E-05	4.8	0.0209	1.33	0.36
9.4	8.50E-05	10.5	0.032	1.34	0.33
12.2	1.10E-04	7.4	0.0204	1.4	0.365
12.5	1.40E-04	3.8	0.0226	1.32	0.32
21.0	1.70E-04	6.1	0.0191	1.39	0.365
30.5	5.30E-04	4.9	0.0603	1.29	0.375
36.3	1.10E-04	8.8	0.0116	1.5	0.385
39.3	1.00E-04	3.8	0.0187	1.31	0.355
61.0	1.30E-04	6.8	0.014	1.39	0.415
76.2	4.00E-03	9	0.0344	1.97	0.445
94.8	2.10E-05	1.1	0.0134	1.21	0.34
152.1	7.50E-04	7.1	0.0141	1.73	0.45
219.2	1.20E-04	0.01	0.0249	1.2	0.32
249.0	2.30E-03	0.01	0.0199	1.2	0.415
Homog	1.88E-04	5.195	0.0207	1.38	0.37

Table 4. PW-3 Hydrogeologic Data (REECo, 1994)

Depth(m)	Ksat cm/s	Residual Water Content	alpha (1/cm)	n	porosity
0.3048	7.20E-04	3.1	0.0103	1.47	0.38
0.9144	3.20E-04	3.2	0.0107	1.48	0.36
15.5448	3.20E-04	4.1	0.0115	1.38	0.34
15.8496	5.60E-05	4.9	0.0114	1.43	0.34
30.7848	6.00E-05	8.6	0.0153	1.37	0.32
39.624	4.40E-04	7.2	0.045	1.48	0.33
152.4	2.40E-03	3	0.0383	1.3	0.32
167.64	1.10E-03	4.7	0.0275	1.38	0.39
Homog	3.60E-04	4.85	0.0179	1.41	0.35

Table 5. Stable Isotope Parameters Used in Simulations

	$H_2{}^{16}O$	$H_2{}^{18}O$	$HD^{16}O$
Equilibrium Fractionation Factor[1]	1	1.0098	1.0850
Henrys Law Constant (MPa)	2.332E-03	2.309E-03	2.149E-03
Free Water Diffusivity (m^2/s)[2,3]	2.26E-09	2.26E-09	2.23E-09
Free Vapor Diffusivity (m^2/s)[2,4]	2.57E-05	2.50E-05	2.51E-05

1 - Merlivat and Coantic (1975)
2 - $H_2{}^{16}O$ diffusivity from Smiles et al. (1995)
3 - calculated from measurements provided in Wang et al.(1953)
4 - $H_2{}^{18}O$ and HDO from Merlivat (1978)

Table 6. Model simulation structure

	PW1	PW2	PW3	Fixed Parameters	Variable Parameters
	4 material sets REECo_hom REECo_het DRI_hom DRI_het	2 material sets REECo_hom REECo_het	2 material sets REECo_hom REECo_het		
Pre-pluvial	↓	↓	↓	Duration 79 ky Root zone = 8MPa	
Pluvial	↓	↓	↓	Duration = 1 ky	Infiltration (best) (mm/yr) PW1_REECo = 3.0 PW1_DRI = 3.5 PW2 = 30.0 PW3 = 9.0
Post-pluvial	↓	↓	↓		Root-zone potential 4 MPa or 8 MPa Duration 13 ky or 26 ky

Table 7. Simulation Index

Identifier (on some figures, only part of the identifier is used)	Borehole	Root Pressure	Pluvial infiltration	Van Genuchten Property set
PW1_REECo_8MPa_homog	PW-1	8 MPa	3 mm/yr	REECo (1994) homogeneous
PW1_REECo_8MPa_heter	PW-1	8 MPa	3 mm/yr	REECo (1994) heterogeneous
PW1_REECo_4MPa_homog	PW-1	4 MPa	3 mm/yr	REECo (1994) homogeneous
PW1_REECo_4MPa_heter	PW-1	4 MPa	3 mm/yr	REECo (1994) heterogeneous
PW1_DRI_8MPa_homog	PW-1	8 MPa	3.5 mm/yr	Young et al. (2002) homogeneous
PW1_DRI_8MPa_heter	PW-1	8 MPa	3.5 mm/yr	Young et al. (2002) heterogeneous
PW1_DRI_4MPa_homog	PW-1	4 MPa	3.5 mm/yr	Young et al. (2002) homogeneous
PW1_DRI_4MPa_heter	PW-1	4 MPa	3.5 mm/yr	Young et al. (2002) heterogeneous
PW2_REECo_8MPa_homog	PW-2	8 MPa	30 mm/yr	REECo (1994) homogeneous
PW2_REECo_8MPa_heter	PW-2	8 MPa	30 mm/yr	REECo (1994) heterogeneous
PW2_REECo_4MPa_homog	PW-2	4 MPa	30 mm/yr	REECo (1994) homogeneous
PW2_REECo_4MPa_heter	PW-2	4 MPa	30 mm/yr	REECo (1994) heterogeneous
PW3_REECo_8MPa_homog	PW-3	8 MPa	9 mm/yr	REECo (1994) homogeneous
PW3_REECo_8MPa_heter	PW-3	8 MPa	9 mm/yr	REECo (1994) heterogeneous
PW3_REECo_4MPa_homog	PW-3	4 MPa	9 mm/yr	REECo (1994) homogeneous
PW3_REECo_4MPa_heter	PW-3	4 MPa	9 mm/yr	REECo (1994) heterogeneous

Table 8. Statistics comparing chloride transport simulations with data for 8 MPa root-zone capillary pressure during post pluvial period.

Well	Property Set	Data Source	Diffusion Model	Post Pluvial (ky)	Pluvial Infiltration Rate (mm)	Root Mean Square of Difference	Mean	Variance
PW1	heter	REECo	MQ	13	3	38.65	-16.06	1236.03
PW1	heter	REECo	MQ	26	3	32.3	-18.53	699.9
PW1	heter	DRI	MQ	13	3.5	28.48	-9.53	720.34
PW1	heter	DRI	MQ	26	3.5	26.37	-9.23	610.32
PW1	homog	REECo	MQ	13	3	27.2	-10.76	626.25
PW1	homog	REECo	MQ	26	3	23	-13.3	353.6
PW1	homog	DRI	MQ	13	3.5	26.16	-10.55	572.87
PW1	homog	DRI	MQ	26	3.5	23.78	-11.47	433.95
PW1	homog	REECo	Conca	13	2	23.7	-3.39	549.95
PW1	homog	REECo	Conca	26	2	29.79	-7.75	827.17
PW2	heter	REECo	MQ	13	30	31.37	15.73	736.39
PW2	heter	REECo	MQ	26	30	37.26	-6.64	1344.38
PW2	homog	REECo	MQ	13	30	31.72	16.57	731.66
PW2	homog	REECo	MQ	26	30	38.12	-5.48	1423.41
PW3	heter	REECo	MQ	13	9	33.57	4.81	1104.07
PW3	heter	REECo	MQ	26	9	38.61	-0.85	1490.25
PW3	homog	REECo	MQ	13	9	36.11	5.78	1270.2
PW3	homog	REECo	MQ	26	9	35.11	1.21	1231.32
PW3	homog	REECo	Conca	13	7	28.75	3.92	811.4
PW3	homog	REECo	Conca	26	7	21.19	-0.99	447.87

REECO - REECo (1994)

DRI - Young et al. (2002)

MQ - Millington Quirk Diffusion Model

Conca - Conca and Wright Diffusion Model

Table 9. Statistics comparing chloride transport simulations with data for 4 MPa root-zone capillary pressure during post pluvial period.

Well	Property Set	Data Source	Diffusion Model	Post Pluvial (ky)	Pluvial Infiltration Rate (mm)	Root Mean Square of Difference	Mean	Variance
PW1	heter	REECo	MQ	13	3	38.92	-16.4	1246.13
PW1	heter	REECo	MQ	26	3	31.96	-18.54	677.83
PW1	heter	DRI	MQ	13	3.5	28.57	-10.03	715.76
PW1	heter	DRI	MQ	26	3.5	24.92	-9.86	523.55
PW1	homog	REECo	MQ	13	3	27.4	-11.15	626.29
PW1	homog	DRI	MQ	26	3	22.65	-13.57	328.91
PW1	homog	DRI	MQ	13	3.5	27.08	-11.06	611.08
PW1	homog	REECo	MQ	26	3.5	23.95	-12.33	421.46
PW2	heter	REECo	MQ	13	30	31.92	15.65	774.16
PW2	heter	REECo	MQ	26	30	33.61	-6.76	1084.1
PW2	homog	REECo	MQ	13	30	32.11	16.44	760.43
PW2	homog	REECo	MQ	26	30	35.43	-5.74	1222.03
PW3	heter	REECo	MQ	13	9	32.7	4.81	1045.97
PW3	heter	REECo	MQ	26	9	36.06	-0.85	1299.9
PW3	homog	REECo	MQ	13	9	32.95	4.28	1067.11
PW3	homog	REECo	MQ	26	9	30.34	-0.87	919.5

REECO - REECo (1994)

DRI - Young et al. (2002)

MQ - Millington Quirk Diffusion Model

8. Figures

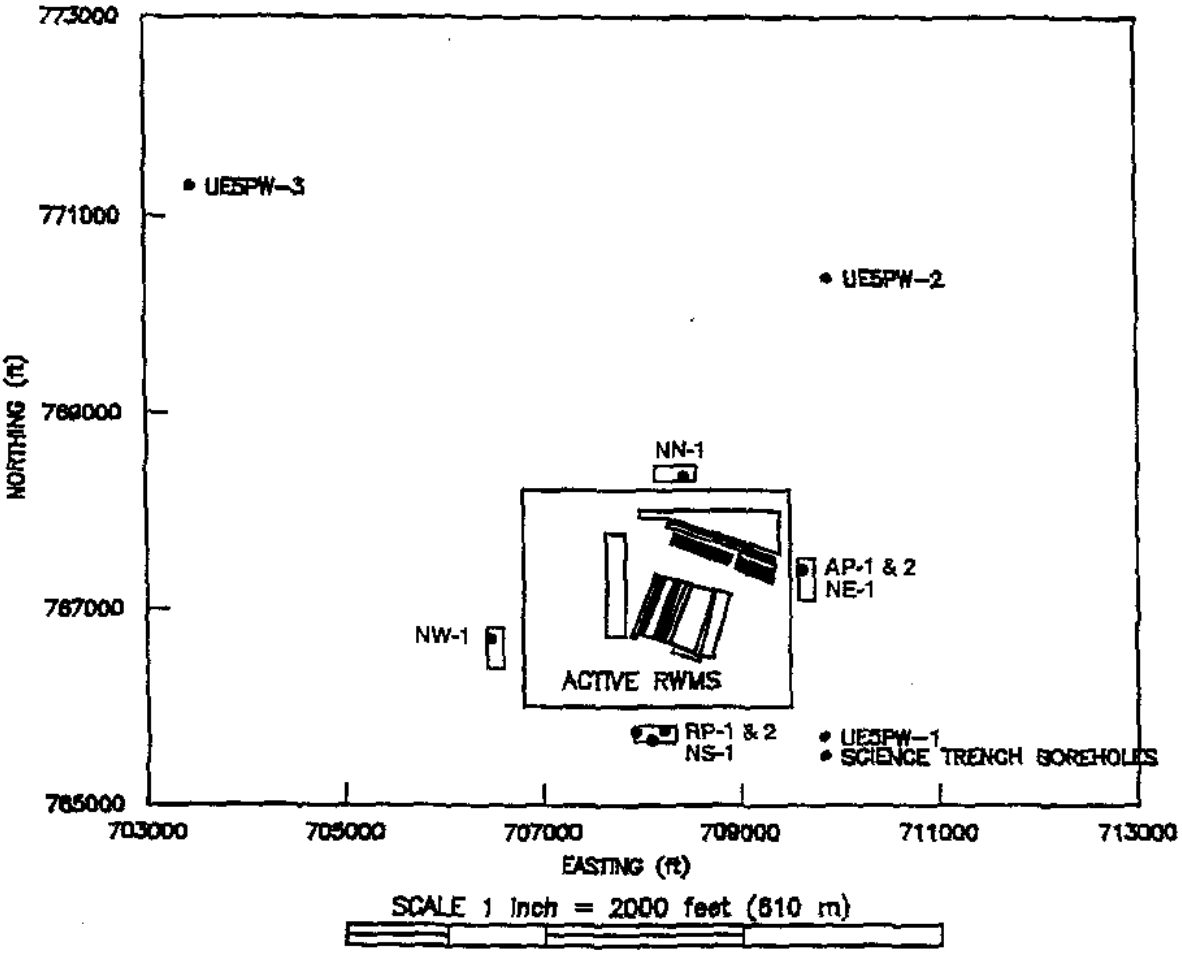

Figure 1. Area 5 RWMS and borehole locations (From Tyler et al. 1999)

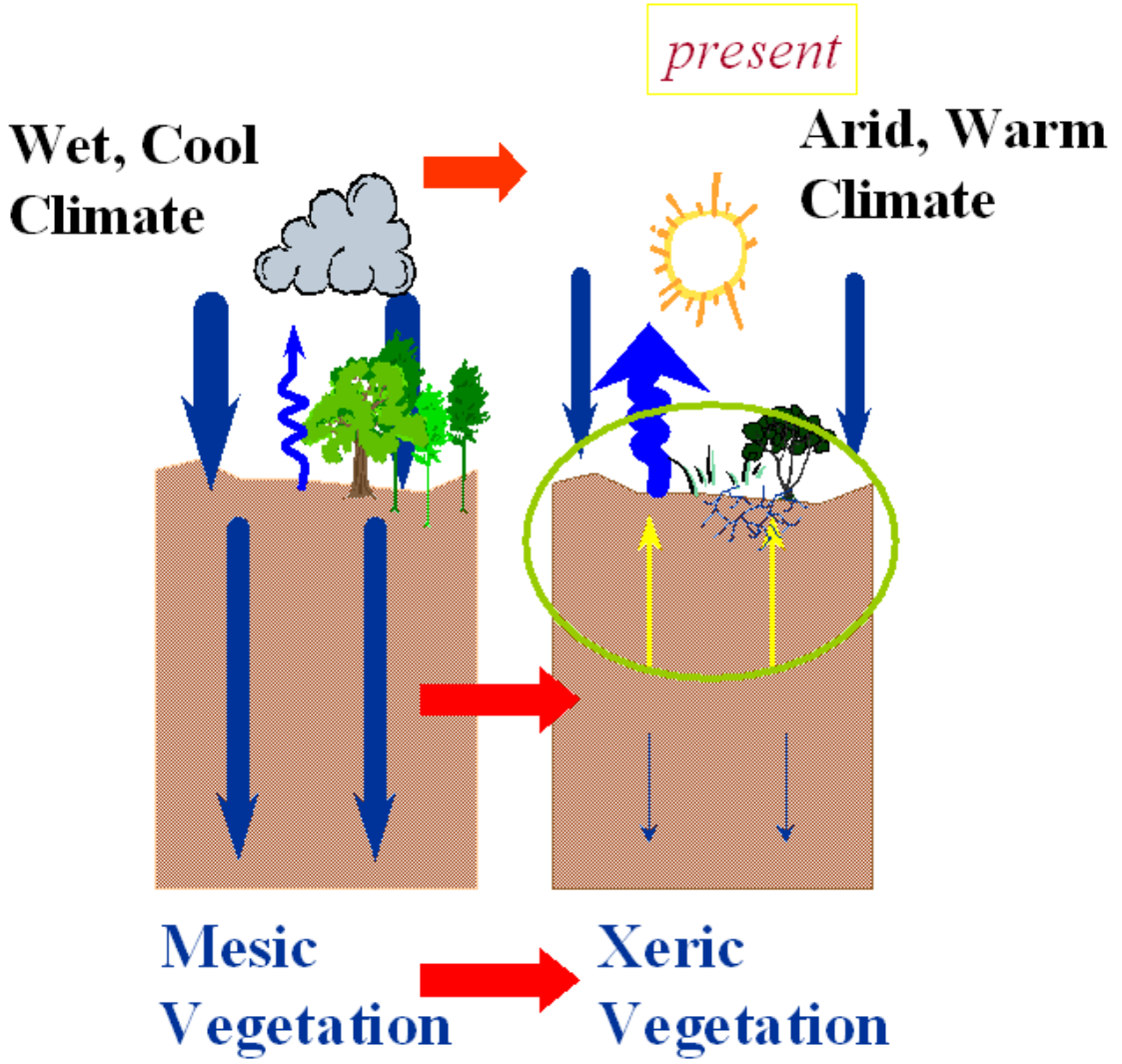

Figure 2. Deep Arid System Hydrodynamics (DASH) conceptual model (From Walvoord et al., 2001). During the transition from a wet, cool climate during the past pluvial period to current dry conditions, large capillary pressures are established in the xeric vegetation root zone, inducing strong upward gradients.

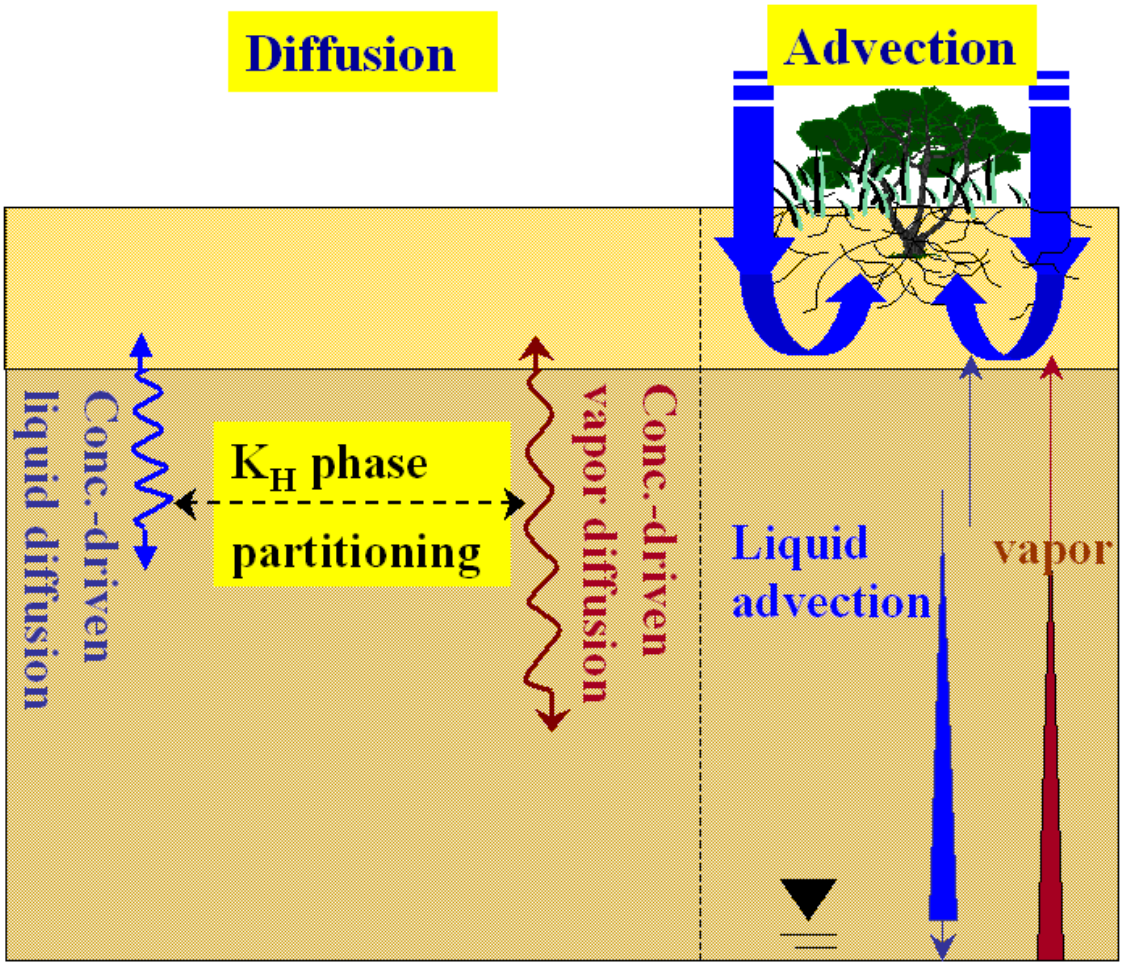

Figure 3. Present climate advective and diffusive solute fluxes in the DASH model (modified from Walvoord et al., 2001 to show upward as well as downward diffusive flux), which are dependent upon the location and direction of the concentration gradient.

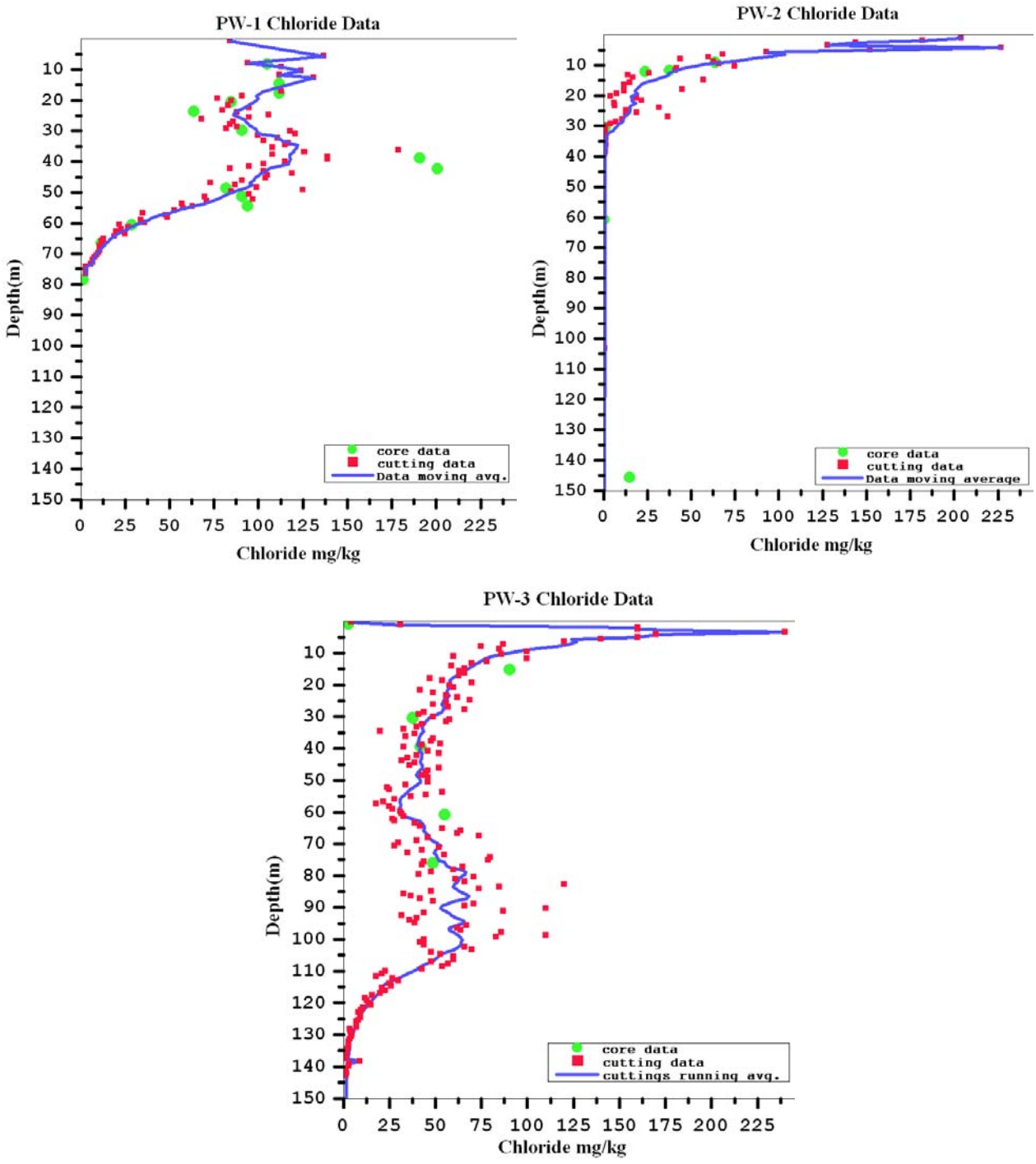

Figure 4. Chloride data measured in core and cuttings in PW-1, PW-2, and PW-3. Blue lines show a moving average of the data.

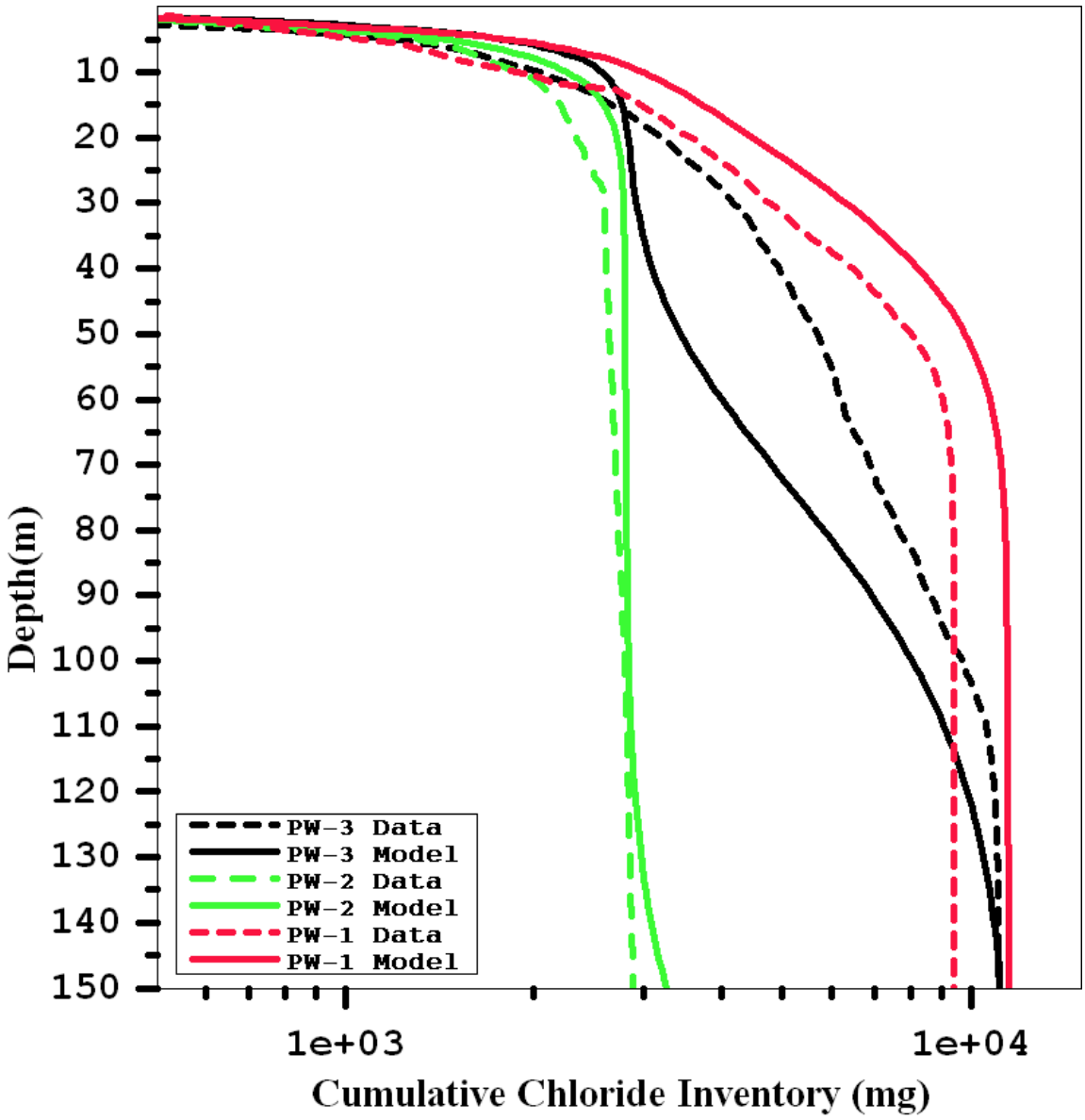

Figure 5. Total chloride inventory - comparing simulations (model) and measurements from cuttings (data). Simulations represent 105 mg/m^2-yr chloride deposition, 8 MPa root-zone capillary pressure and 26 ky since last pluvial period.

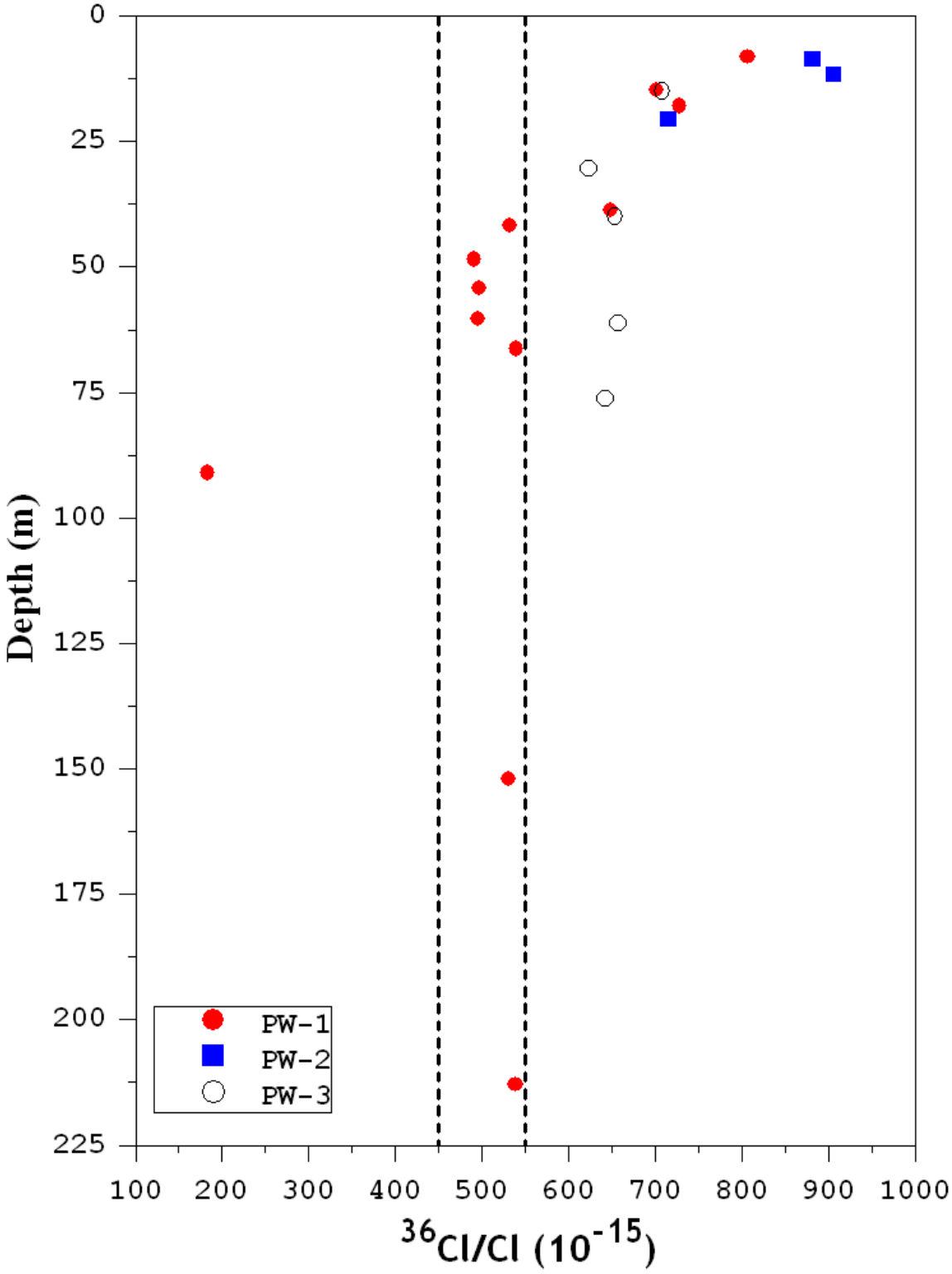

Figure 6. Chlorine-36 data with depth in PW-1, PW-2, and PW-3 (data from REECo, 1994). Dashed lines show range of modern-day pre-bomb fallout.

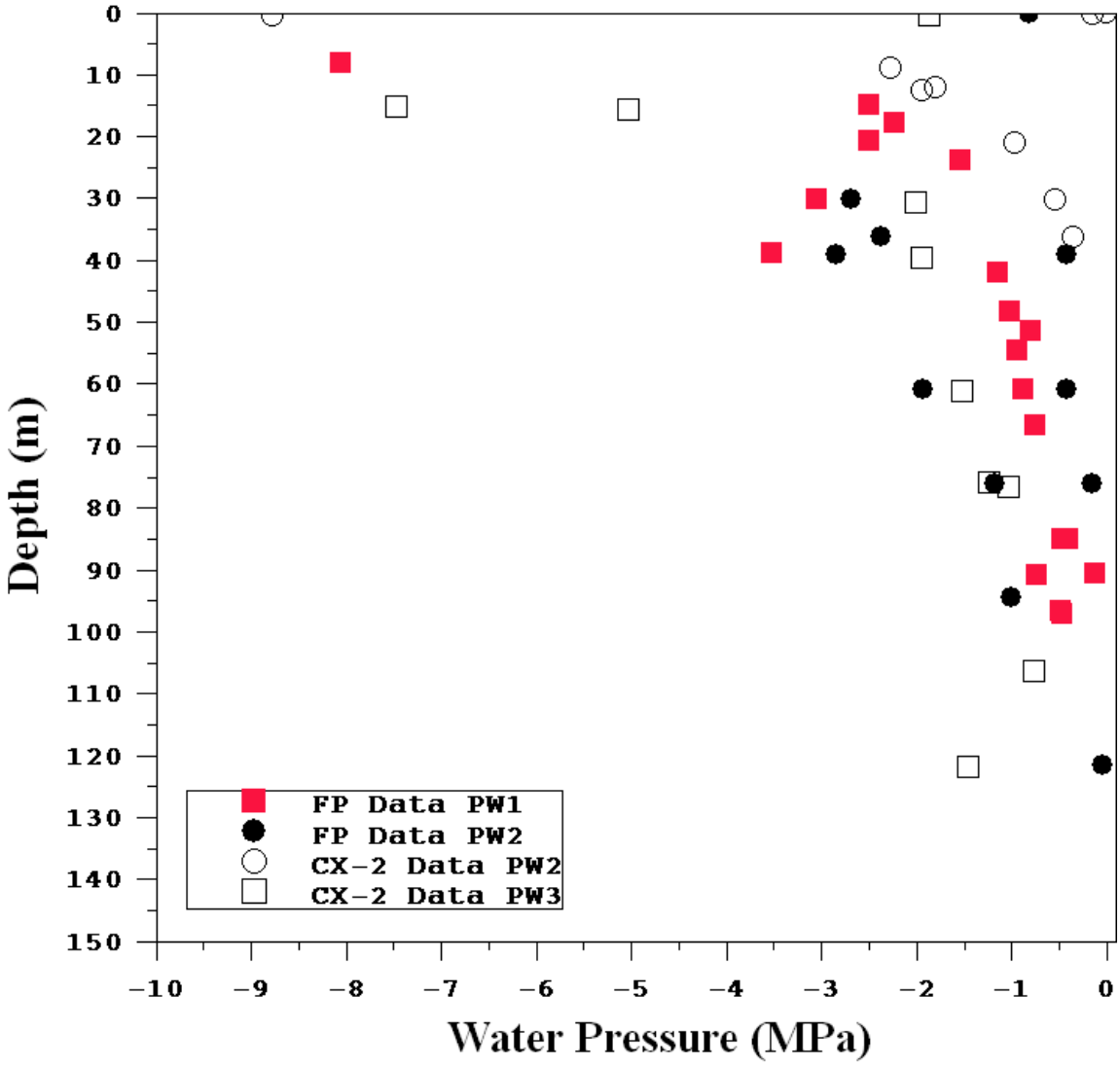

Figure 7. Measured water pressures with depth in the three wells (REECo, 1994). See section 1.4.3 for discussion. Capillary pressures are effectively the absolute values of the water pressures, as discussed in Section 1.2.

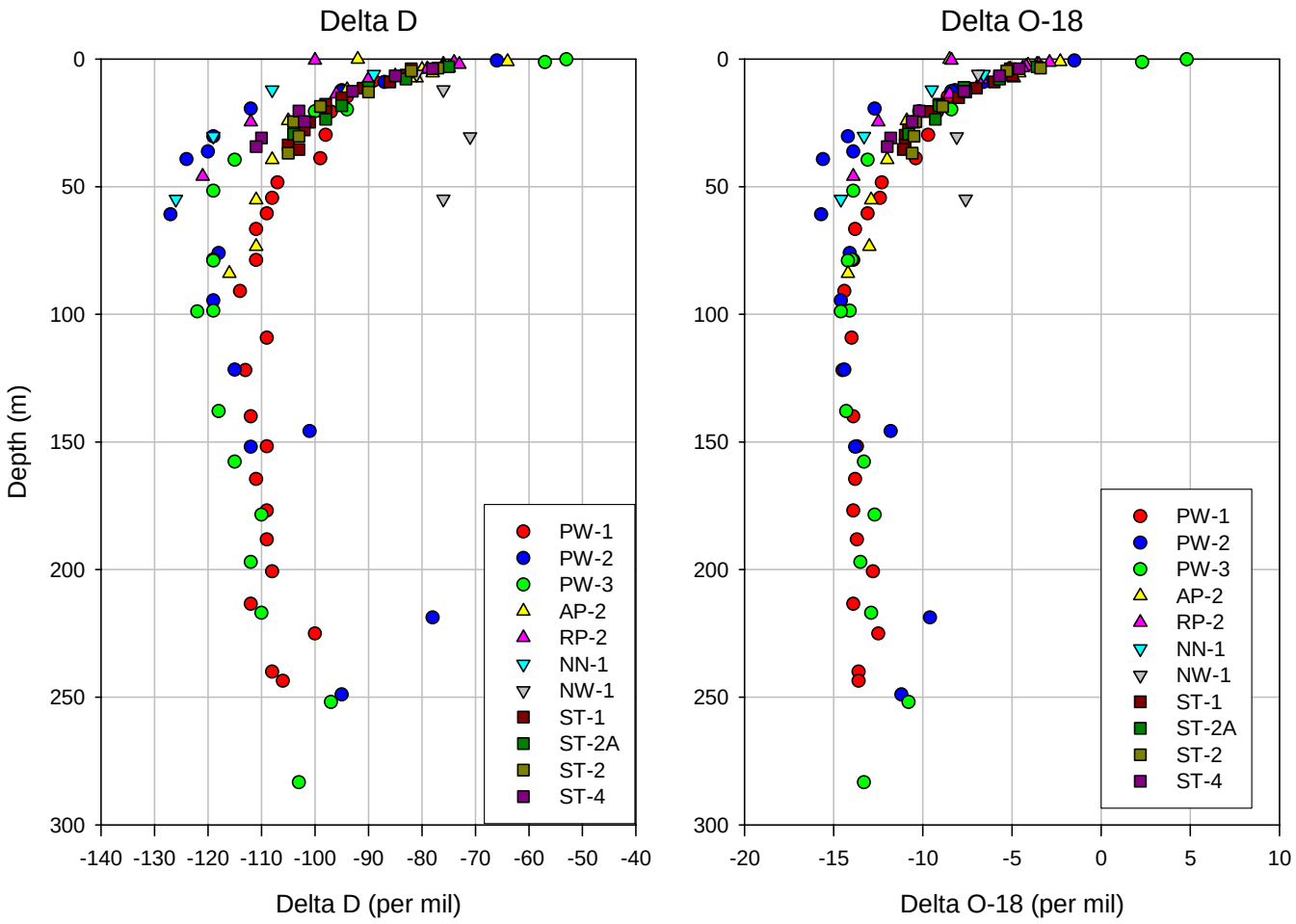

Figure 8. Stable isotope profiles for multiple wells near the Area 5 RWMS (Tyler et al. 1999).

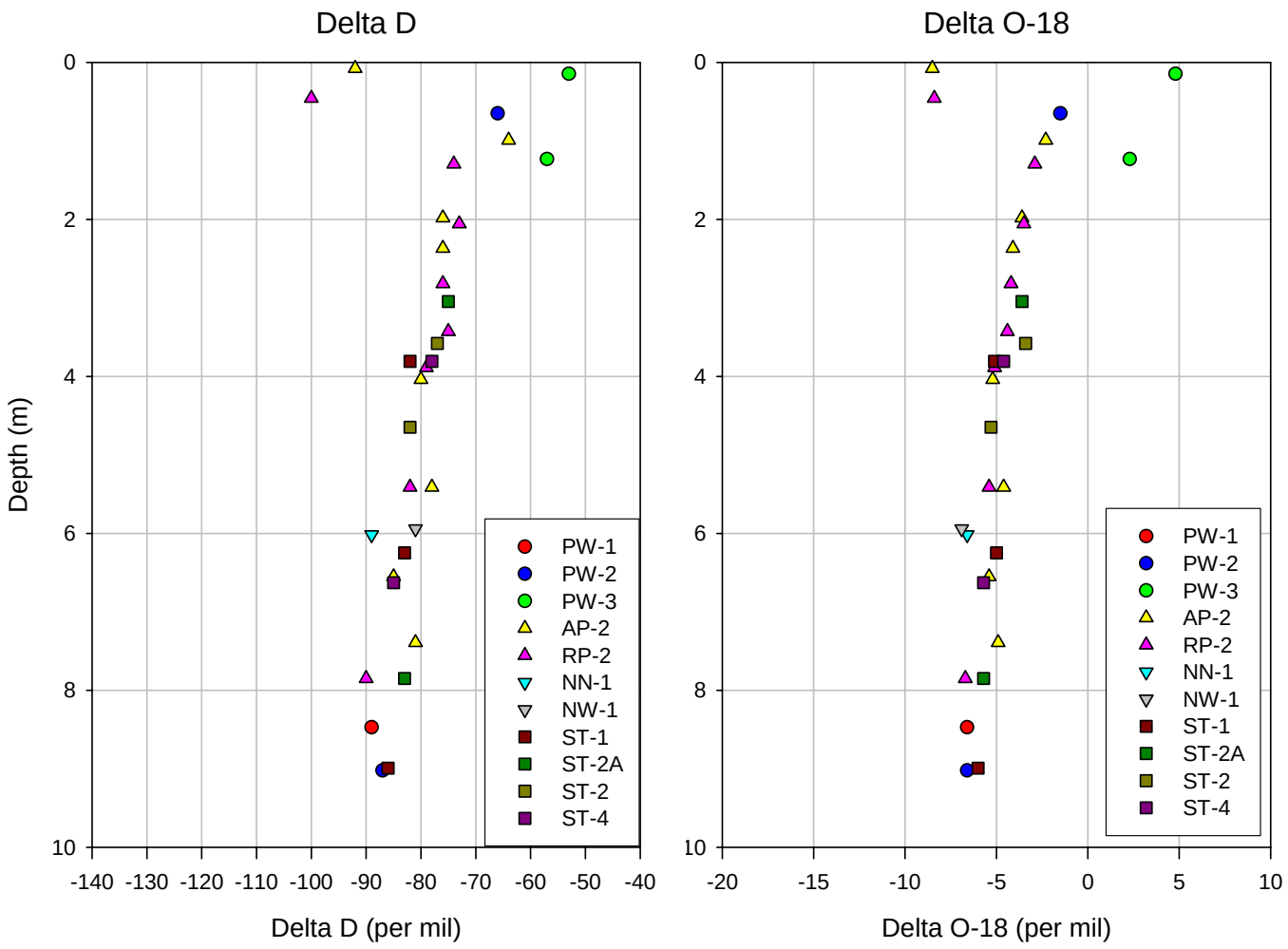

Figure 9. Shallow profiles of stable isotopes as used to set model boundary conditions.

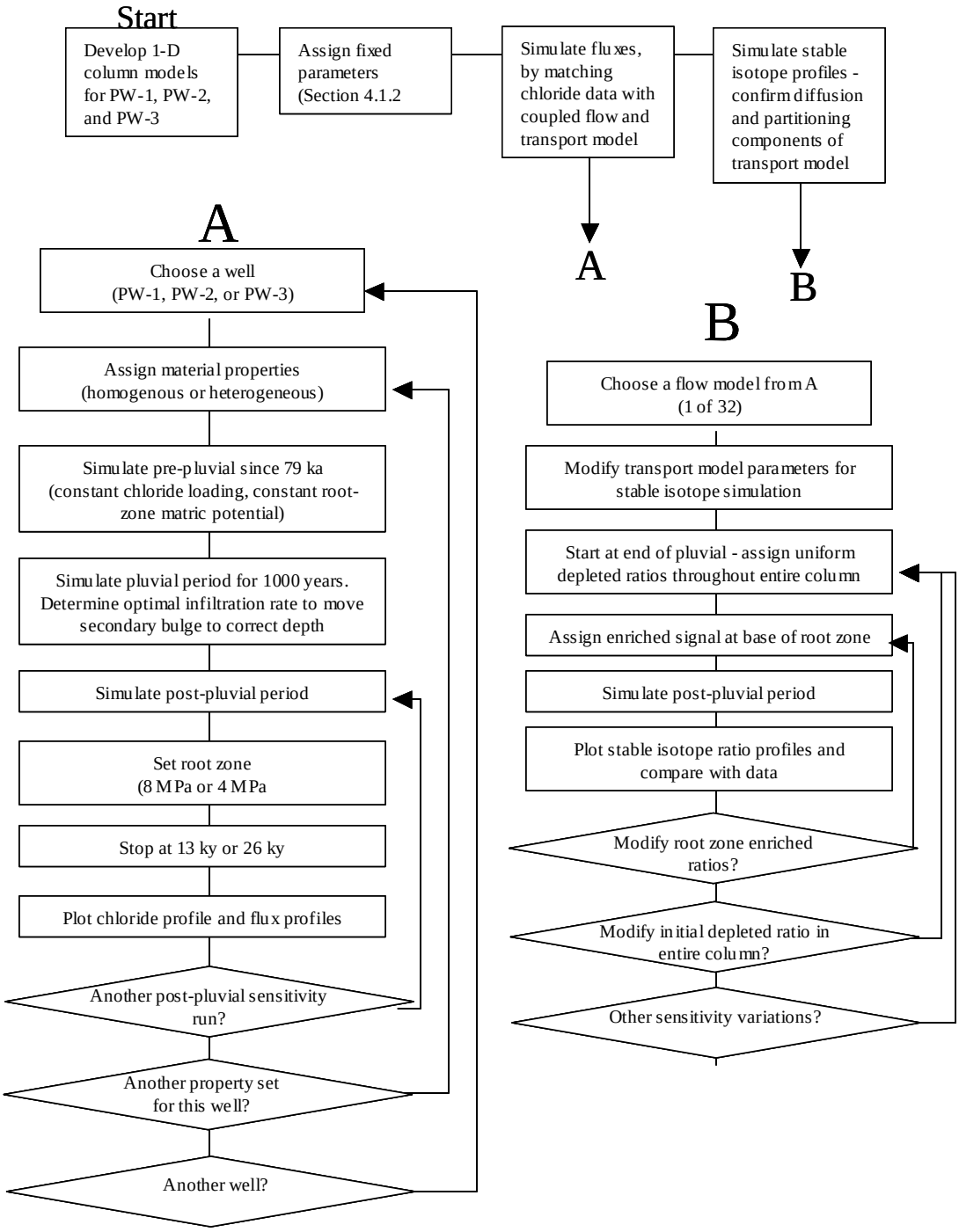

Figure 10. Storyboard of modeling process

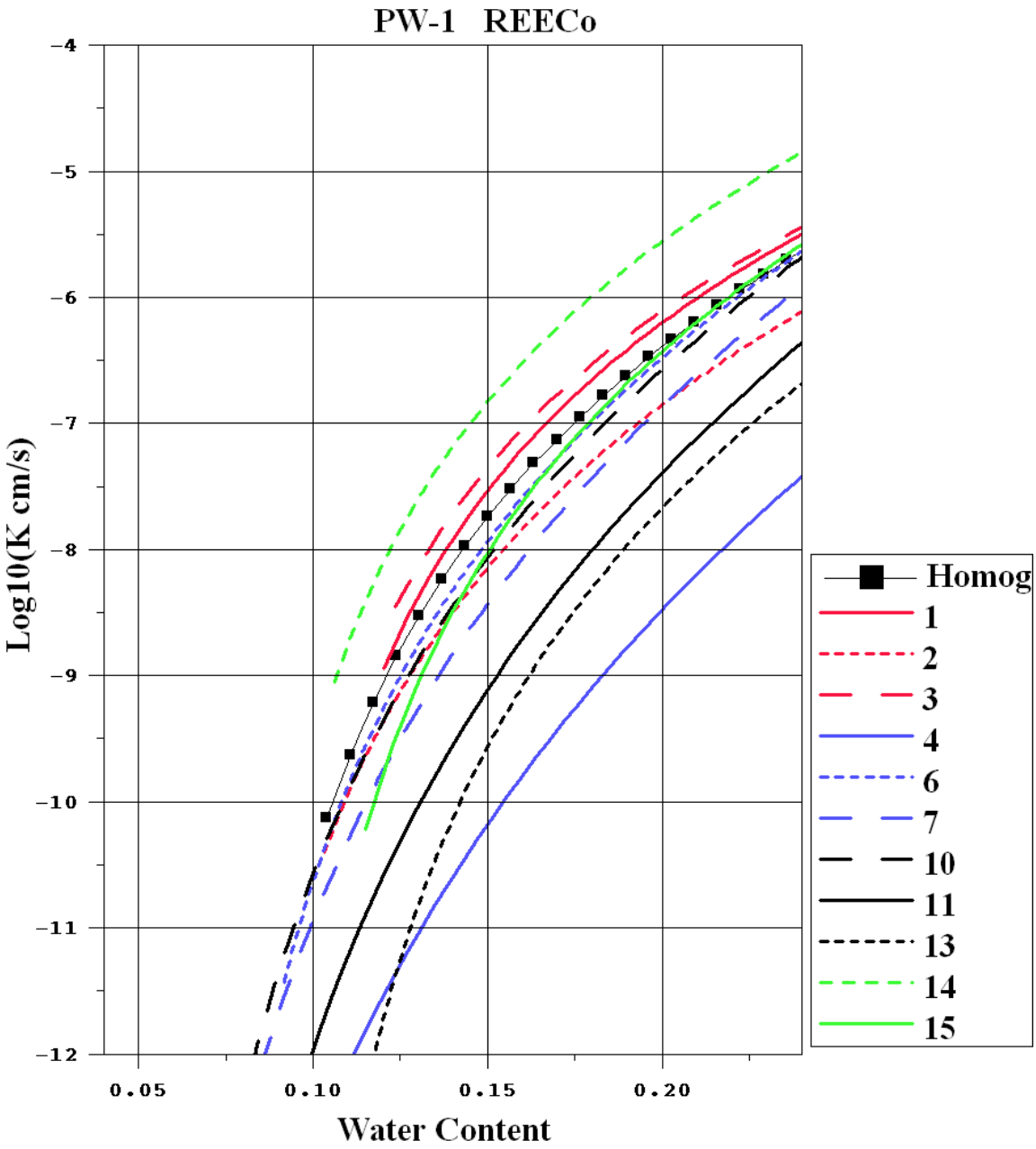

Figure 11. Vadose-zone water content/hydraulic conductivity relationships for borehole PW-1 samples, computed from REECo (1994) parameters. See Section 2.1 for sample description. Curve numbers correspond with sequential data lines in Table E.2.10 of REECo (1994).

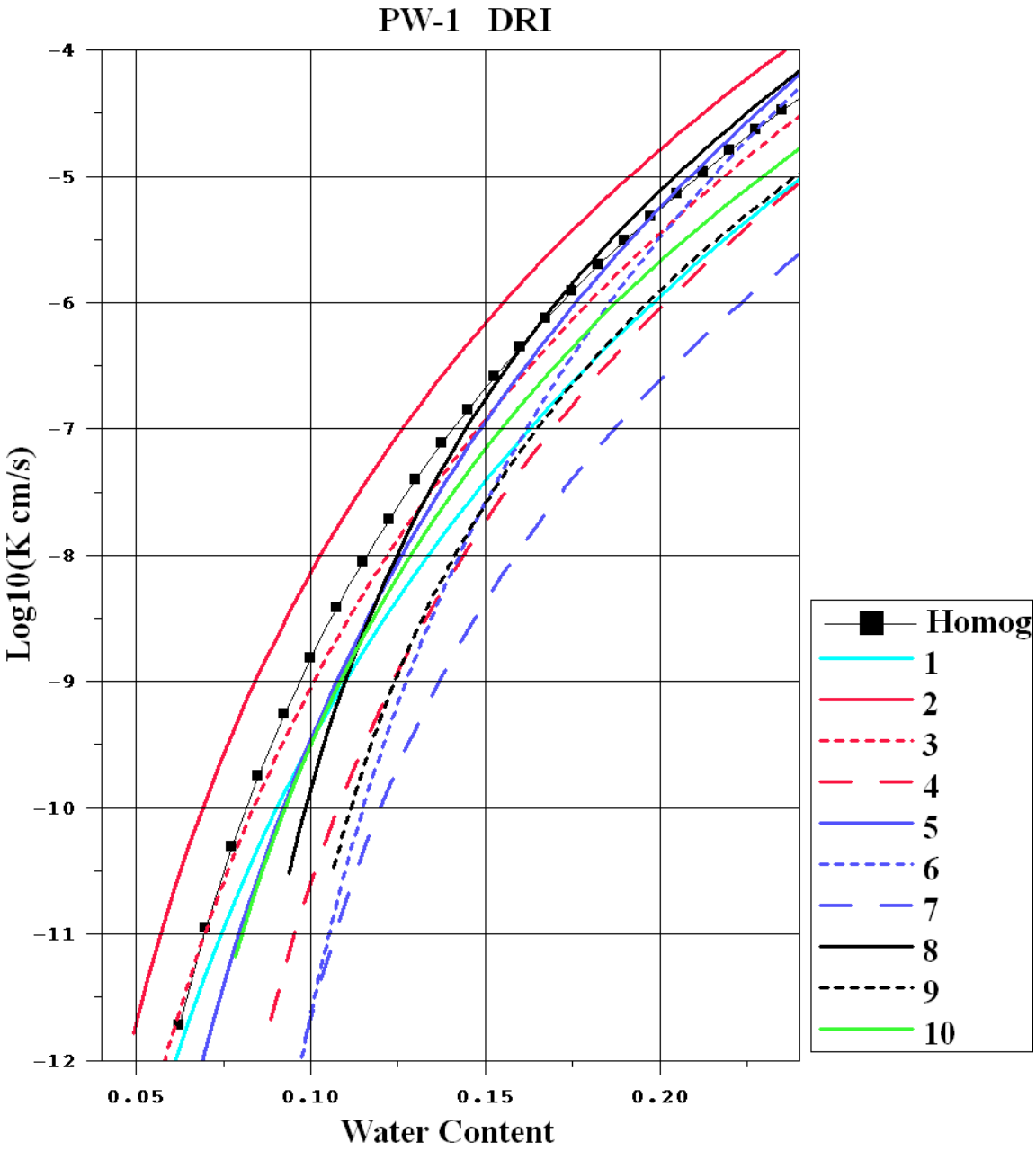

Figure 12. Vadose-zone water content/hydraulic conductivity relationships for borehole PW-1 samples, computed from Young et al. (2002) parameters. See 2.1 for sample description. Curve numbers correspond with sequential data lines in Table 3 of Young et al. (2002).

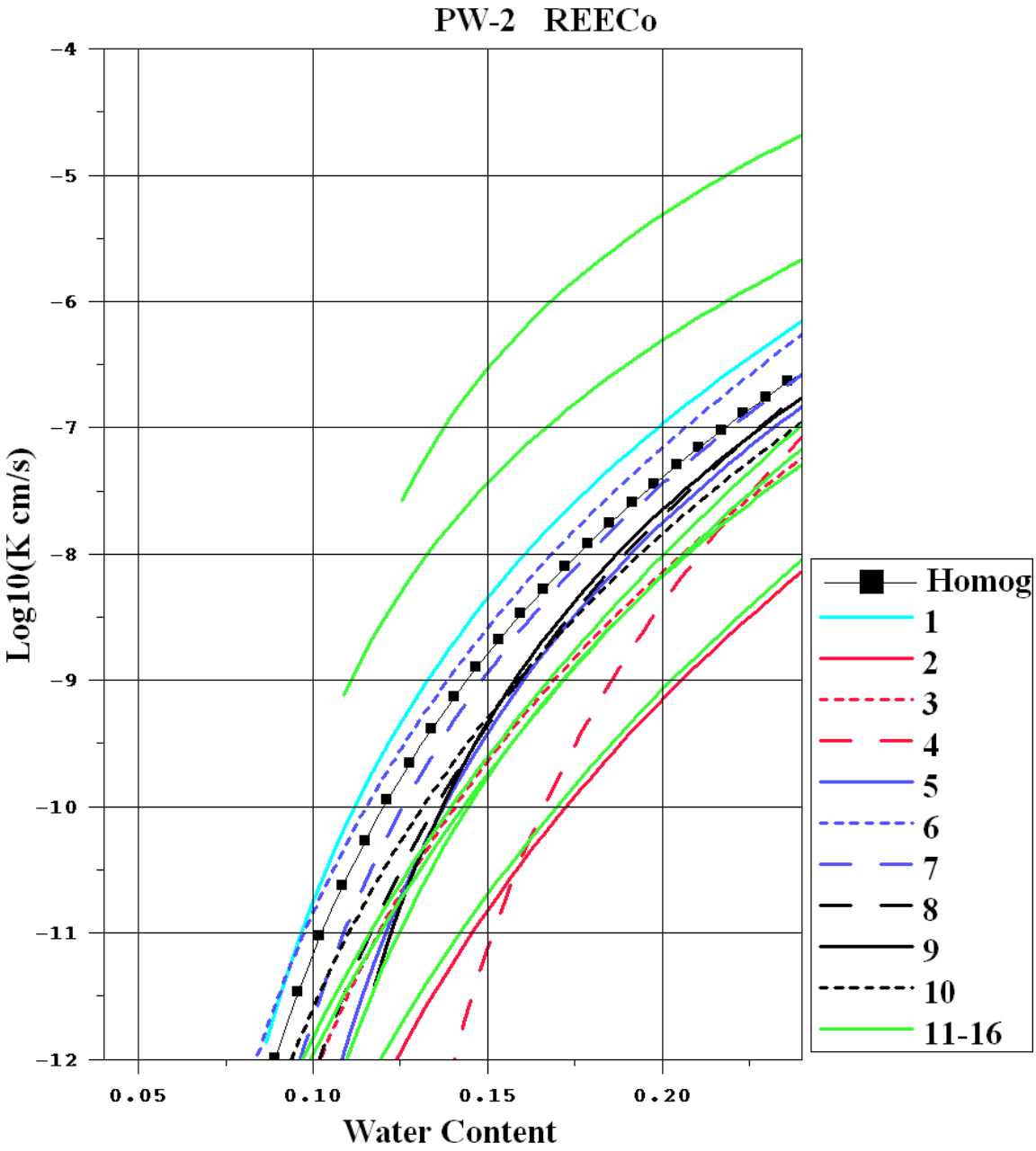

Figure 13. Vadose-zone water content/hydraulic conductivity relationships for borehole PW-2 samples, computed from REECo (1994) parameters. See 2.1 for sample description. Curve numbers correspond with sequential data lines in Table E.2.10 of REECo (1994).

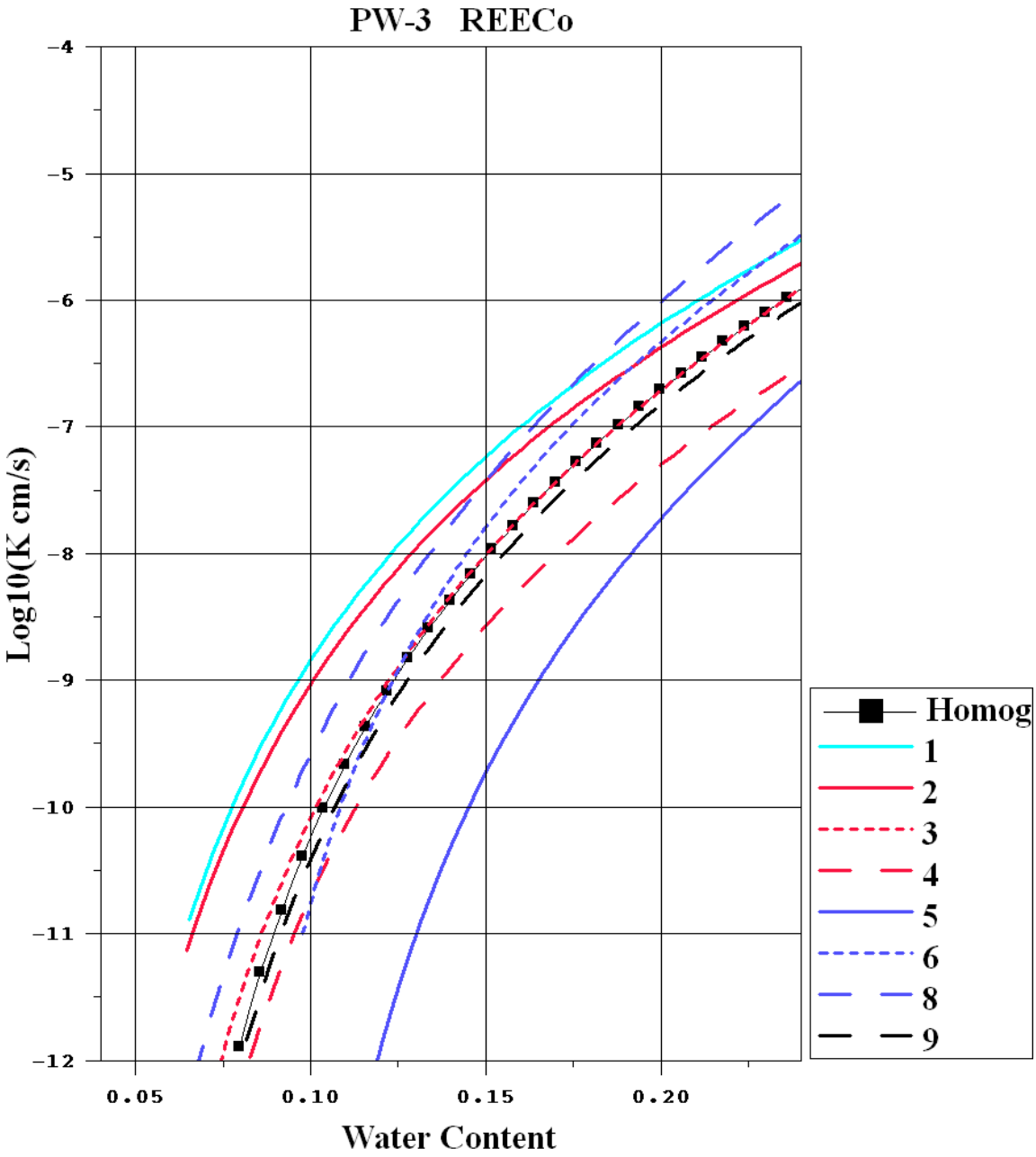

Figure 14. Vadose-zone water content/hydraulic conductivity relationships for borehole PW-3 samples, computed from REECo (1994) parameters. See Section 2.1 for sample description. Curve numbers correspond with sequential data lines in Table E.2.10 of REECo (1994).

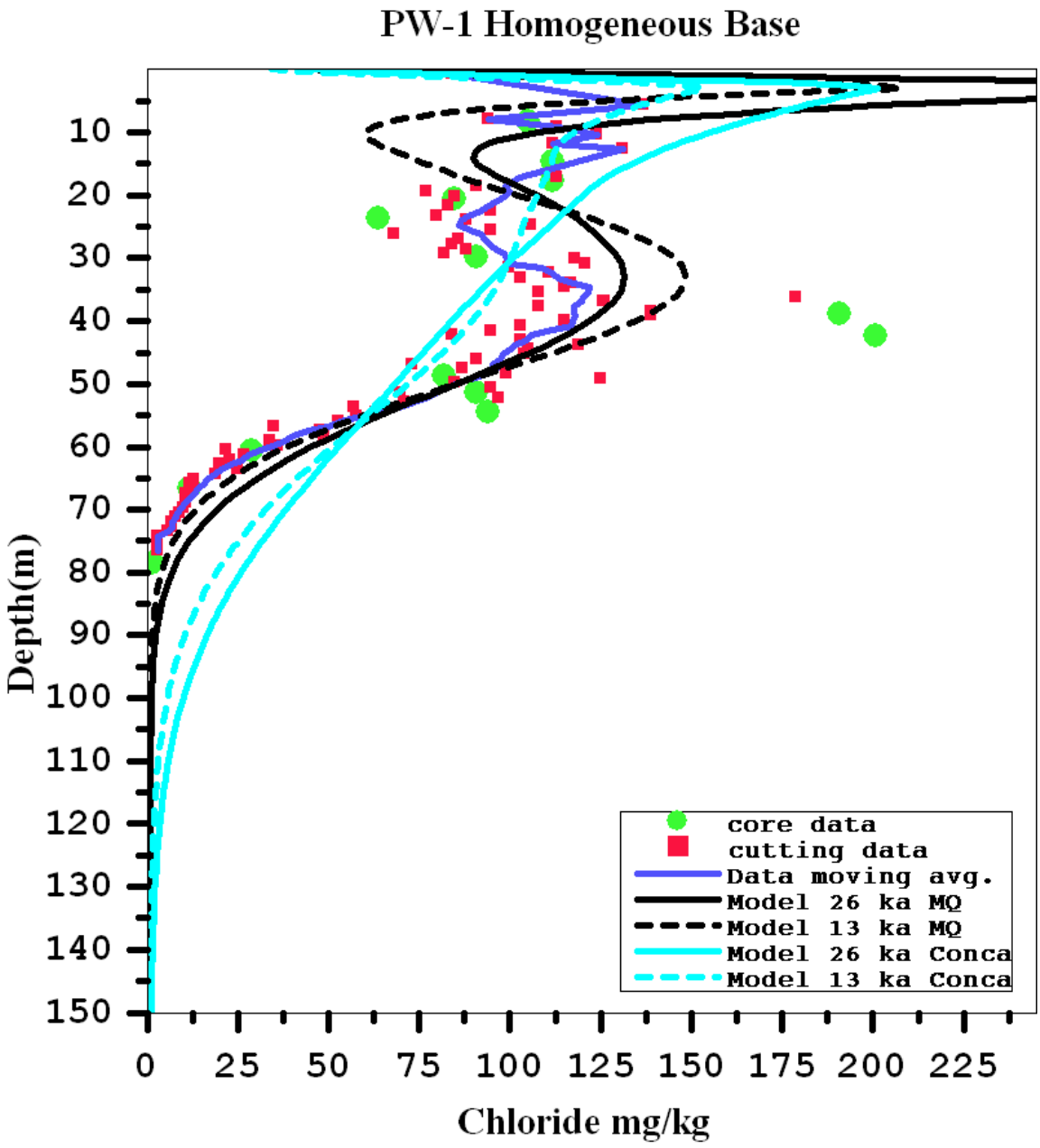

Figure 15. Observed and simulated chloride mass concentrations in **PW-1** for root-zone potential of 8 MPa. Figure shows differences for 26 and 13 thousand years of high root-zone capillary pressure since last pluvial period. Model results show the difference in diffusive mass transport simulated with Conca-Wright and Millington-Quirk models. **Homogeneous** hydraulic properties based on **REECo (1994)** sample analyses.

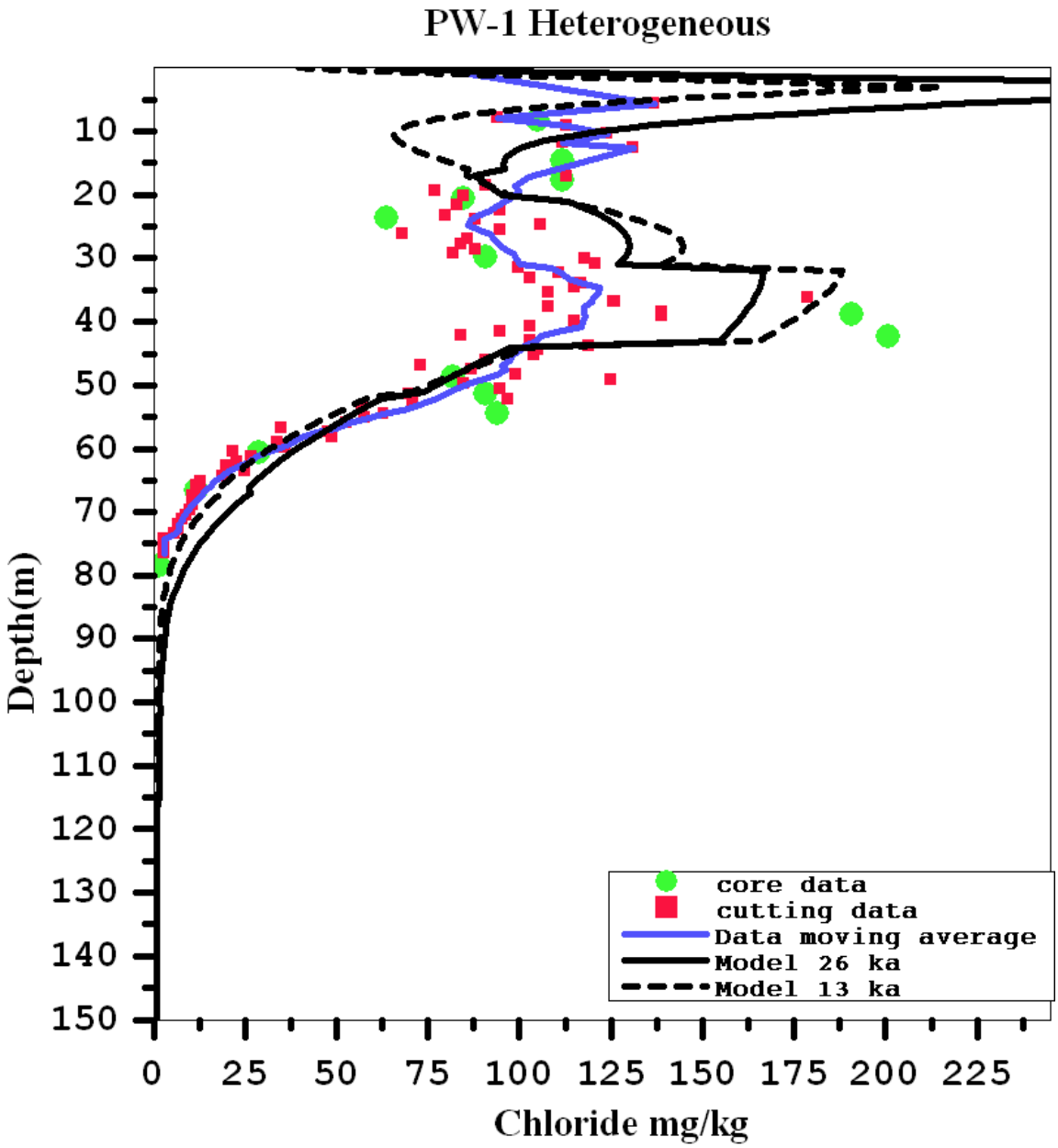

Figure 16. Observed and simulated chloride mass concentrations in **PW-1** for root-zone potential of 8 MPa. Figure shows differences for 26 and 13 thousand years of high root-zone capillary pressure since last pluvial period. Only Millington-Quirk diffusion model results are shown in this figure. **Heterogeneous** hydraulic properties based on **REECo (1994)** sample analyses.

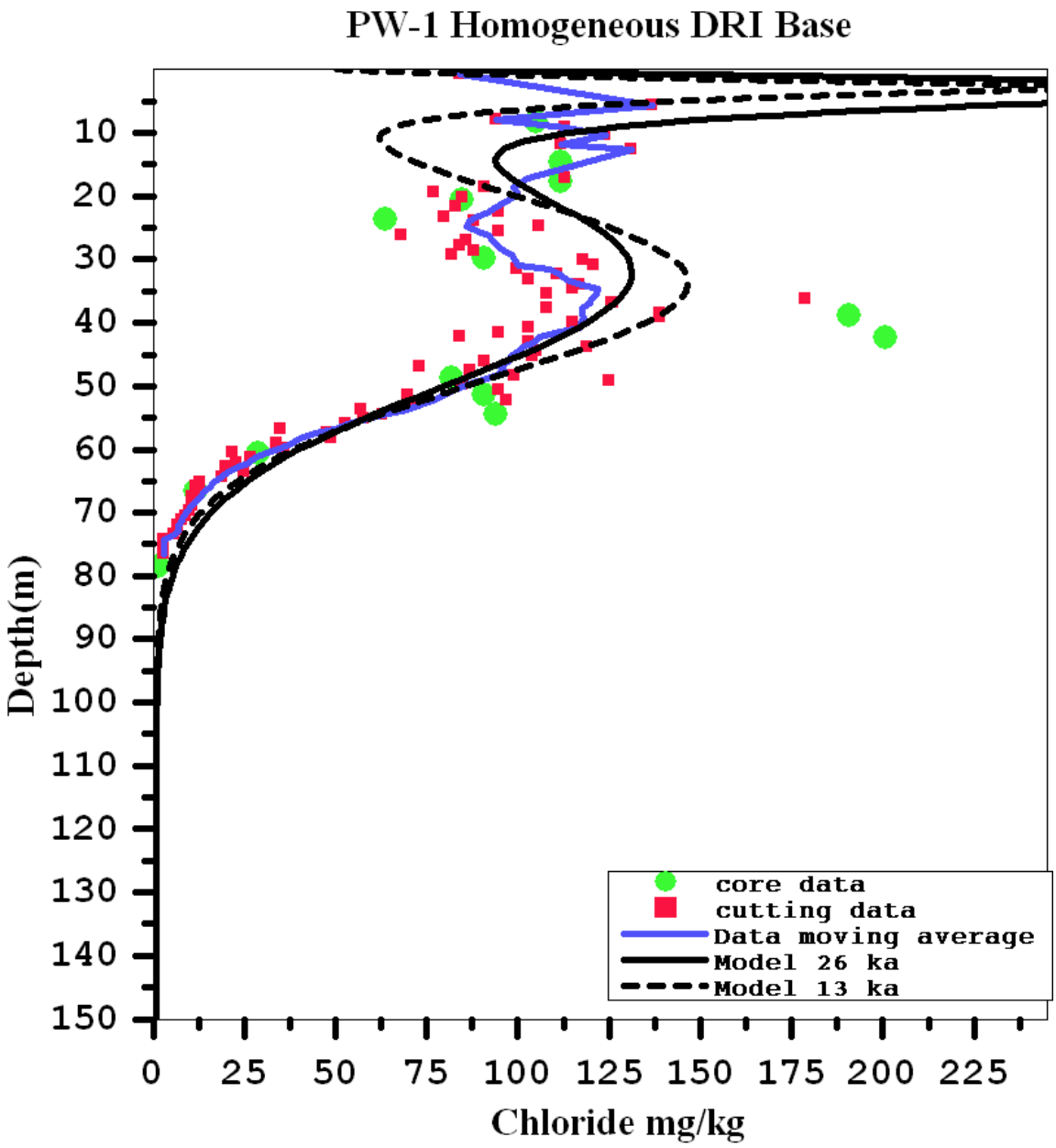

Figure 17. Observed and simulated chloride mass concentrations in **PW-1** for root-zone potential of 8 MPa. Figure shows differences for 26 and 13 thousand years of high root-zone capillary pressure since last pluvial period. Only Millington-Quirk diffusion model results are shown in this figure. **Uniform** hydraulic properties based on geometric mean of **Young et al. (2002)** parameters.

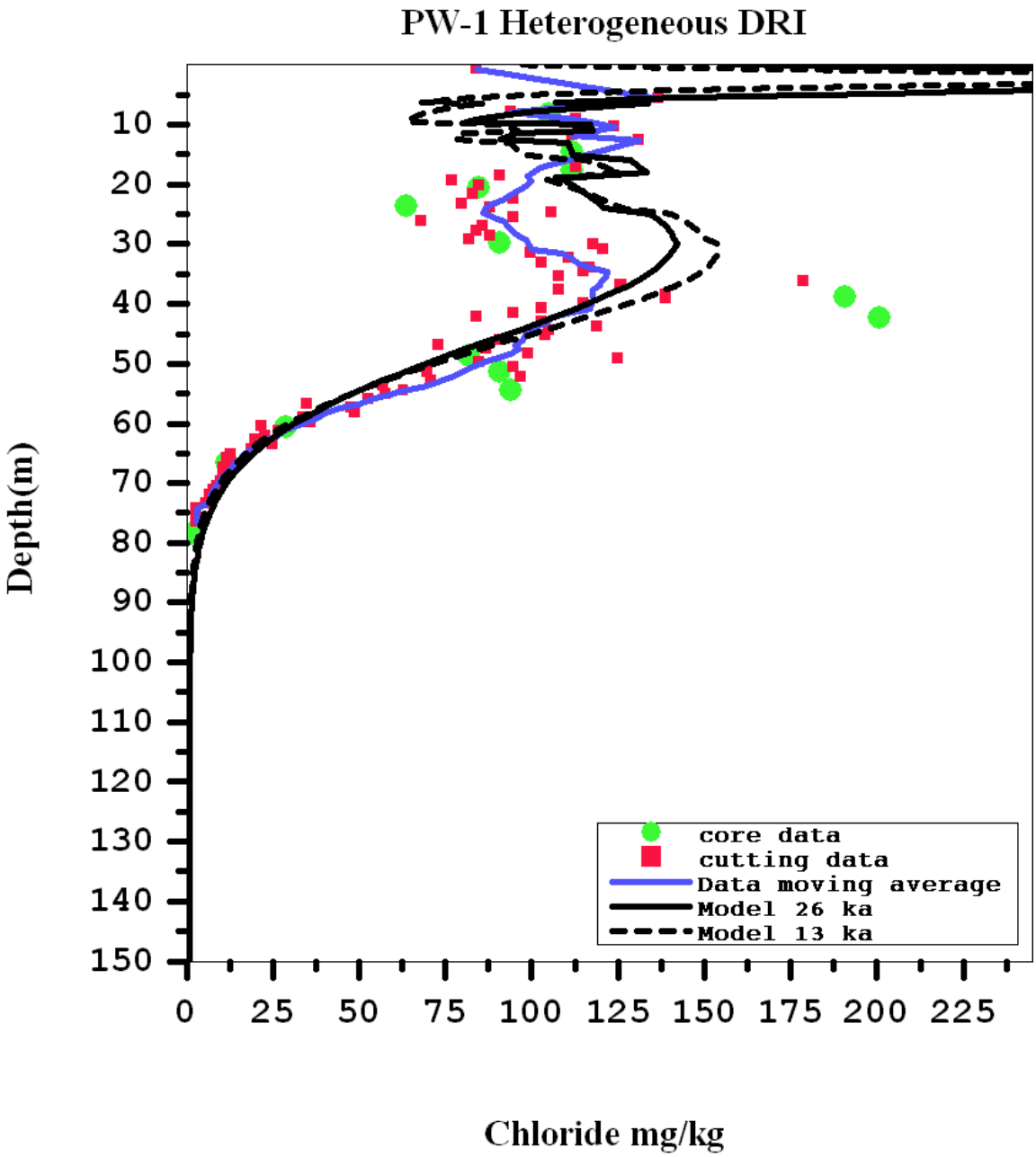

Figure 18. Observed and simulated chloride mass concentrations in **PW-1** for root-zone potential of 8 MPa. Figure shows differences for 26 and 13 thousand years of high root-zone capillary pressure since last pluvial period. Only Millington-Quirk diffusion model results are shown in this figure. **Heterogeneous** hydraulic properties based on **YOUNG ET AL. (2002**) sample analyses.

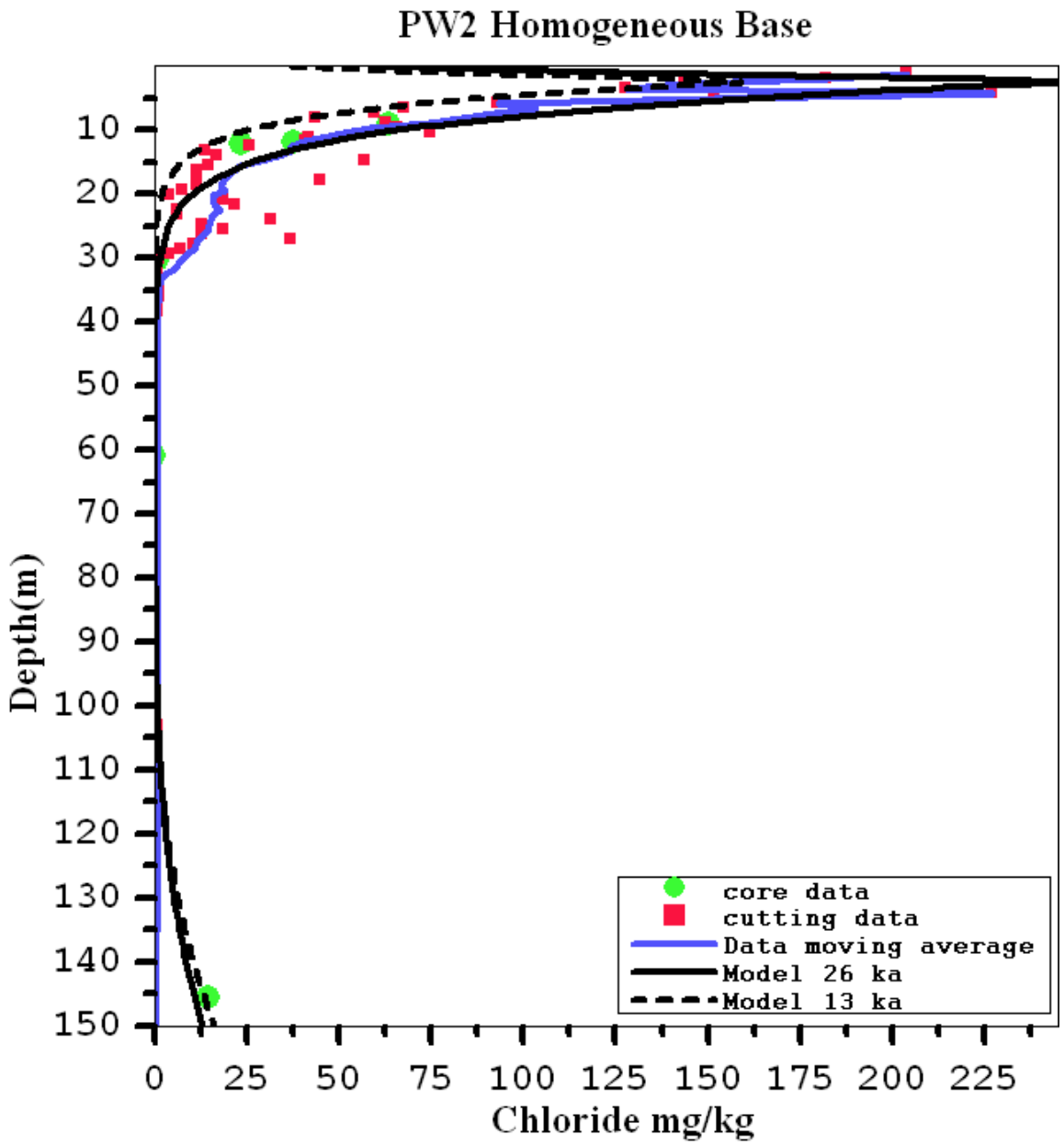

Figure 19. Observed and simulated chloride mass concentrations in **PW-2** for root-zone potential of 8 MPa. Figure shows differences for 26 and 13 thousand years of high root-zone capillary pressure since last pluvial period. Only Millington-Quirk diffusion model results are shown in this figure. **Uniform** hydraulic properties based on geometric mean of **REECo (1994)** parameters.

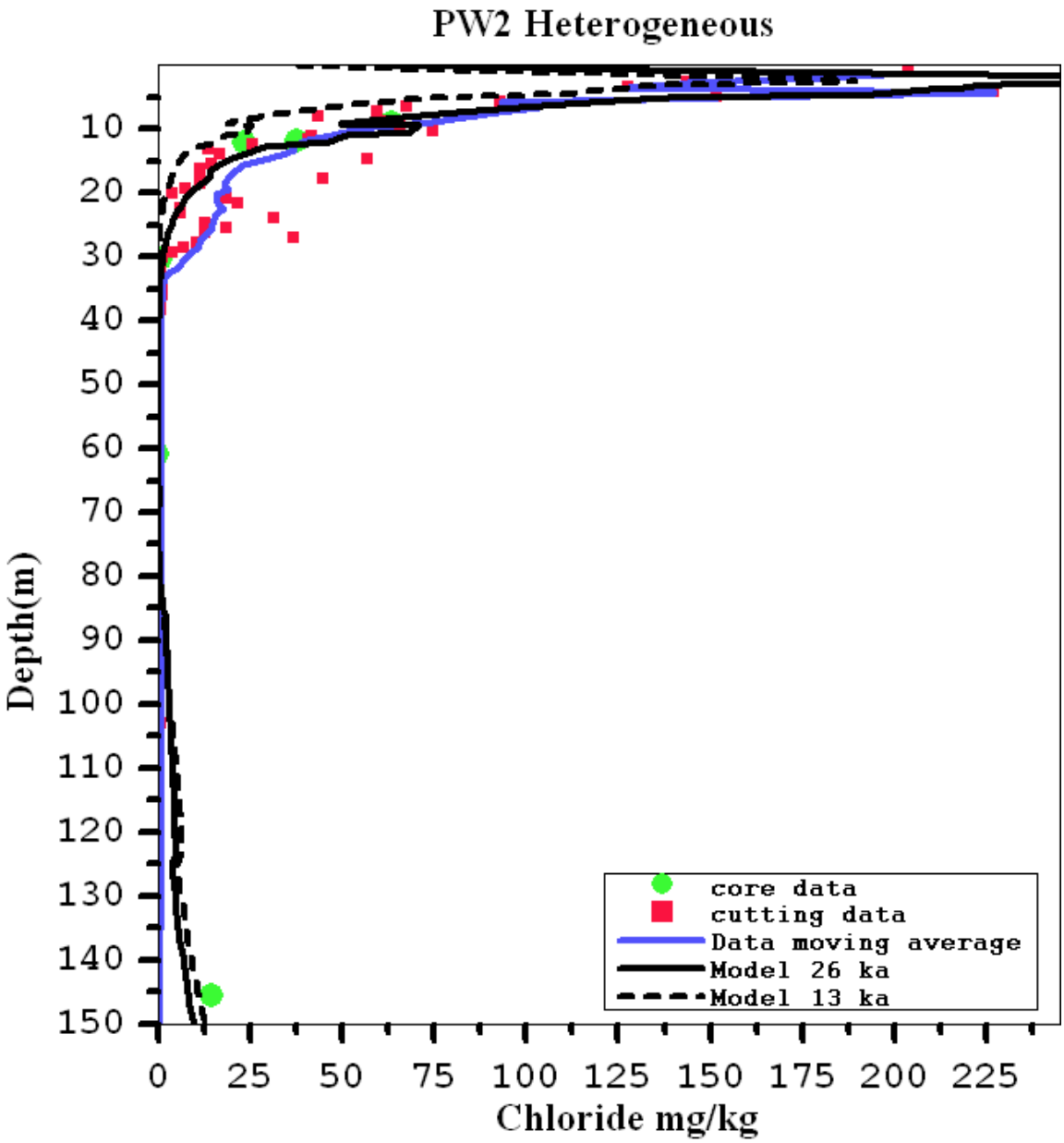

Figure 20. Observed and simulated chloride mass concentrations in **PW-2** for root-zone potential of 8 MPa. Figure shows differences for 26 and 13 thousand years of high root-zone capillary pressure since last pluvial period. Only Millington-Quirk diffusion model results are shown in this figure. **Heterogeneous** hydraulic properties based on **REECo (1994)** sample analyses.

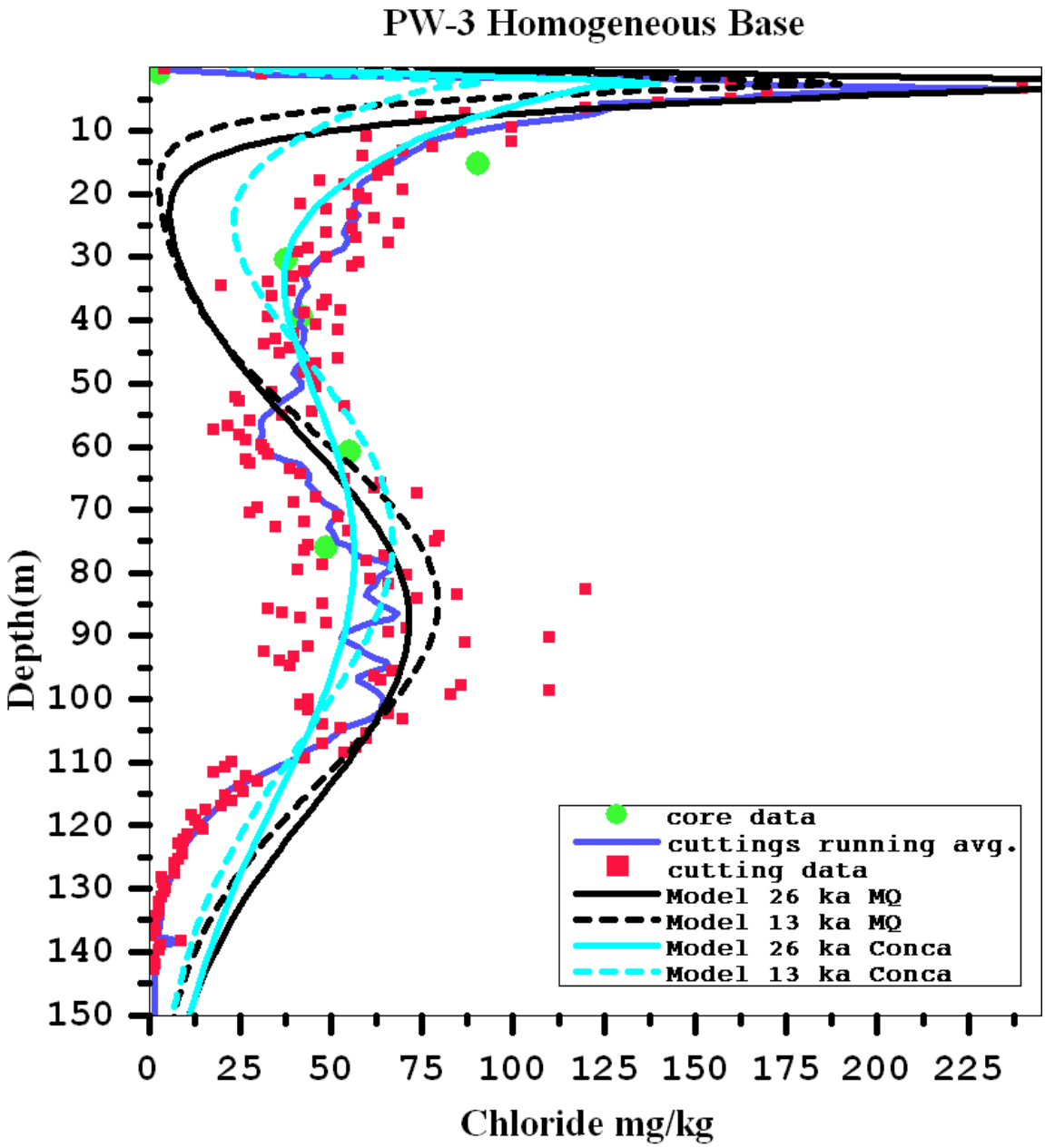

Figure 21. Observed and simulated chloride mass concentrations in **PW-3** for root-zone potential of 8 MPa. Figure shows differences for 26 and 13 thousand years of high root-zone capillary pressure since last pluvial period. Model results show the difference in diffusive mass transport simulated with Conca-Wright and Millington-Quirk models. **Uniform** hydraulic properties based on geometric mean of **REECo (1994)** parameters.

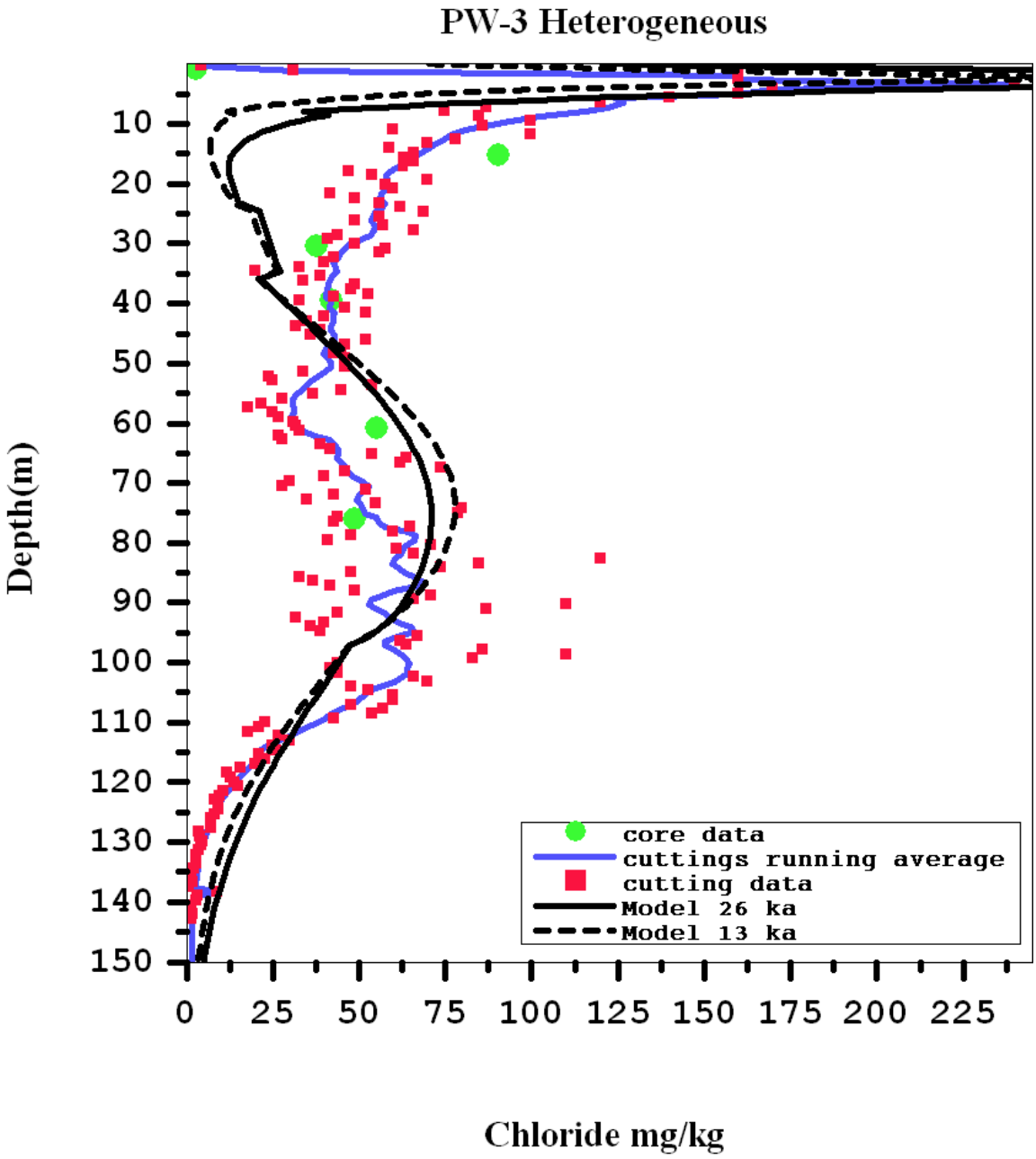

Figure 22. Observed and simulated chloride mass concentrations in **PW-3** for root-zone potential of 8 MPa. Figure shows differences for 26 and 13 thousand years of high root-zone capillary pressure since last pluvial period. Only Millington-Quirk diffusion model results are shown in this figure. **Heterogeneous** hydraulic properties based on **REECo (1994)** sample analyses.

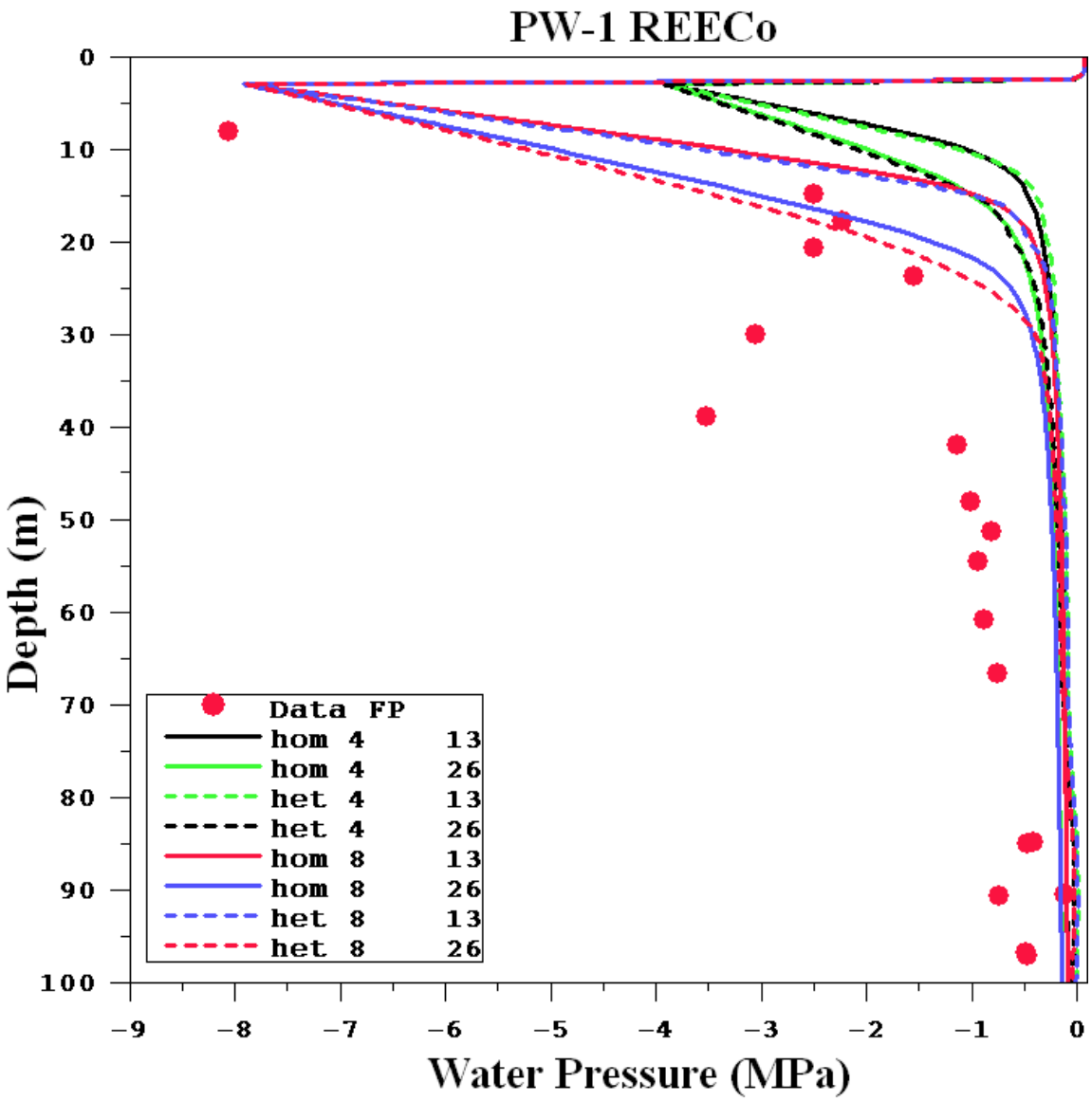

Figure 23. Observed and simulated water pressures (negative capillary pressure) at PW-1 using REECo (1994) properties. Simulations for homogenous (hom) and heterogeneous (het) properties with post-pluvial root-zone capillary pressure set at 4 MPa (4) and 8 MPa (8) and post-pluvial duration of 13 ky and 26 ky.

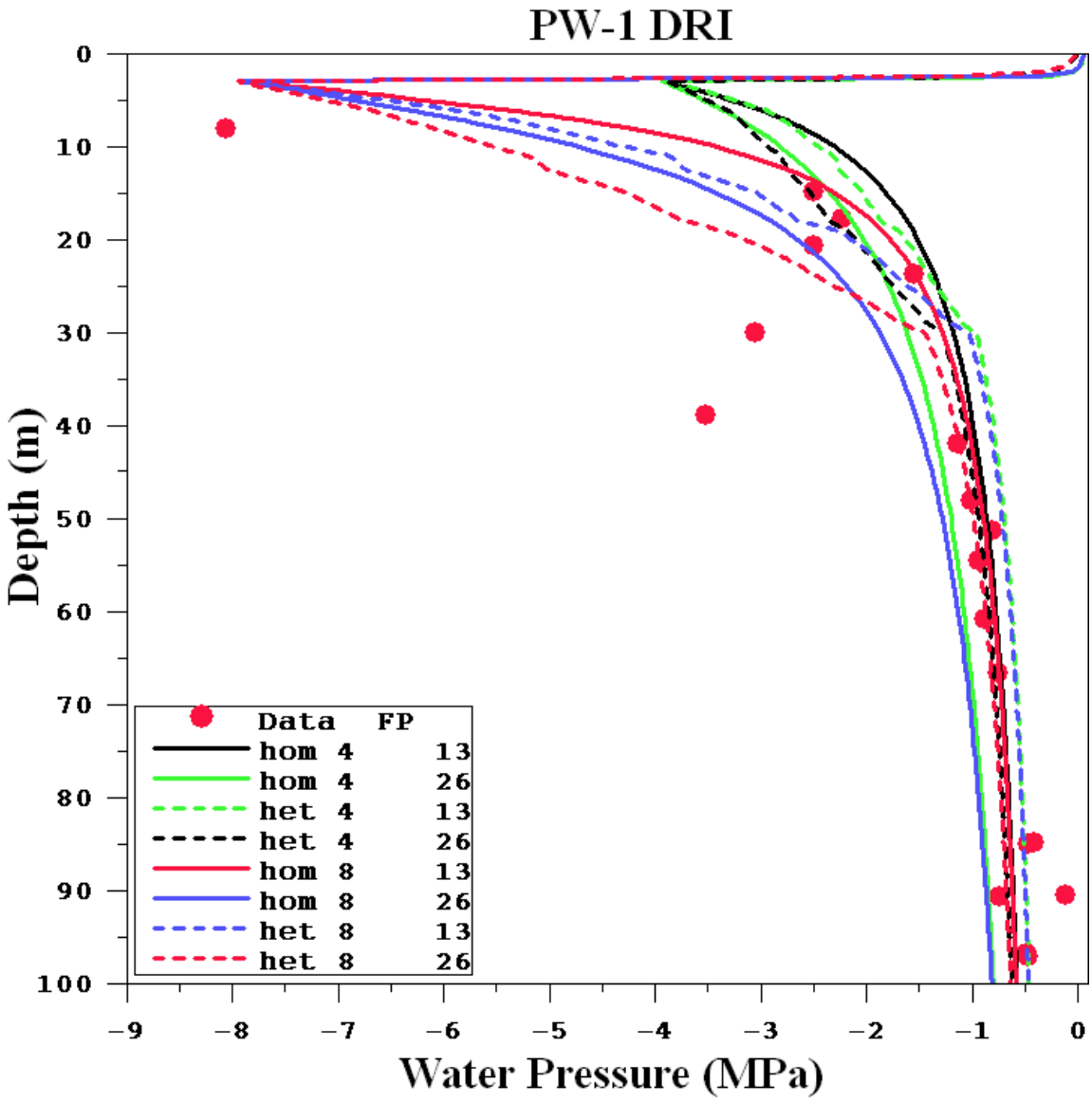

Figure 24. Observed and simulated water pressures (negative capillary pressure) at PW-1 using Young et al. (2002) properties. Simulations for homogenous (hom) and heterogeneous (het) properties with post-pluvial root-zone capillary pressure set at 4 MPa (4) and 8 MPa (8) and post-pluvial duration of 13 ky and 26 ky.

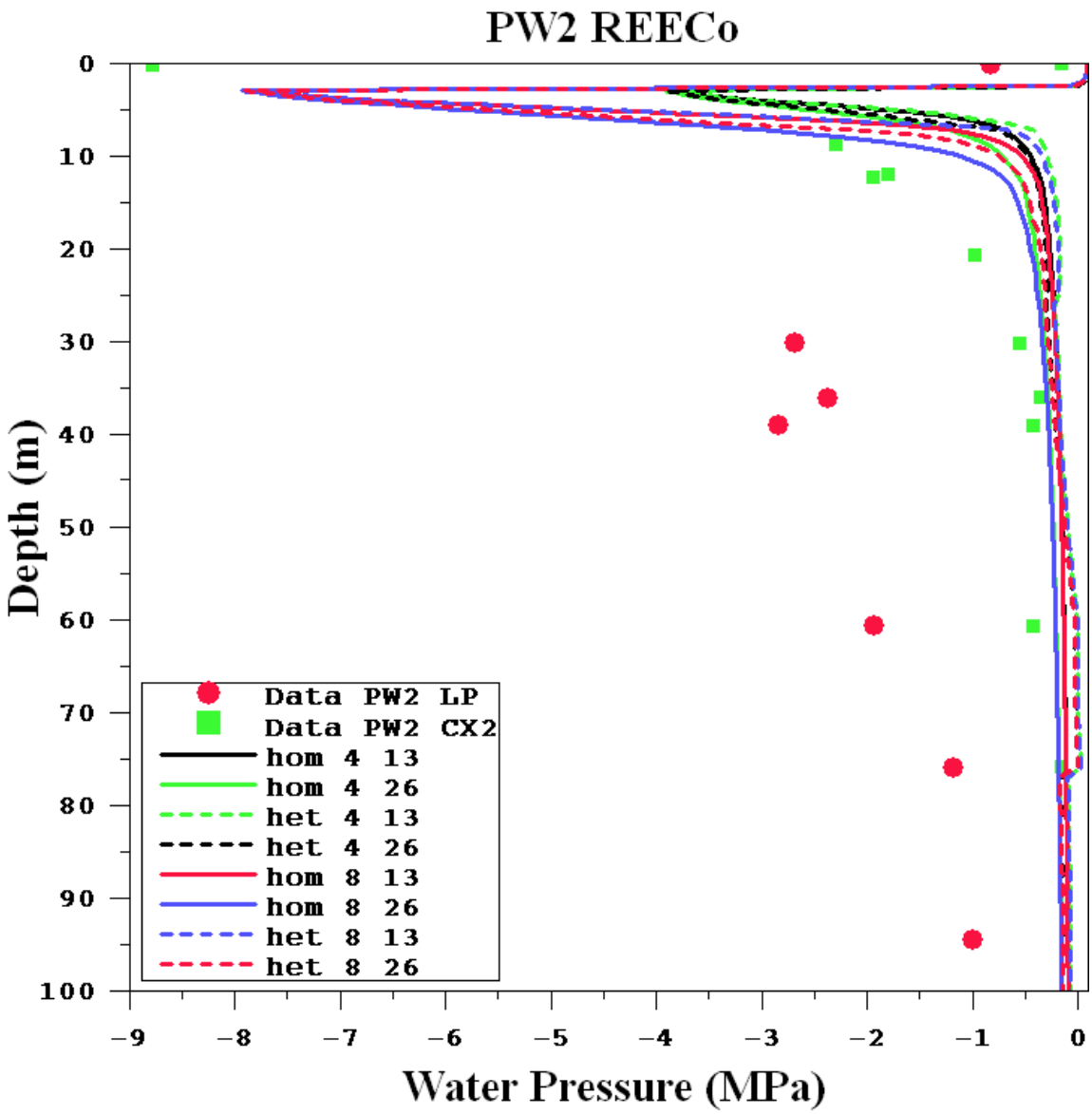

Figure 25. Observed and simulated water pressures (negative capillary pressure) at PW-2 using REECo (1994) properties. Simulations for homogenous (hom) and heterogeneous (het) properties with post-pluvial root-zone capillary pressure set at 4 MPa (4) and 8 MPa (8) and post-pluvial duration of 13 ky and 26 ky.

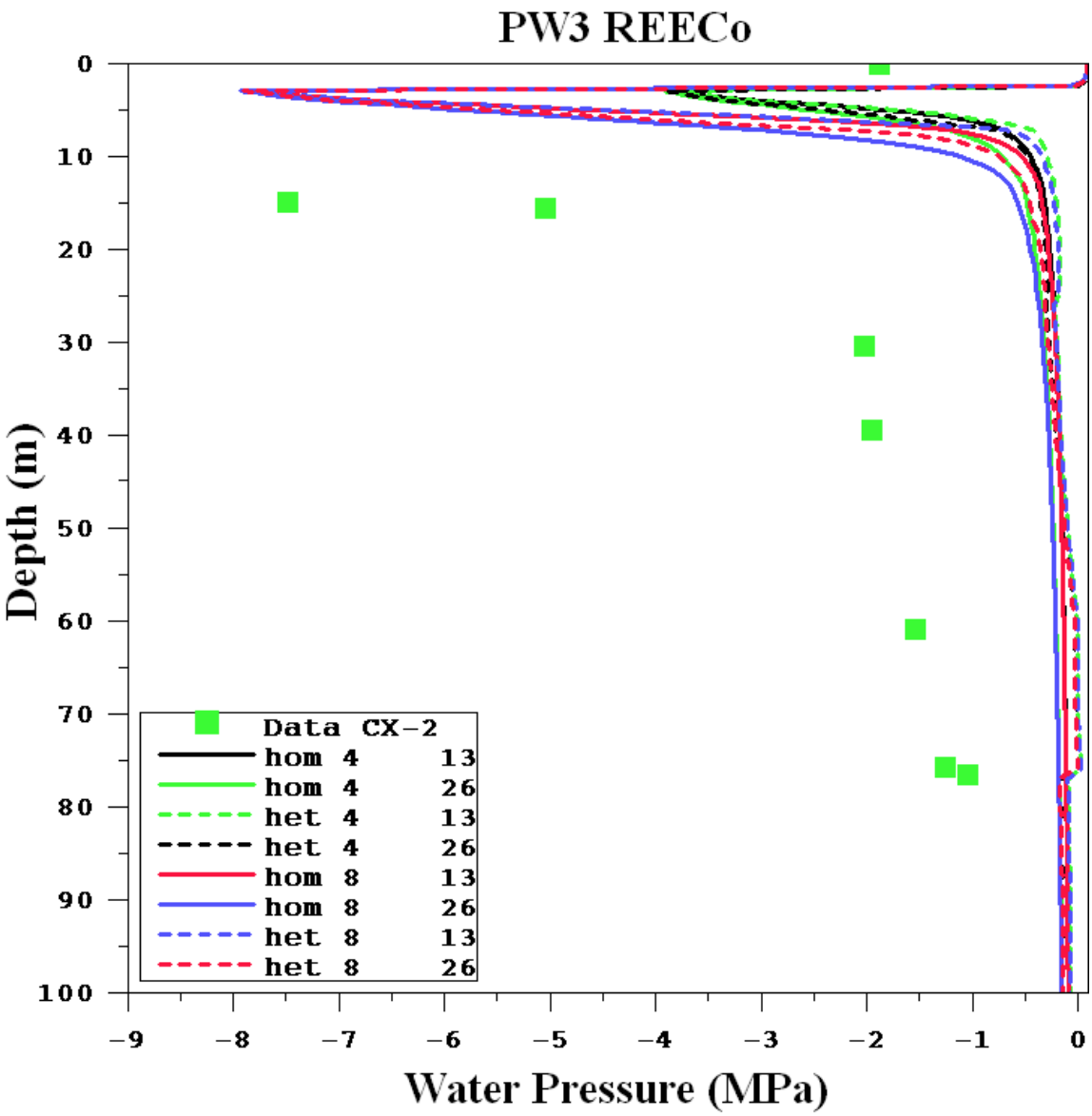

Figure 26. Observed and simulated water pressures (negative capillary pressure) at PW-3 using REECo (1994) properties. Simulations for homogenous (hom) and heterogeneous (het) properties with post-pluvial root-zone capillary pressure set at 4 MPa (4) and 8 MPa (8) and post-pluvial duration of 13 ky and 26 ky.

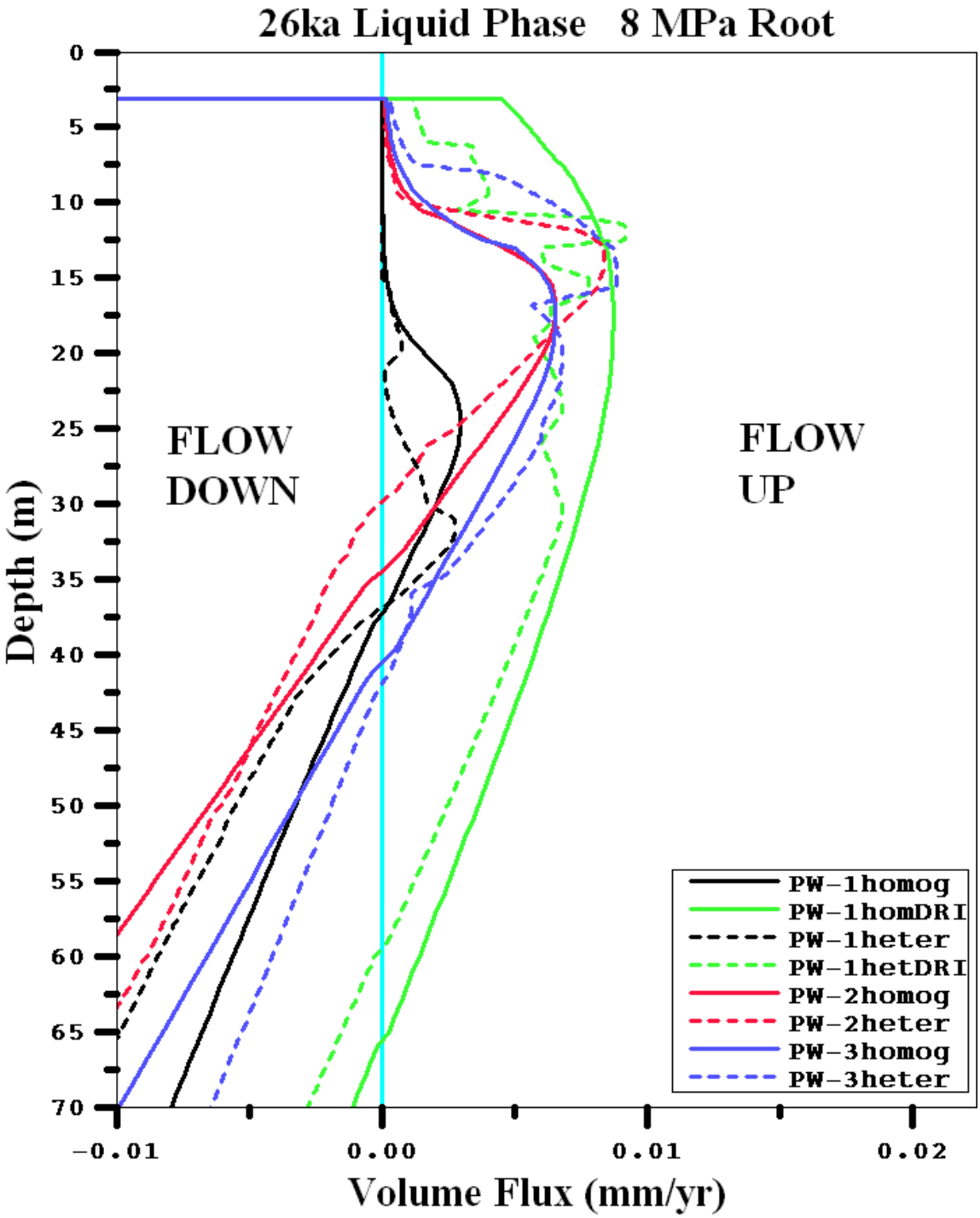

Figure 27. Simulated liquid fluxes vs. depth with an 8 MPa root-zone capillary pressure for 26 ky since the last pluvial period. Legend indicates location and material properties as listed in Table 7.

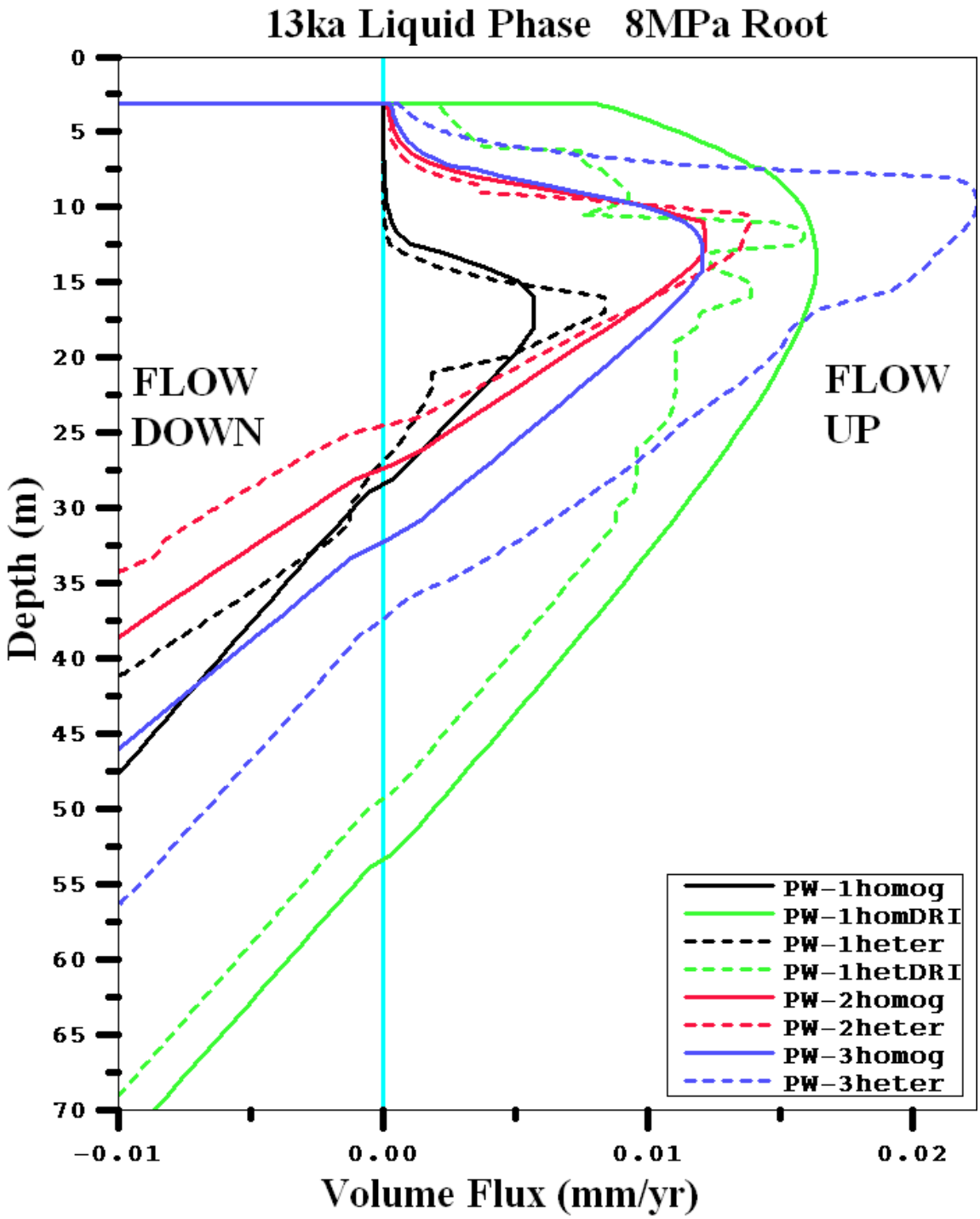

Figure 28. Simulated liquid fluxes vs. depth with an 8 MPa root-zone capillary pressure for 13 ky since the last pluvial period. Legend indicates location and material properties as listed in Table 7.

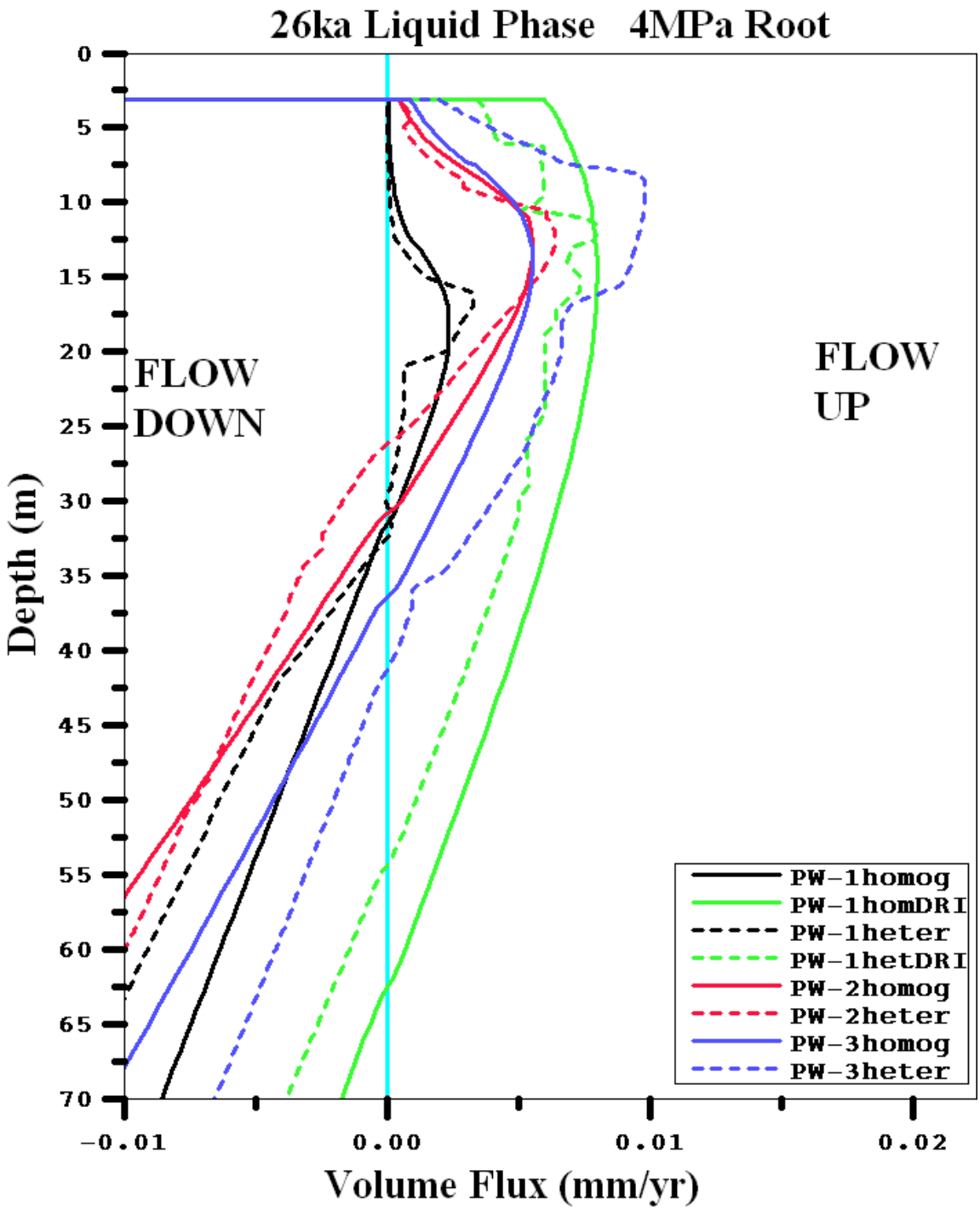

Figure 29. Simulated liquid fluxes vs. depth with a 4 MPa root-zone capillary pressure for 26 ky since the last pluvial period. Legend indicates location and material properties as listed in Table 7.

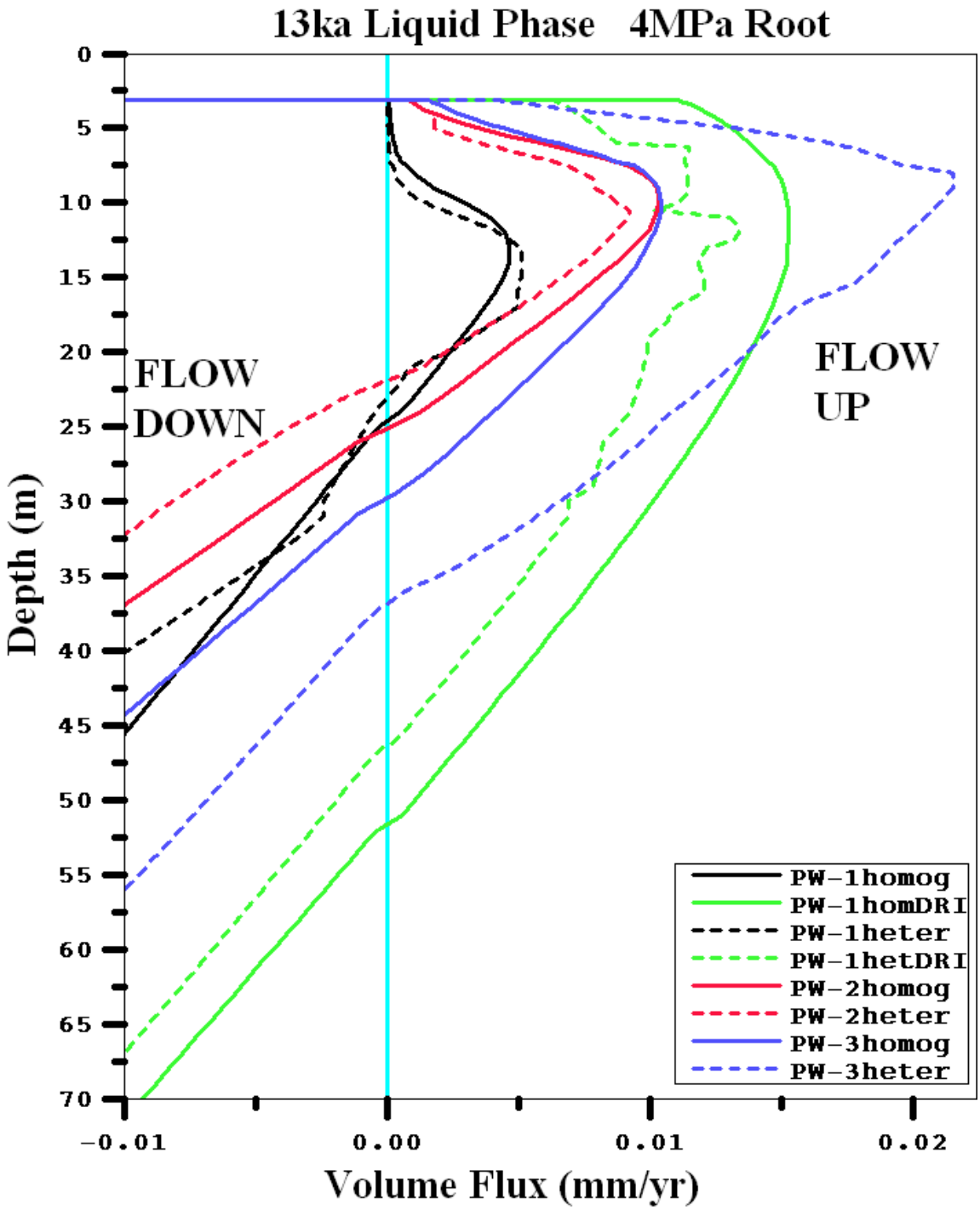

Figure 30. Simulated liquid fluxes vs. depth with a 4 MPa root-zone capillary pressure for 13 ky since the last pluvial period. Legend indicates location and material properties as listed in Table 7.

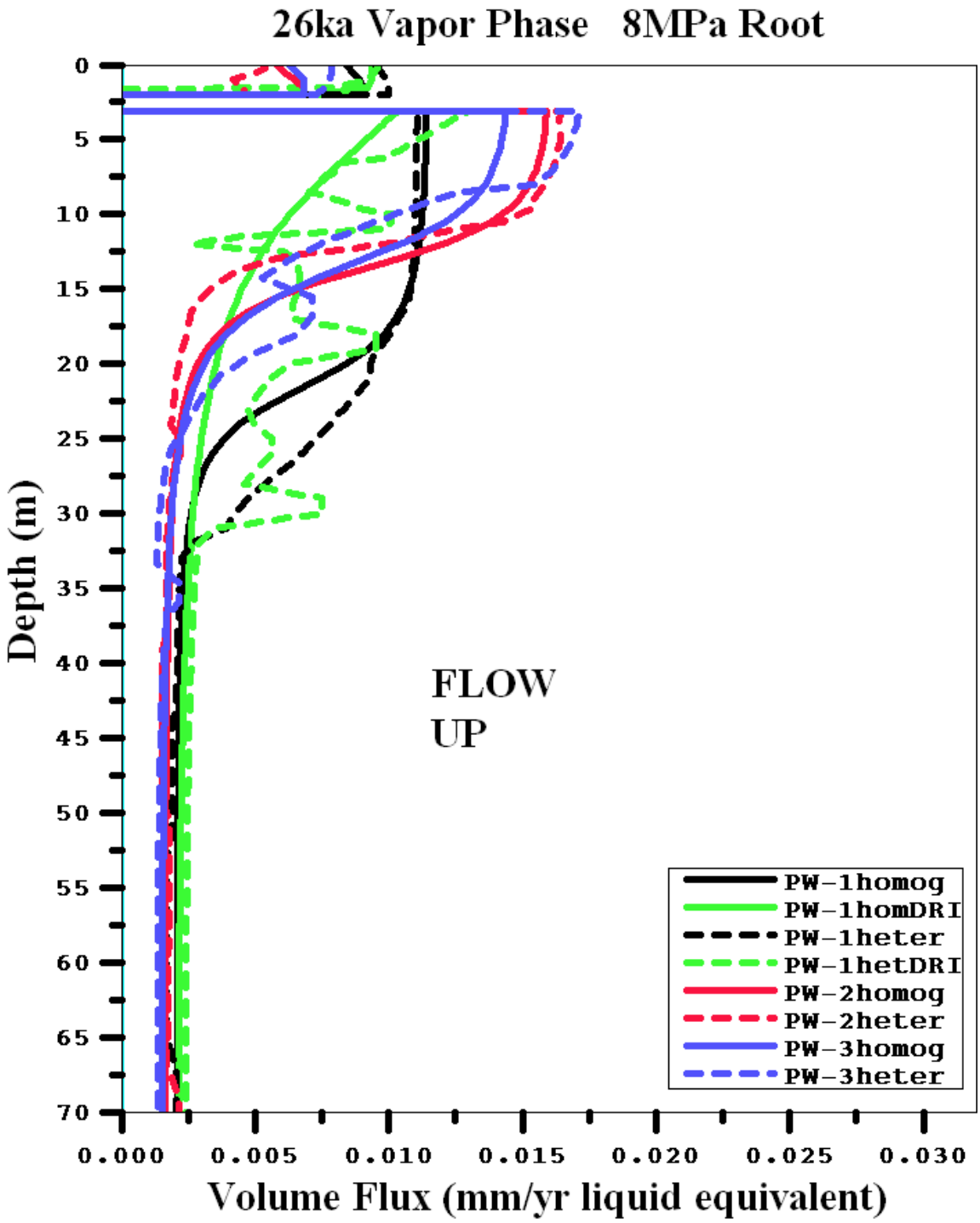

Figure 31. Simulated vapor fluxes vs. depth with an 8 MPa root-zone capillary pressure for 26 ky since the last pluvial period. Legend indicates location and material properties as listed in Table 7.

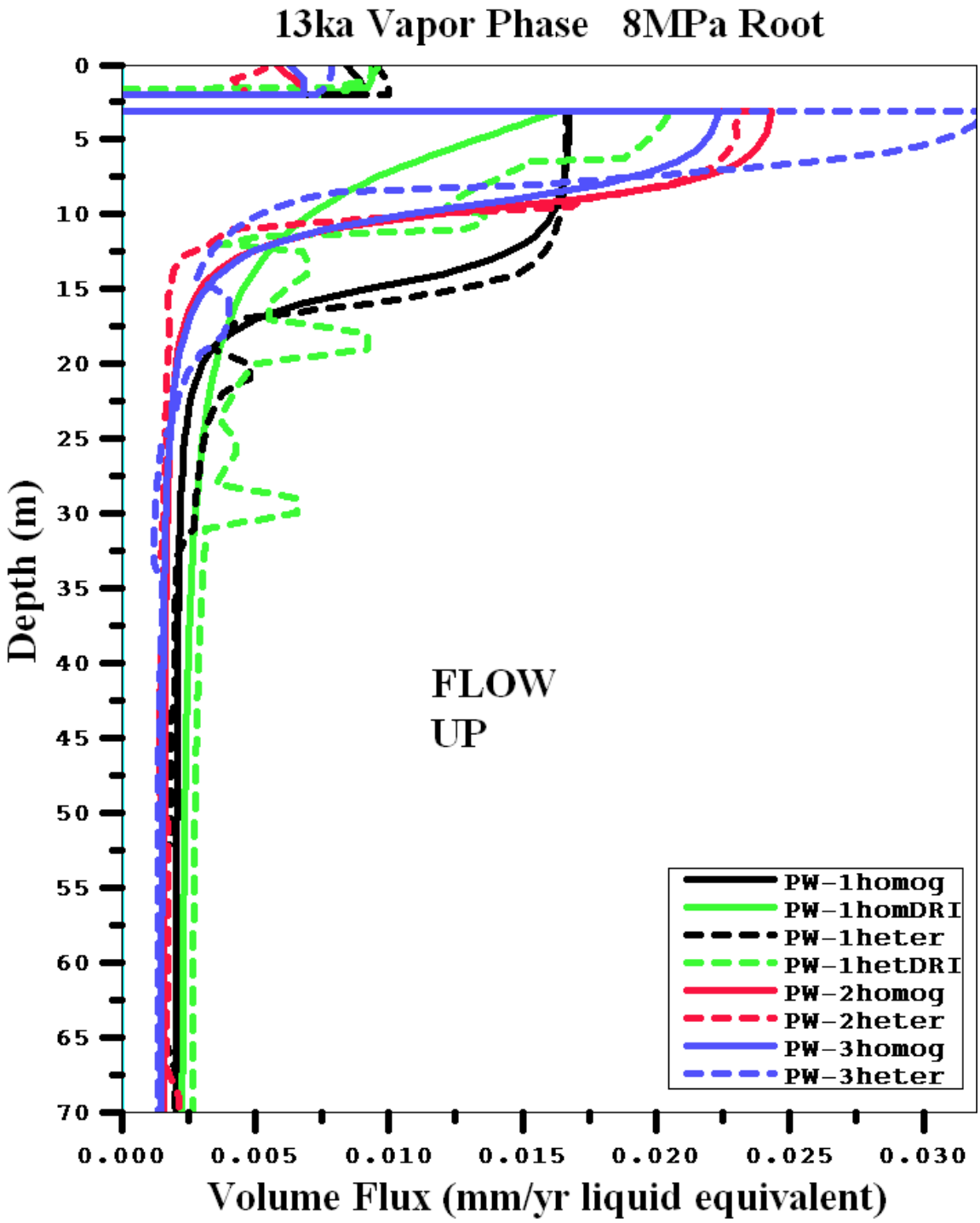

Figure 32. Simulated vapor fluxes vs. depth with an 8 MPa root-zone capillary pressure for 13 ky since the last pluvial period. Legend indicates location and material properties as listed in Table 7.

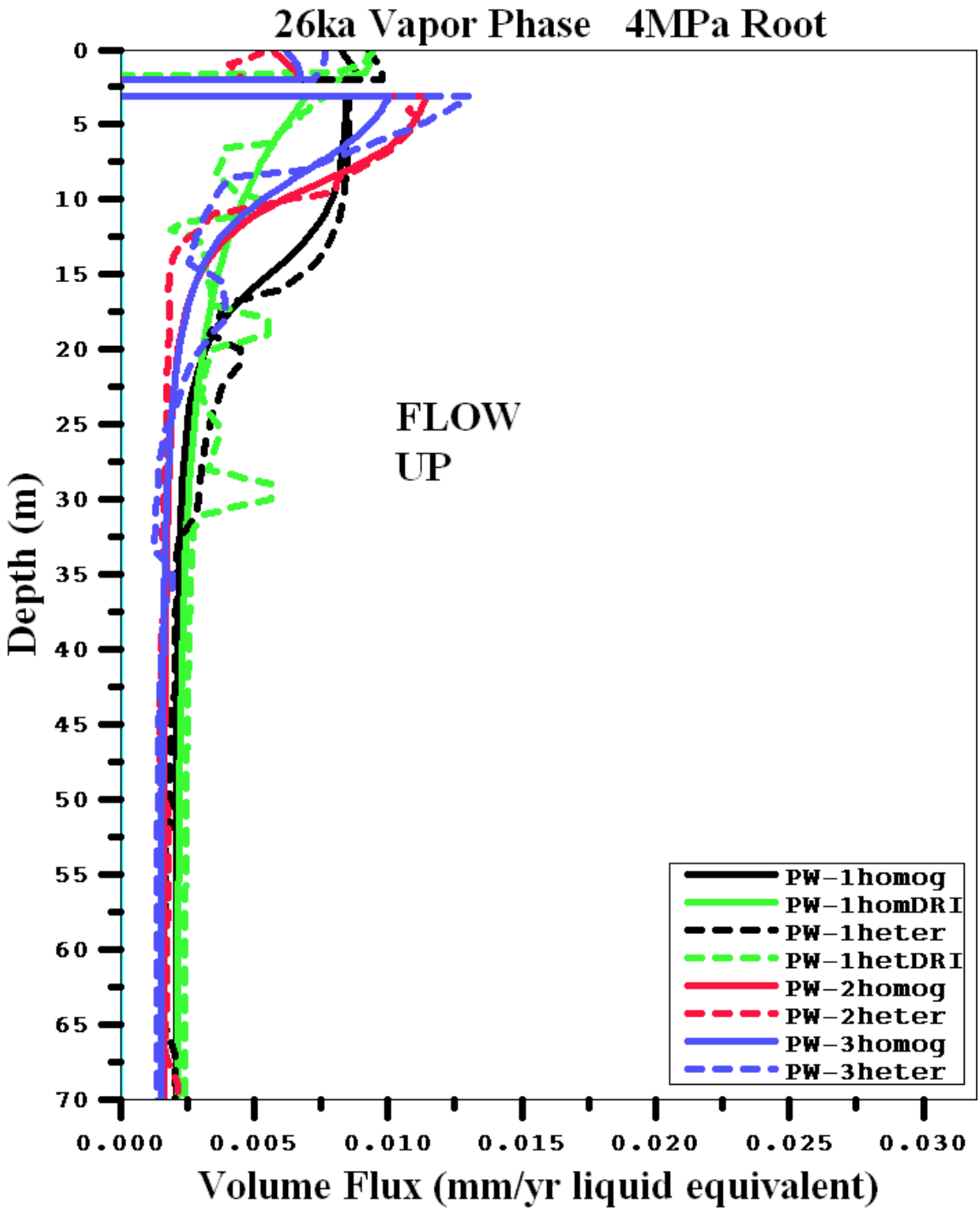

Figure 33. Simulated vapor fluxes vs. depth with an 4 MPa root-zone capillary pressure for 26 ky since the last pluvial period. Legend indicates location and material properties as listed in Table 7.

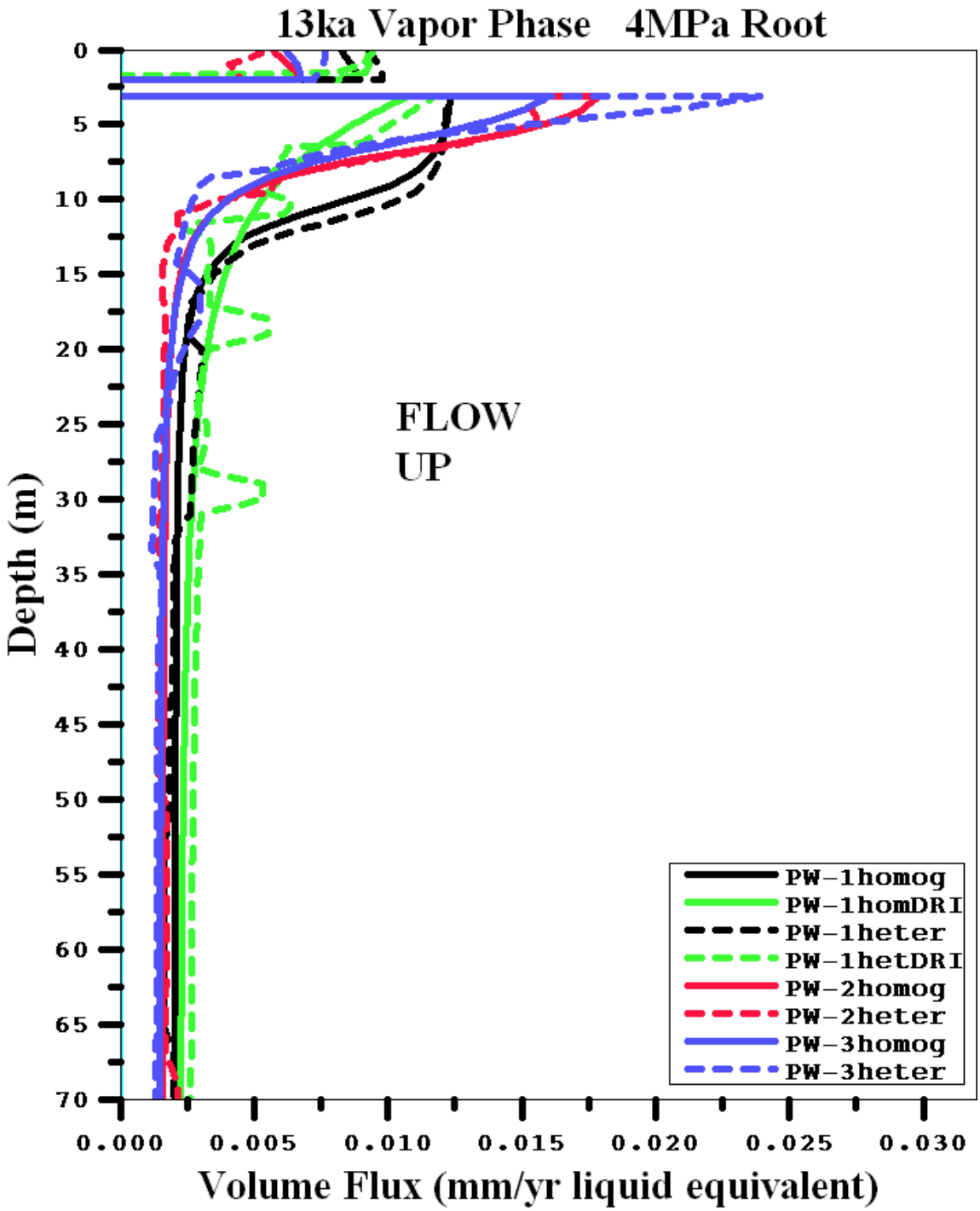

Figure 34. Simulated vapor fluxes vs. depth with an 4 MPa root-zone capillary pressure for 13 ky since the last pluvial period. Legend indicates location and material properties as listed in Table 7.

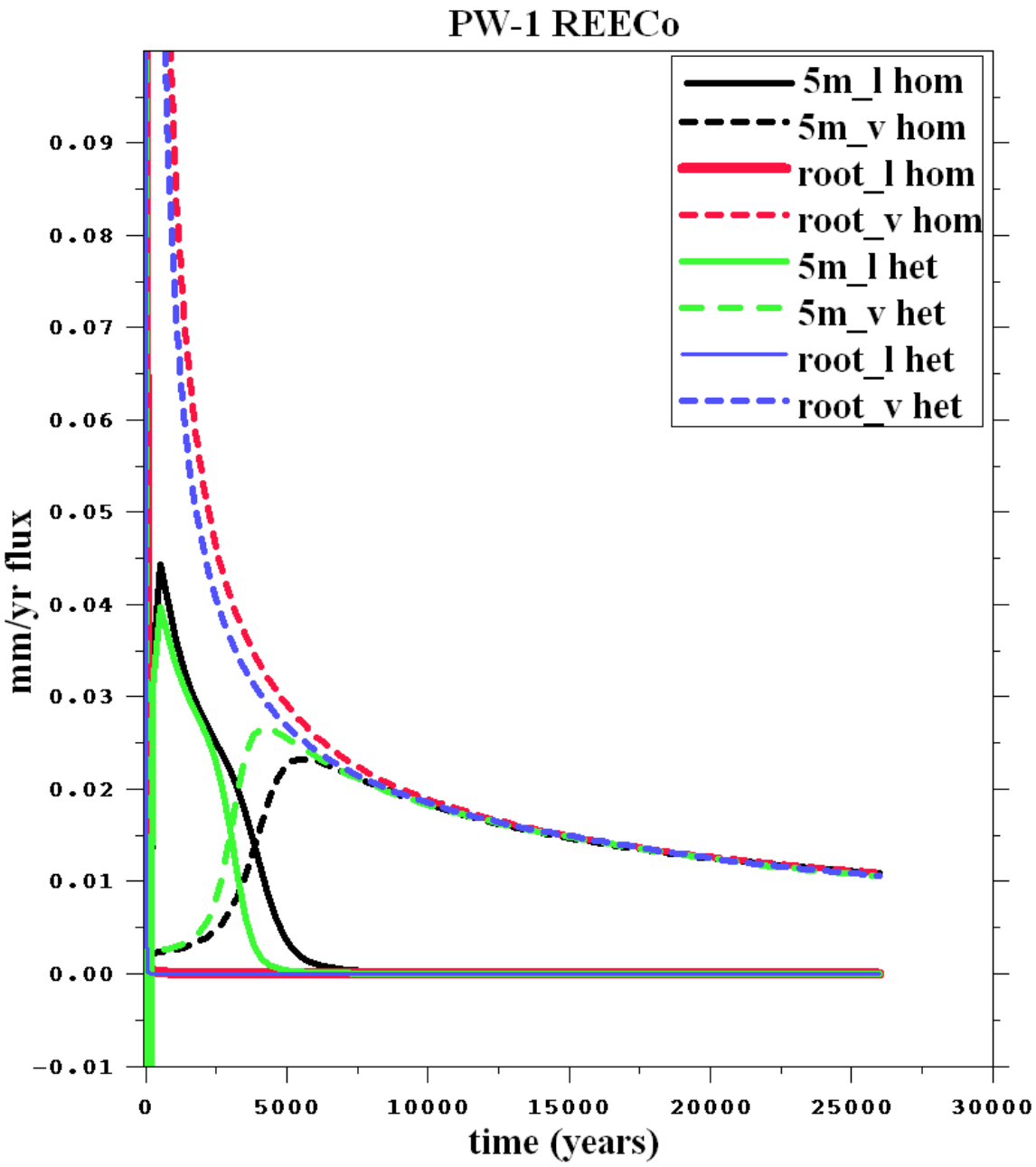

Figure 35. Liquid (l) and vapor (v) flux as a function of time since the last pluvial period (time = 0) at the root zone (r) and 5 m below the root zone (5m) for the 8 MPa root-zone capillary pressure simulations at PW-1 using the homogenous (hom) and heterogeneous (het) properties based on REECo (1994) data.

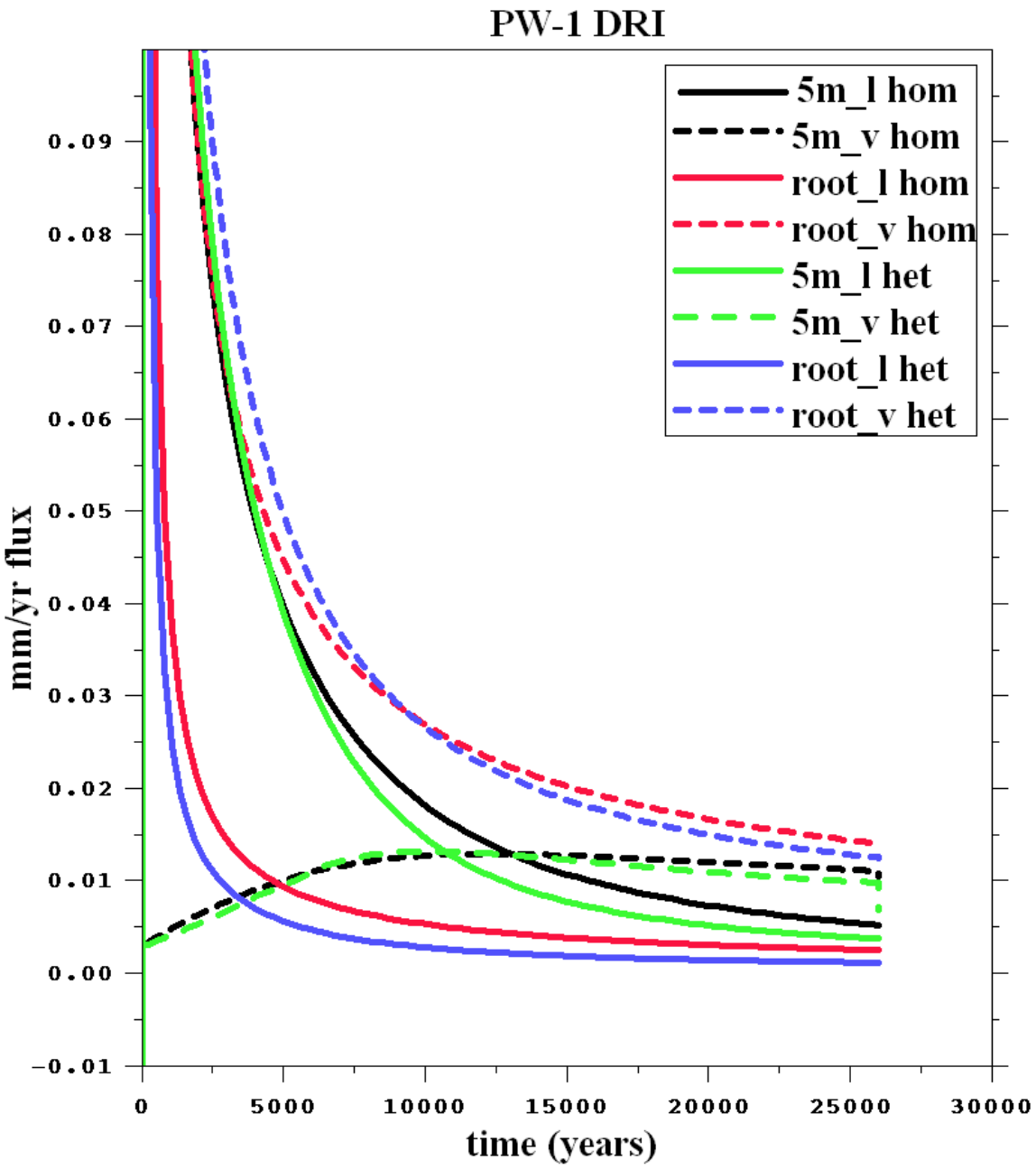

Figure 36. Liquid (l) and vapor (v) flux as a function of time since the last pluvial period (time = 0) at the root zone (r) and 5 m below the root zone (5m) for the 8 MPa root-zone capillary pressure simulations at PW-1 using the homogenous (hom) and heterogeneous (het) properties based on Young et al. (2002) data.

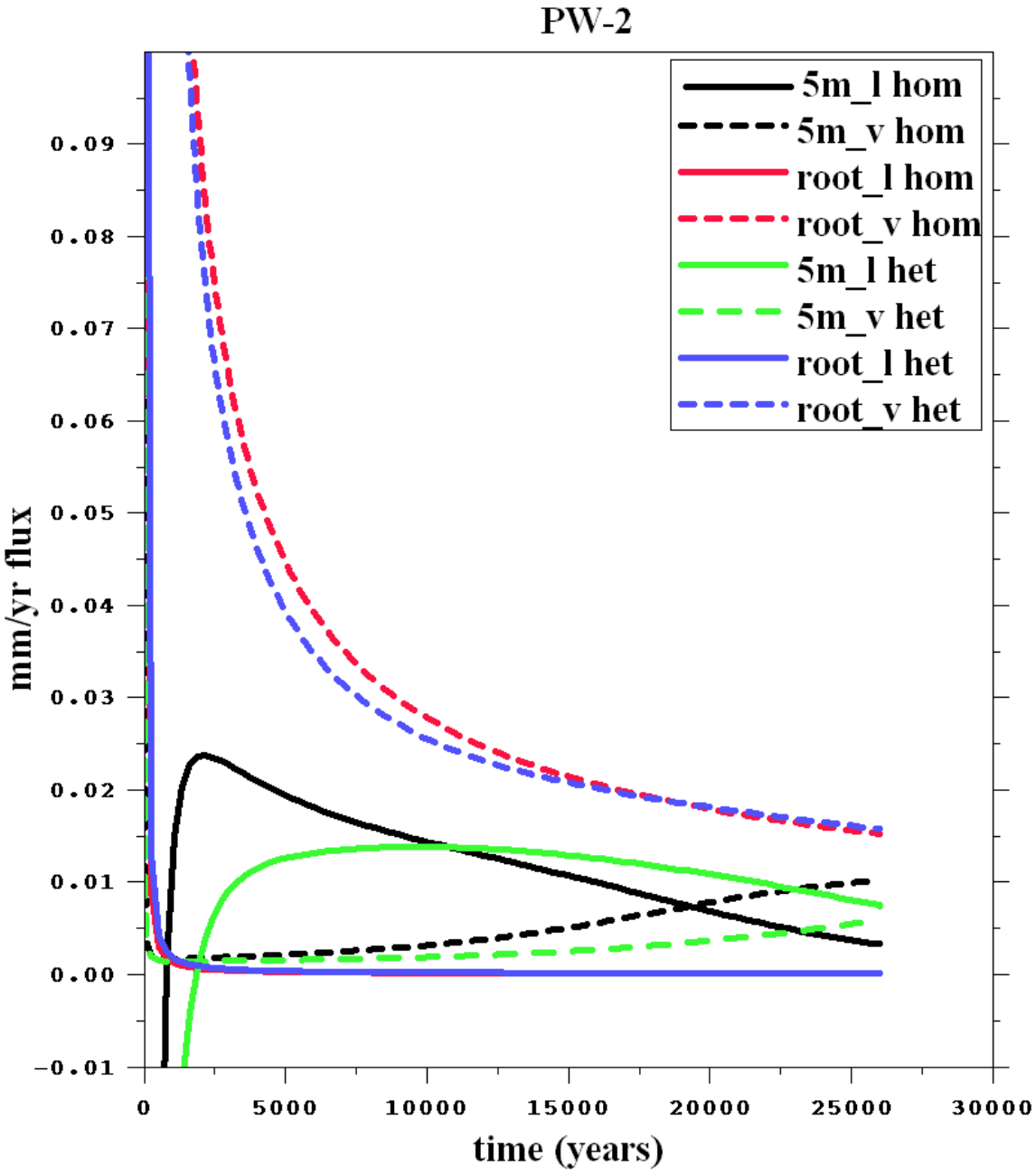

Figure 37. Liquid (l) and vapor (v) flux as a function of time since the last pluvial period (time = 0) at the root zone (r) and 5 m below the root zone (5m) for the 8 MPa root-zone capillary pressure simulations at PW-2 using the homogenous (hom) and heterogeneous (het) properties based on REECo (1994) data.

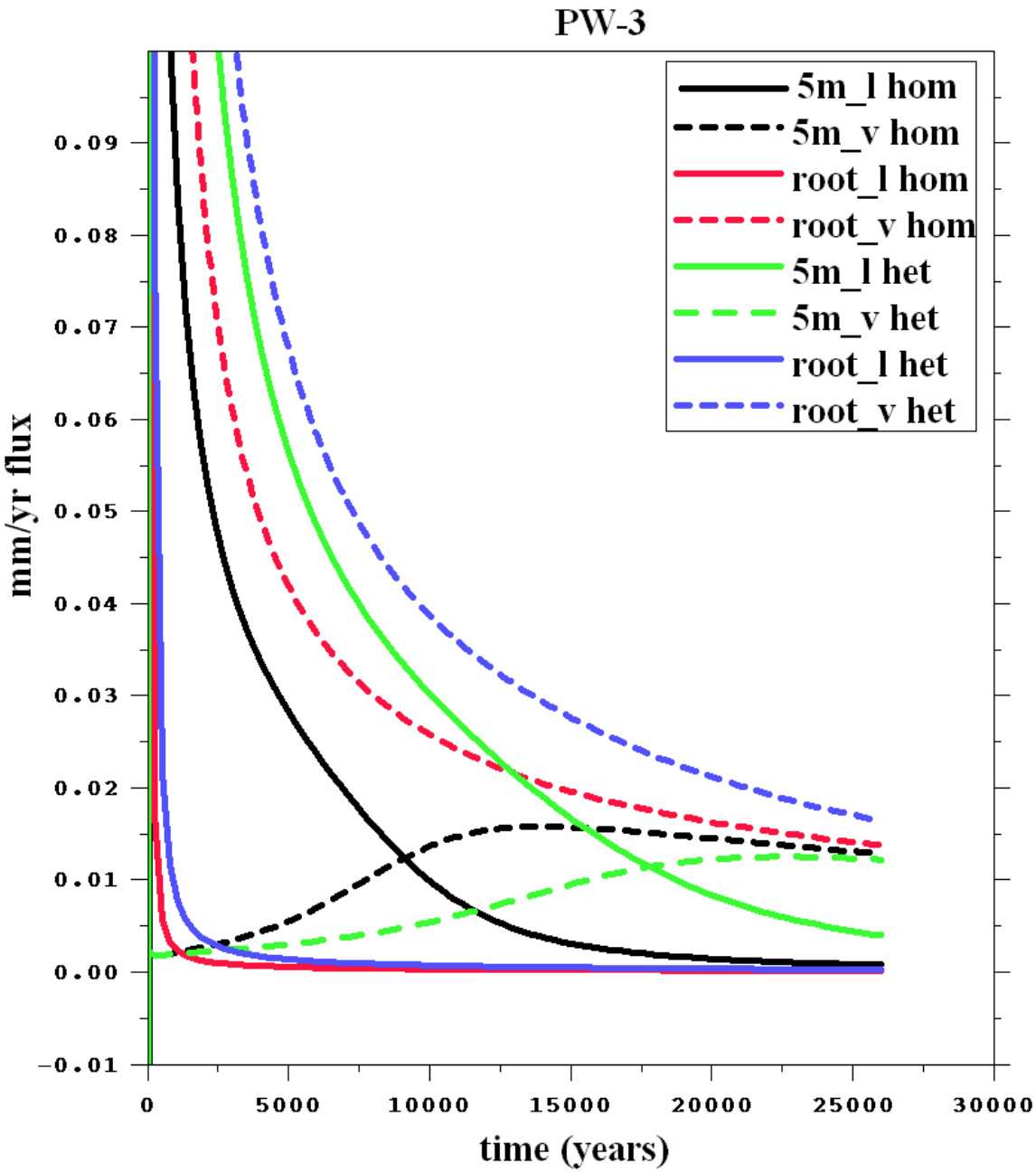

Figure 38. Liquid (l) and vapor (v) flux as a function of time since the last pluvial period (time = 0) at the root zone (r) and 5 m below the root zone (5m) for the 8 MPa root-zone capillary pressure simulations at PW-3 using the homogenous (hom) and heterogeneous (het) properties based on REECo (1994) data.

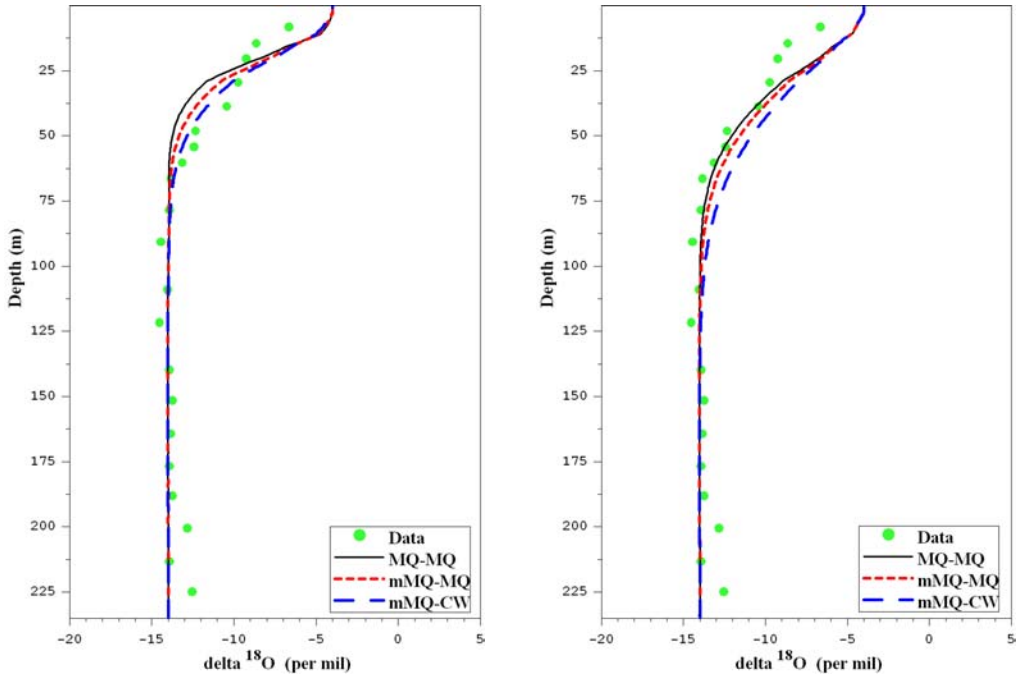

Figure 39. Comparison of simulated and measured stable oxygen isotope profiles for post-pluvial warm periods of 13 ky (left), and 26 ky (right) at **PW-1** using **heterogeneous** Young et al. (2002) properties and an 8 MPa root-zone capillary pressure boundary condition. Diffusion models include combinations of different vapor-phase and liquid phase diffusion models discussed in the text. For vapor, the models are Millington-Quirk (MQ) and modified Millington-Quirk (mMQ). For liquid the models are Millington Quirk (MQ) and Conca-Wright (CW).

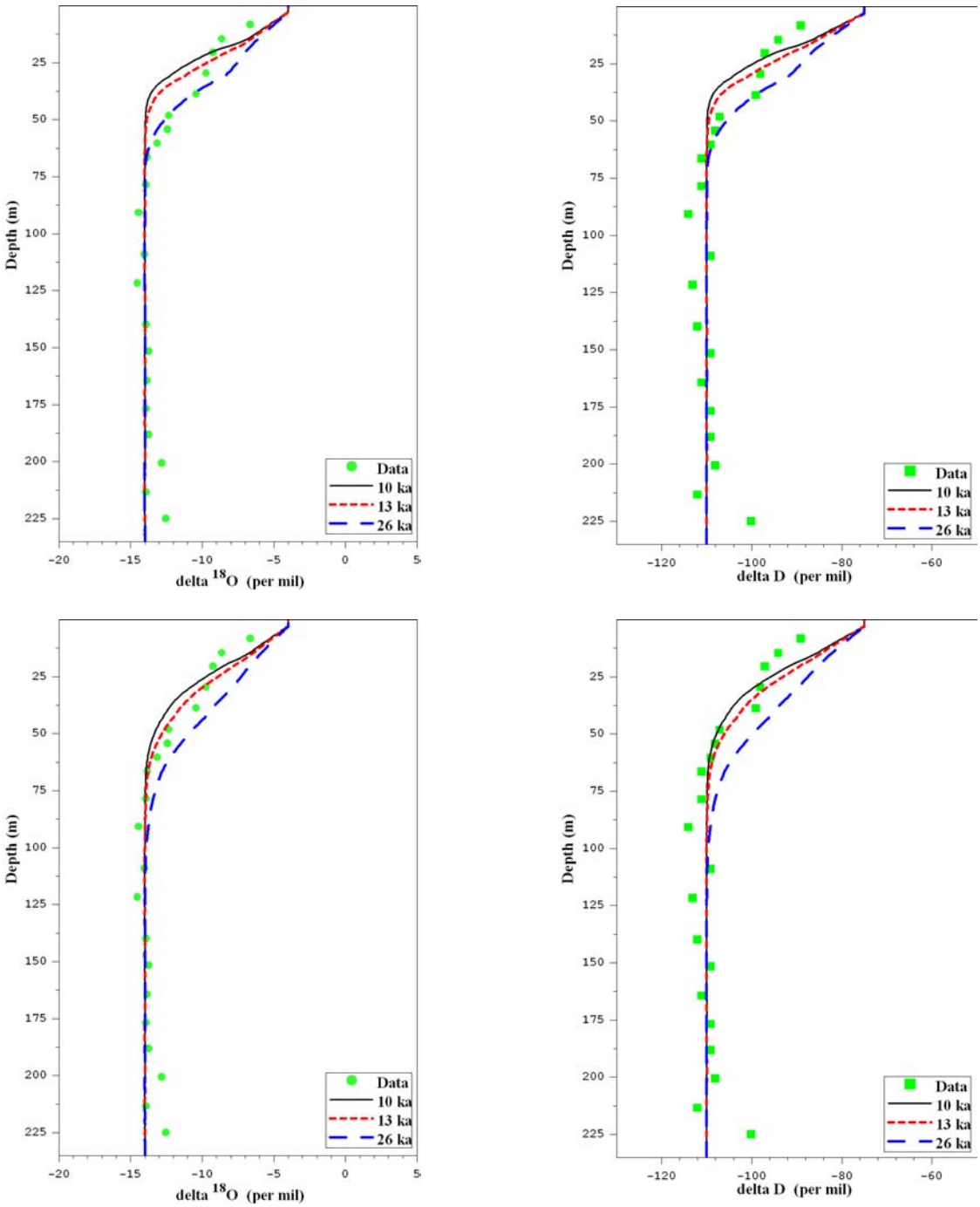

Figure 40. Simulated and measured stable isotope profiles for post-pluvial warm periods of 10, 13, and 26 ky at **PW-1** using heterogeneous **REECo (1994)** properties and an 8 MPa root-zone capillary pressure boundary condition. Upper figures use Millington-Quirk (MQ) for both liquid and vapor. Lower Figures use modified Millington-Quirk (mMQ) for vapor and Conca-Wright (CW) for liquid.

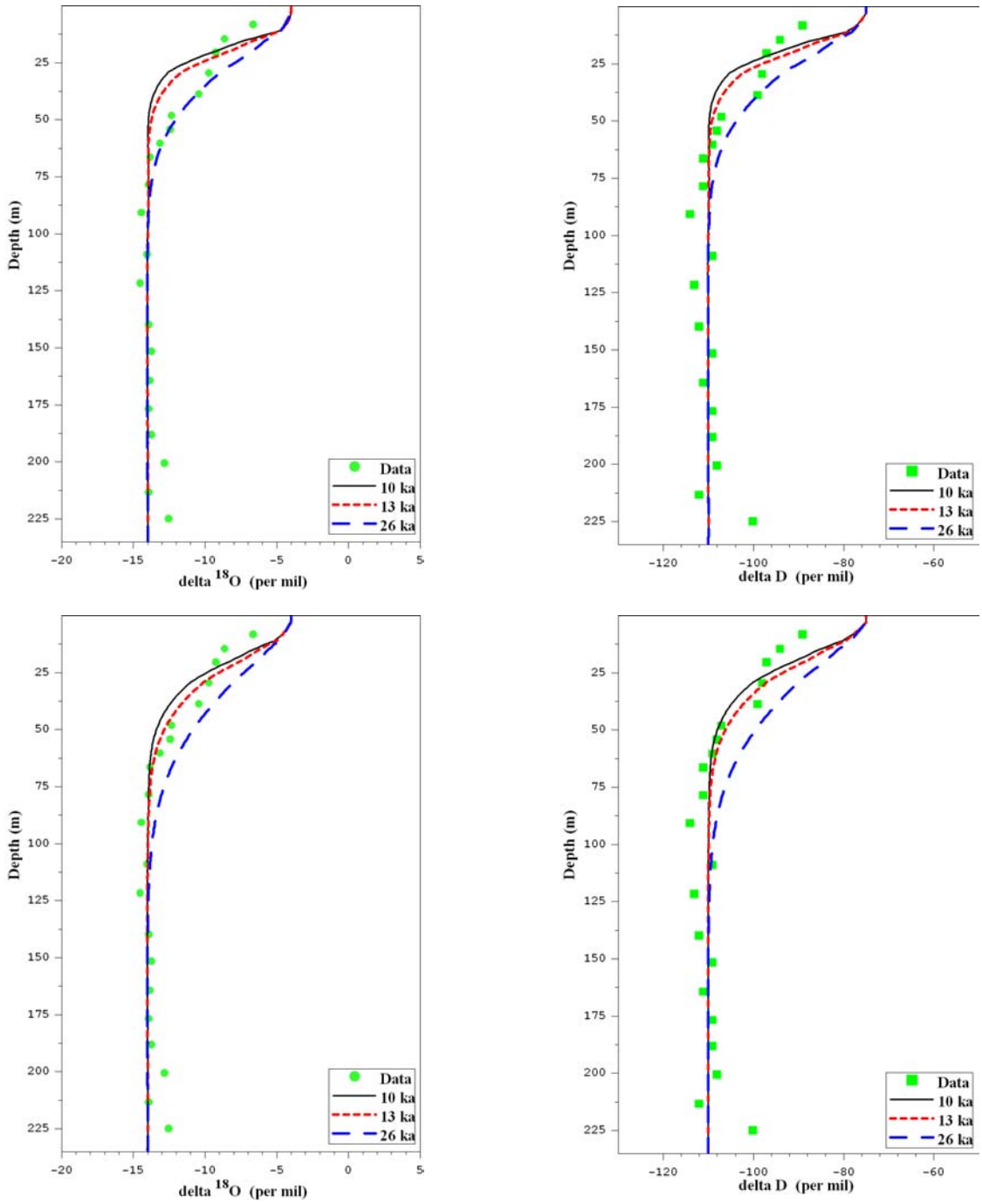

Figure 41. Simulated and measured stable isotope profiles for post-pluvial warm periods of 10, 13, and 26 ky at **PW-1** using heterogeneous **Young et al. (2002)** properties and an 8 MPa root-zone capillary pressure boundary condition. Upper figures use Millington-Quirk (MQ) for both liquid and vapor. Lower figures use modified Millington-Quirk (mMQ) for vapor and Conca-Wright (CW) for liquid.

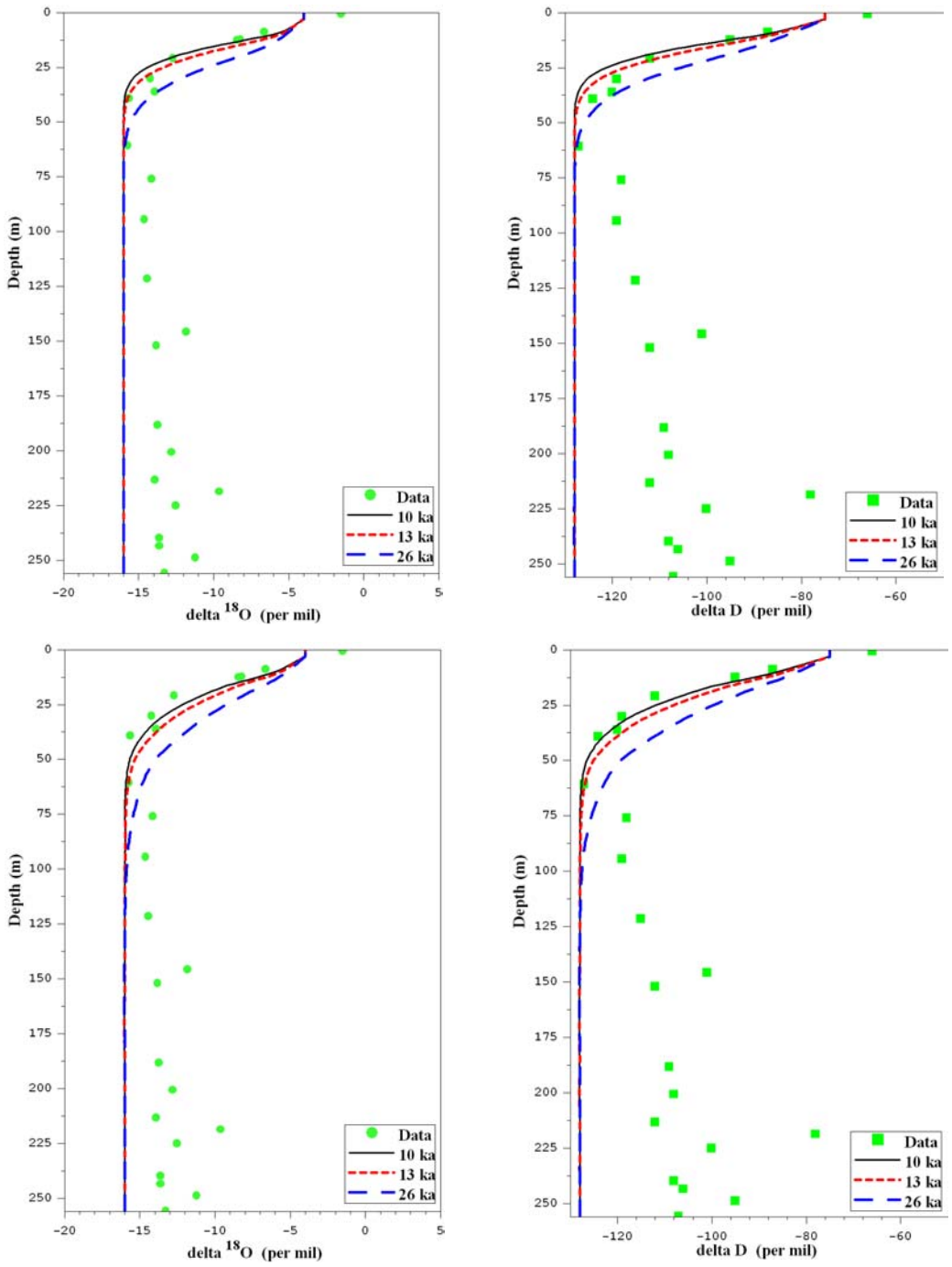

Figure 42. Simulated and measured stable isotope profiles for post-pluvial warm periods of 10, 13, and 26 ky at **PW-2** using heterogeneous **REECo (1994)** properties and an 8 MPa root-zone capillary pressure boundary condition. Upper figures use Millington-Quirk (MQ) for both liquid and vapor. Lower figures use modified Millington-Quirk (mMQ) for vapor and Conca-Wright (CW) for liquid.

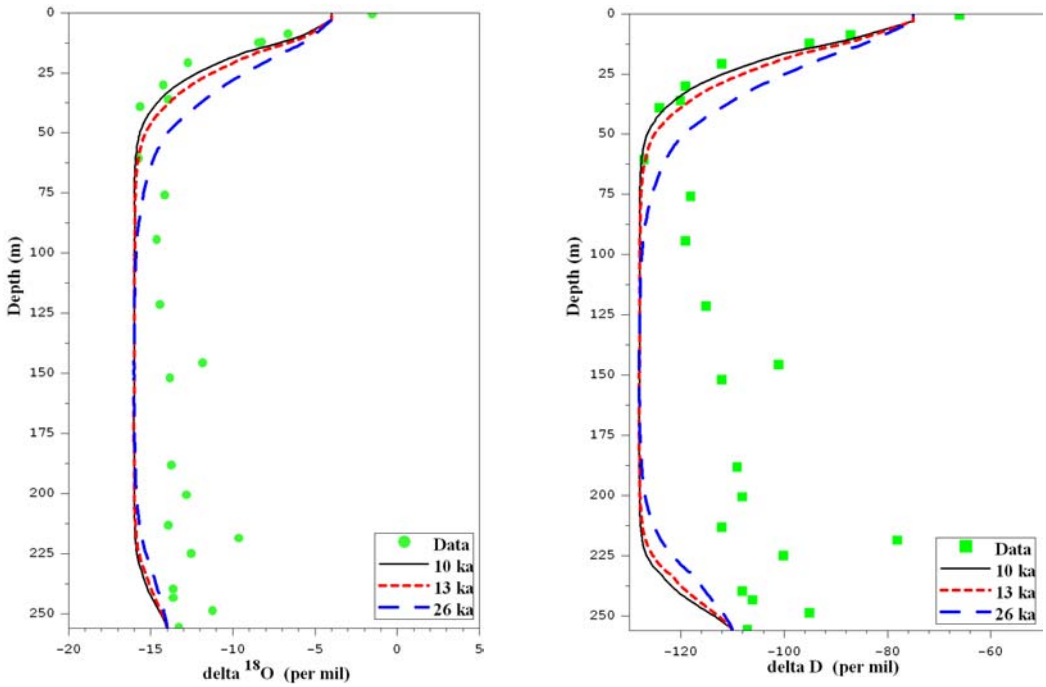

Figure 43. Simulated and measured stable isotope profiles for post-pluvial warm periods of 10, 13, and 26 ky at **PW-2** using heterogeneous **REECo (1994)** properties and an 8 MPa root-zone capillary pressure boundary condition, **and contemporary isotopic ratios at the water table boundary.** The results do not match the lower, enriched portions of the profiles, but the provide an indication that those portions of the profiles may be a result of both upper and lower boundary condition changes over time.

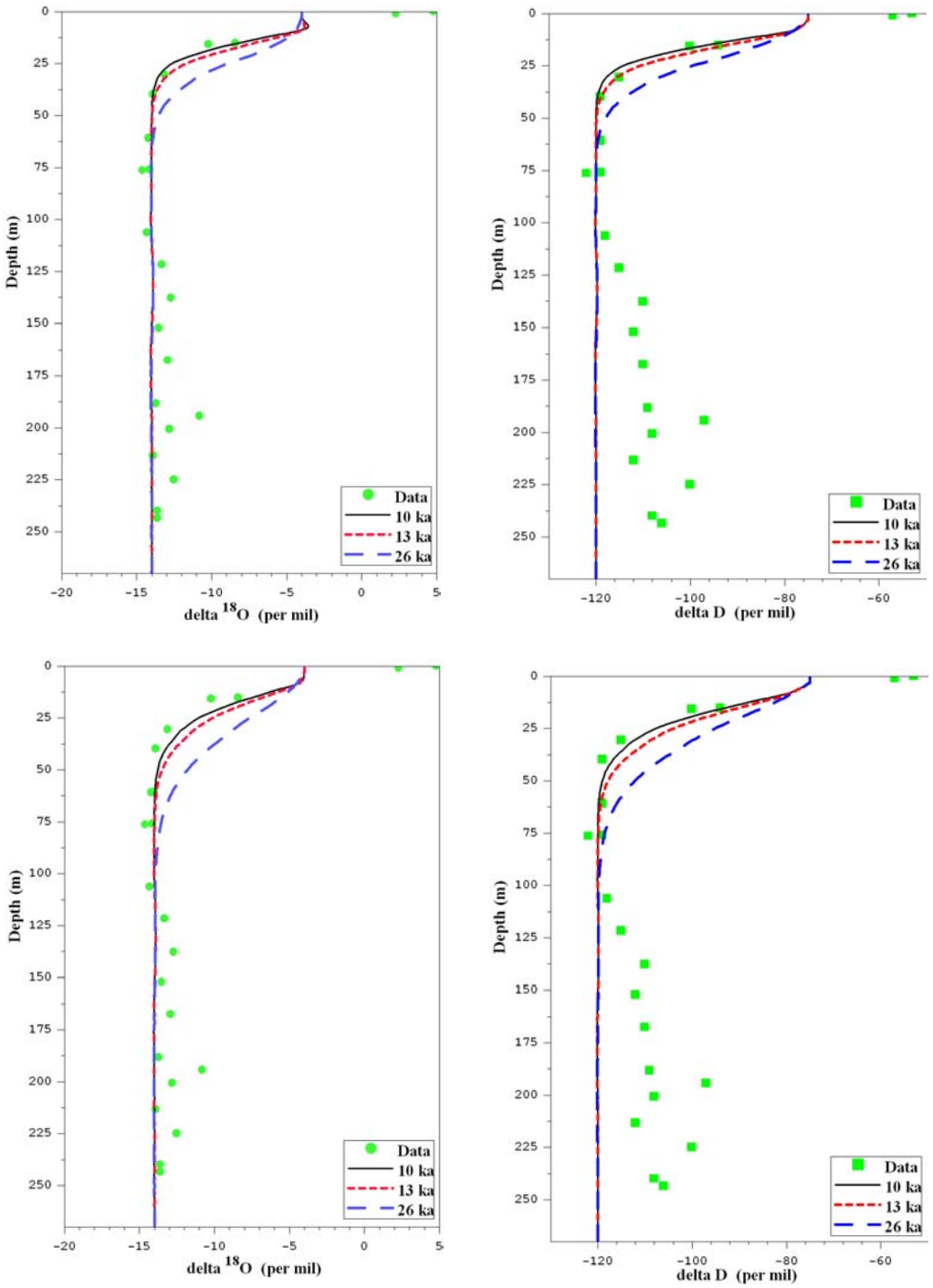

Figure 44. Simulated and measured stable isotope profiles for post-pluvial warm periods of 10, 13, and 26 ky at **PW-3** using heterogeneous **REECo (1994)** properties and an 8 MPa root-zone capillary pressure boundary condition. Upper figures use Millington-Quirk (MQ) for both liquid and vapor. Lower figures use modified Millington-Quirk (mMQ) for vapor and Conca-Wright (CW) for liquid.

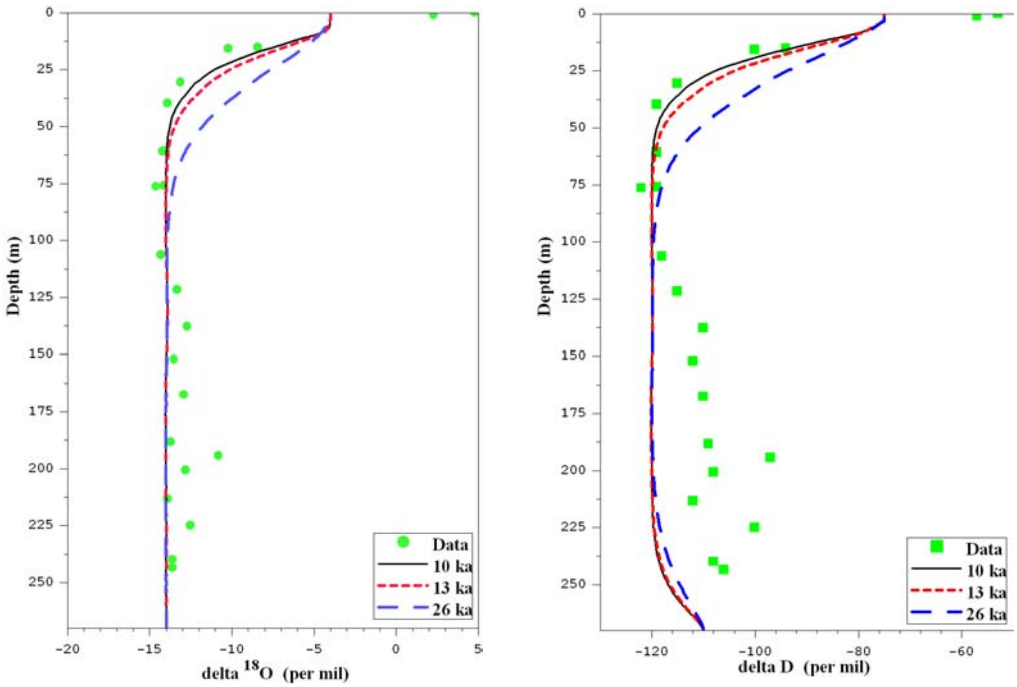

Figure 45. Simulated and measured stable isotope profiles for post-pluvial warm periods of 10, 13, and 26 ky at **PW-3** using heterogeneous **REECo (1994)** properties and an 8 MPa root-zone capillary pressure boundary condition, **and contemporary isotopic ratios at the water table boundary**. Diffusion modeled with modified Millington-Quirk (mMQ) for vapor and Conca-Wright (CW) for liquid

Distribution List

Jhon Carilli
U.S. Department of Energy
National Nuclear Security Agency
AMEM Mail Stop 505
232 Energy Way
North Las Vegas, NV 89030

Bruce Crowe
Los Alamos National Laboratory
U.S. Department of Energy
National Nuclear Security Agency
AMEM Mail Stop 505
232 Energy Way
North Las Vegas, NV 89030

Paul Black
Neptune and Company, Inc.
2031 Kerr Gulch Road
Evergreen, CO 80439

John Tauxe
Neptune and Company, Inc.
1505 15th Street Suite B
Los Alamos, New Mexico 87544

David Shafer
Division of Hydrologic Sciences
Desert Research Institute (DRI)
755 East Flamingo Road
Las Vegas, NV 89145

Vefa Yucel
Bechtel Nevada
Mailstop: NLV081
2621 Losee Road
North Las Vegas, NV 89030

Michelle Walvoord
National Research Council Postdoctoral
Associate
U.S. Geological Survey - WRD
Denver Federal Center, Box 25046
MS 413
Lakewood, CO 80225-0046

U.S. Department of Energy
National Nuclear Security Administration
Nevada Site Office
Technical Library
P.O. Box 98518
Las Vegas, NV 89193-8518

U.S. Department of Energy
National Nuclear Security Administration
Nevada Site Office
Nuclear Testing Archive,
M/S 400
P.O. Box 98521
Las Vegas, NV 89193-8521

U.S. Department of Energy
Office of Scientific and Technical Information
P.O. Box 62
Oak Ridge, TN 37831-0062

Los Alamos NM 87545